2019

Decoding and Optimizing Magnesium Phosphate Binders for Additive Construction Applications

Hashem Khaled Almashaqbeh
University of Mississippi

DECODING AND OPTIMIZING MAGNESIUM PHOSPHATE BINDERS FOR ADDITIVE CONSTRUCTION APPLICATIONS

A Dissertation

presented in partial fulfillment of requirements

for the degree of Doctor of Philosophy

in the Department of Civil Engineering

The University of Mississippi

by

Hashem K. Almashaqbeh

May 2019

ABSTRACT

The inclusion of 3D printing (3DP) technologies in the construction field has the potential to solve many structural related problems and will reduce construction cost and time. 3DcP technology is facing some drawbacks, such as scarcity of printable materials, accompanied by material science challenges, including production process, process-related material requirements, construction-related material requirements, and handling of non-homogeneous and time-dependent material properties. Therefore, extensive work is needed to improve and utilize materials for AC applications. The two main challenges that need to be urgently investigated, to incorporate 3DP in construction (3DcP) applications are (1) development of the 3DcP process for non-homogeneous materials to facilitate the production of multilateral mason materials and (2) improvement of the printing process.

Modified magnesium phosphate cement (MPC) composites have a high potential for AC applications due to its superior properties such as high compressive strength, rapid setting time, and excellent durability.

This work aims to give more insight about the physical, mechanical, thermal, and chemical performance of the MPC paste composites. Our primary outcome from this research is to improve the MPC composites with different additives, including boric acid, GnP, and acetic acid for potential utilization in 3DcP applications. Furthermore, Martian and Lunar regolith simulants can be mixed with the MPC composites to create mortars as a possible extraterrestrial 3DP in-situ construction material mainly to support the NASA habitation exploration mission.

Before adjusting the required properties for an AC application, many aspects need to be studied in depth to provide a better understanding of MPC behavior under different conditions. The main highlights of the experimental results show that each additive can change the phase compositions of the MPC pastes and affect its physical and mechanical performance towards fitting the 3DcP requirements. Moreover, the research conducted creatively utilized artificial neural networks (ANN) to investigate and subsequently optimize both the MPC pastes and composite formulation for desirable in-service performance.

The novel approach and terminology proposed in this dissertation are expected to provide critical fundamental scientific bases on a new class of construction material for both extraterrestrial habitats and terrestrial construction applications, where sand and clay can replace regolith.

DEDICATION

I dedicate this dissertation to my wonderful parents (Mr. Khaled Al Mashaqbeh and Mrs. Hiyam Al Mashaqbeh), my lovely wife and my stunning sister who supported me through my long journey with all the source of love, enthusiasm, and encouragement.

ACKNOWLEDGMENTS

Firstly, I would like to express my sincere gratitude to my advisor, Dr. Hunain Alkhateb, for her support, patience, motivation, enthusiasm, immense knowledge and encouragement during these past four years. Dr. Alkhateb has been inexhaustibly supportive and has given me the freedom to pursue various projects of personal interest without objection. It has been invaluable to work under an advisor that consistently takes the time to listen to all the little problems and roadblocks that one encounters along the way. She has shown the generous ability to solve dilemmas and provide aid without hesitation. Without her help, this work would not exist.

I would like to thank the Department of Civil Engineering; I could not have financed my studies without their assistantship. Also, I would like to thank the members of my graduate committee: Professor Ahmed Al-Ostaz, Professor Yacoub Najjar, and Dr. Alexander Lopez, for their guidance and suggestions.

Special thanks go Dr. Najjar and Dr. Al-Ostaz for their support during this research and for their insight and counsel.

I would like to offer my special thanks to my parents and my wife for their help and support during this work.

I am also particularly grateful for the assistance given by my colleagues: Fielding Ables and Rami Alsughier. Also, I would like to acknowledge the help provided by Dr. Amrita Mishra, Damian Stoddard and Nick Scott of the Mechanical Engineering Department/The University of Mississippi.

I would like to thank Dr. Sanjay of the University of Memphis and his graduate student Tej P. Poudel for conducting the XRD testing for my specimens. Thanks are due as well to Dr. Hongyu Zhou of the University of Alabama in Huntsville and his graduate student Adam L. Brooks for facilitating the thermal conductivity test used in this work. Also, I would like to thank Chris Watters, Hitachi High Technologies America Inc, and Dr. Lax Saraf at Clemson's EMF, for offering the SEM images of this research.

Finally, I want to thank NASA for funding this research and to all others who have participated in this research, regardless of the magnitude of their efforts.

TABLE OF CONTENTS

CHAPTER I: INTRODUCTION AND LITERATURE REVIEW

CHAPTER II: MATERIALS AND METHODS

LIST OF TABLES

LIST OF FIGURES

CHAPTER I

INTRODUCTION AND LITERATURE REVIEW

1.1 INTRODUCTION

Construction industries have always been inflexible, difficult to change, slow in evolution, and the latest in adapting to modern technology. Although the construction industries seem unchangeable, many researchers have indicated that the construction industry will be engaged to the world of digital technology. Some examples of insertion of modern technology in the construction field include machine learning, virtual reality, and three-dimensional printing (3DP).

3DP, which is also known as Additive Manufacturing (AM), is the coming soon technology that will change the industry world. This year, NASA announced that it will build its new spacecraft by assembling more than 100 3D printed parts, which will perform some lunar missions by the next year. Moreover, NASA aspires to build the first lunar and Martian habitat using 3DP technology. On Earth, a 37-square-meter house was built in a suburb of Moscow in less than 24 hours by using 3DP technology; and in last June, A French family has become the first family in the world to live into a four-bedroom 3D printed house.

The goal of embedding AM technology in the construction industry is to reduce time and cost. The ability to create larger structures in a very short time may become possible with this technology, especially in the case of emergencies, such as the establishment of emergency shelters

after earthquakes and natural disasters. The benefits of embedding AM in the field of construction are not limited to that, also, it can reduce the number of on-site labor and reduce the material waste.

1.2 ADDITIVE MANUFACTURING (AM)

Additive Manufacturing (AM) is a developing deposition process for creating manufactured objects, by placing a specific material layer by layer to obtain the acquired 3D object. The object which is produced by AM is a projection of a 3D software drawing. The printing process in AM is composed of a computerized system that connects the printing machine with the 3D design model, such as a Computer-Aided Design (CAD) model or Additive Manufacturing File (AMF).

AM has many attracting advantages such as the high quality of the products finishing, the accuracy of correspondence to the software models, the reduction in the time needed for manufacturing processes, the minimization of the number of laborers needed for fabricating products and the reduction in the production waste [1]. Despite the many advantages of AM, there are some challenges that face this technology including (1) limitation in adequate materials (2) difficult implementation in large structure productions and (3) high cost compared to traditional industry. Hence, more work is needed to utilize materials that can be used for AM technologies and different applications. [1,2]

1.2.1 HISTORY OF 3D PRINTING

AM term was inspired by the 3-dimensional printing (3DP) technique, which is creating objects by adding layer upon layer. The development of equipment and methods for AM

technology were established in the 1980s. In 1984, Méhauté with a group of French inventors, initiated the stereolithography (SLT) process to be used in AM applications [3]. Two years later, Chuk Hull developed the SLT process where the material layers were formed from photopolymers and cured by ultraviolet (UV) light lasers [4]. The process depends on creating cross sections for the desired object. Hull's contribution in stereolithography strategy is involved in many applications today [4, 5]. In 1988, S. Scott Crump improved a unique application of plastic extrusion called fused deposition modeling (FDM), this process is the most technology used by the 3DP applications until these days [6]. In 2009, the FDM 3DP procedure patents expired.

There are several AM technologies that were determined according to the method of 3D printing; based on the machine used, and the material's type and consistency which include: (1) vat photopolymerization, (2) material jetting, (3) Powder Bed Fusion (PBF), (4) binder jetting, (5) directed energy deposition, (6) and material extrusion.

In the vat photopolymerization method, the model is constructed layer by layer, though, the material used should be in a liquid phase during the process. The vat polymerization process uses plastics and polymers, and the resin is cured and hardened using UV light. 3D Systems ProX 950 machine is an example of the vat photopolymerization method. The vat photopolymerization is known for its high-quality finishing and rapid procedure, moreover, its ability to get out relatively large-scale objects. On the other side, it is considered relatively expensive compared to the other methods [7].

Material jetting applies a similar method of the inkjet document printing in the 2D printing system, but instead of dropping the ink onto a paper, the PolyJet 3D printers drops the photopolymer liquid onto a build sheet. The material will be projected to create a layer over layer until completion of the final model, and then, the object will be cured using a UV light to get the

final solid shape of the sample. In the material jetting technique, a gel-like material is required during the process to work as a mold and to support the desired model. This technology is known of its high accuracy and smooth finishing; however, it is relatively slow [1,8-10].

The PBF process is based on spreading the powder material over the previous layers. Some of the drawbacks of this method include the slow process, a deficiency in the structural properties for the produced objects and the size limitations of the products. However, it is relatively inexpensive compared to other methods and includes a wide range of material options [11].

In the binder jetting method, a powder-like material is used to create layers of powered material including plastics, ceramics, and metals. Then, a liquid bonding agent is injected between the layers to form the desired object. This method is considered to be cost-effective [12].

In the material extrusion process, which is also known as Fused Deposition Modelling (FDM), the material is dropped from a nozzle and deposited on a pre-created surface layer by layer, under constant pressure, and a constant speed, the bonding between layers occurs by applying temperature or using chemical agents. Generally, this process is used for polymers and plastics. Recently, cement and concrete materials have been utilizing in this method. One of the disadvantages of this process is the physical limitation due to the nozzle used. In addition, it needs a more time to complete the AM process compared to other processes [13].

Directed energy deposition applies similar principles to the material extrusion process, except that the extruder nozzle can rotate freely at multiple axes. This method is used for joining a new part to an existing object; it is usually used for metals such as cobalt-chromium and titanium [14].

After the great development in the field of AM, especially in the binder jetting and material extrusion techniques, AM applications have been expanded to the construction industry. An equivalent technology to the material extrusion and inkjet printing has been developed to introduce the AM technology into the field of construction [15]. As the concrete is the most used material for construction, it has received more attention to be utilized in 3DP technologies. Recently, using AM technologies in construction has evolved towards delivering full-scale objects and large structural elements [16]. The use of AM technology in the field of construction has been called Additive Construction (AC).

1.2.2 ADDITIVE CONSTRUCTION (AC)

The beginning of AM application in the construction industry has taken a significant interest to open the door for constructing more complex architectural models that were difficult to be created in usual conditions and by means of traditional construction methods. AC is a digital controlling process of creating construction elements from building material and join them together to form a final structural shape. AC has alternative terms, such as 3D Construction Printing (3DCP), Large-Scale Additive Manufacturing (LSAM), and Freeform Construction (FC). Since the concrete is the most commonly used material in construction, concrete-extrusion technologies predominately dominate the scope of additive construction. A more specialized term used to refer to concrete extrusion is '3D printed Concrete'. [2,16, and 17].

The potential advantages of applying 3DCP are; saving time, decreasing the on-site labor requirements on site, optimizing suitable materials which reduces material waste, improving the high-finishing quality, allowing an increase in the structural geometrical complexity, and

reducing the overall construction cost, with the capability of eliminating the presence of traditional formworks [17,18].

AC technology is facing some drawbacks such as scarcity of printable materials accompanied with material science challenges including production process, process-related material requirements, construction-related material requirements, and handling of non-homogeneous and time dependent material properties. Therefore, immense work is needed to improve the AC processes and to utilize materials that have a potential in AC applications [2,18, and 19]. The main two challenges that need to be investigated to improve the quality of AC production are: (1) developing of 3DP process of the non-homogeneous materials in order to facilitate the production of multilateral mason materials (2) improving new materials that delivers unique specifications and properties which are needed for both the printing process and the construction durability [18 and 19].

In the extrusion-based method, which is the primary method for AC, specific process-related characteristics are needed to evaluate, control and improve the performance of AC production [20], the main four process-related characteristics are:

a) Pumpability: is the ability of the material to move through the delivery system [21].
b) Printability: is the yielding shear strength development of the material during the transformation and deposition of the 3D printing procedure [22].
c) Buildability: is the ability of the wet layers of the material to resist the deformation due to applying self-weight loading conditions as the added layers are becoming cumulative, this process-related characteristic controls the thickness and the numbers of the layers that can be obtained in a certain 3DP event [22].

d) Open time: is the time that the 3DP material can conserve the features mentioned above within a reasonable predetermined toleration specification [20,21].

Recently, many researchers studied the possibility of obtaining high-precision concrete objects using AC technology. Anatasiou et al. proved mathematically that any 3D structure (whatever its shape) could be built by layer upon layer deposition approach [23]. Thus, many researchers have studied the main material properties that can affect the efficiency of printed products. For the concrete-like material, the rheological non-homogenous fresh properties are the most critical aspects that can affect the performance of the AC production. Some of these critical fresh properties are:

a) Setting time: is the time required for the material to transform from the liquid or viscous state to the plastic state, the setting time for any concrete-like material depends on several factors including water content, temperature, salt amounts, and chemical combinations [24].
b) Thixotropy: is the subsequent reduction of the paste viscosity with time, when the sample is under shear stress. [25]
c) Green strength: is the strength of the concrete at the early aged hardening and before achieving the full-time curing [26].
d) Workability: is the ease of handling and processing the concrete paste without any segregation [27].

In 3DPC, the mix design must satisfy the required fresh and hardened properties. For example, the required setting time and workability should be obtained, meanwhile, the mix should meet the required green strength to support additional layers. Jianchao et al. tried to find the optimal mix design for 3DP using different types of cementitious binders. The results showed that

the optimal mix design was related to several parameters including pumping rate, used temperature, and required compressive strength [28]. Also, Paul et al. studied the ability of different concrete mixtures to be used for AC applications. They reported that the rheological properties and thixotropic behavior of concrete are the most critical factors for 3DPC [29].

Many construction additives have been investigated to improve the material properties to enable better 3DP. Zhang et al. tried to develop a new concrete ink for 3DP applications. They investigated the effects of several additives on the fresh properties of concrete ink including fluidity, workability, and green strength. The results demonstrated that the buildability of the concrete ink was improved by using nano-clay (NC) and silica -fume (SF) by 150% and 117%, respectively. After trying many concrete mixtures, they were able to build 260 millimeters, in height, of concrete by using a mega-scale 3D printer with a nozzle diameter of 20 mm and a building rate of 8000 mm/min [30]. Soltan et al. designed a reinforced cementitious binder with short polymer fibers to be used for 3DP programs. The rheological properties (workability and thixotropy) were adjusted for a 3D printer with a circular nozzle of 8-13 mm diameters. In order to achieve good printability, they investigated the influence of many additives including; calcium aluminate (CA), micro silica (MS), ground silica (GS), and Attapulgite nano-clay (ANC). The results indicated that a small dosage of CA could increase the hardening rate and the initial flow of the system. Moreover, the hardening rate was increased, and the initial flowability was maintained by adding a small dosage of MS and GS. Finally, using small amounts of ANC can improve the cohesion of the mixture, but it had a slight effect on the hardening rate. [31]. Asprone et al. have suggested a new 3D printing technique to produce a 3 m reinforced concrete beam. They divided the member into different segments, and they printed each one of them separately, then all the parts were assembled together with the steel reinforcement. The results indicated that

the shear damage at the interfaces between different RC beam segments caused a large deflection, which led to reducing the overall performances of the RC beams [32]. Kazemian et al. reported that the using of SF and NC enhanced the shape-stability of 3D printed cement paste [33].

Due to the limited available material for AC applications, the concept of utilizing new materials for AC application has begun to take great global attention. Perrot et al. studied the possibility of using an earth-based material with the 3DP application. They used a 3D printer with two extruders including circular cross-section extruder of 35 mm in diameter and rectangular cross-section extruder of 21 x 40 mm^2. The maximum flow rate was 40 L/min, while the max pressure in the pump was 20 bar. The results indicated that using earth-based material in 3D printing application was possible [34]. Ketela et al. adjusted the rheology properties of a silicate-based slurry to study the possibility of printing this material with a 3D printer using laser triangulation-based 3D-scanning. After investigating the relations between the rheological properties and the printability of the slurry, they suggested using a printability index -to evaluate the extent of the mismatch between what is designed on a digital CAD and what is actually printed- to control and evaluate the 3D printed slurry. The results indicated that using of silicate-based slurry in 3DP needed further work [35].

Recently, some evidence has indicated that the use of AC may reduce environmental pollution by reducing carbon dioxide emissions rate. Achillas et al. reported that the AC techniques could reduce the amount of carbon dioxide in the atmosphere. The carbon dioxide produced by AC is less compared to that produced by traditional construction methods, this could be connected to the reduction in the material waste generated by AC technologies compared to traditional construction technologies. Moreover, taking into consideration that AC techniques do not require molding and casting operations [36].

According to many researchers, the inclusion of AM technologies in the field of construction will solve many structural related problems and will reduce cost and time. Therefore, applying AC technologies under multiple construction conditions is becoming a pressing necessity. In addition, utilizing concrete alternatives which can withstand difficult construction conditions is becoming a demanding requirement in the field of AC; also, the properties of these materials must be suitable for 3DP. In the last decade, magnesium-based binders (MBBs) have shown a great promise to be used in different AC applications.

MBBs exhibit many superior properties such as high compressive strength, high initial setting time, excellent volume stability, and excellent durability, the ability to harden at low temperature, low drying shrinkage, fire-proof behavior, and excellent resistance to abrasion [37 and 38]. Therefore, MBBs are strong candidate materials for 3DP application in both biomedical and construction fields [39 and 40].

1.3 MAGNESIA BASED BINDERS (MBBS)

Cement is a substance that sets and hardens which is used to bind or hold materials together through a chemical reaction. Cement is usually used to produce concrete by binding sand and gravel together. Globally, concrete is the second most consumed material after water, more than 5 billion cubic yards of concrete are produced annually [41]. Therefore, cement has become one of the essential materials for all kinds of construction. Generally, cementitious binders can be classified as hydraulic or non-hydraulic cements. The hydraulic cement hardens due to the chemical reaction between the anhydrous ingredients and water, this type of cement, once initially set, it can continue setting and developing strength under water, such as Portland cement. For the non-hydraulic cement, no water is required to complete the setting and the strength development.

Portland cement is the most common type used in concrete production, due to its high mechanical properties, excellent durability, in addition to the abundant availability of its raw materials. The two primary raw materials used in the cement industry are limestone and clay, limestone ($CaCO_3$) provides calcium (CaO), and it is decomposed at 1000 ◦C; clay provides silicates (SiO_2), and it is decomposed at 600◦ C. Usually in the manufacturing process of OPC, the raw materials are heated in a rotary kiln to very high temperatures (up to 1400 ◦C) to produce the clinker, this process requires intense energy. Producing OPC is not only energy consuming but also it is associated with high carbon dioxide emissions into the atmosphere [42]. The energy consumed to produce 1 ton of hydraulic cement exceeds 5 billion joules of electrical power and fuel energy, and it generates about 0.9 ton of carbon dioxide [43].

With the significant growing concern about global warming and environmental pollution, researchers focused more on studying cement-like materials and alternatives that are more sustainable and environmental-friendly than OPC. For instance, some of the newly developed cement-like materials include chemically bonded ceramics (CBCs) [43]. In general, CBCs are obtained from an acid-base chemical reaction, which is basically an aqueous phase formation between a metal cation and an oxyanion source (formula of $A_xO^{-z}_y$) [44]. When the magnesium oxide (MgO) is used as a metal cation, magnesia-based binders are obtained.

MgO can be formed by heating magnesite ($MgCO_3$) at a temperature to around 750 ◦C [45]. The reactivity of the magnesia depends on two main factors, the calcination temperature, and the particle size. MgO has the ability to absorb CO_2 from the atmosphere to form carbonates and hydroxycarbonates; this ability has led to an increasing interest in magnesia-based binders (MBB)s [46]. Besides, magnesium-based cement (MBC) needs much less energy for production and

releases less carbon dioxide compared to OPC. The mentioned earlier qualifications for MBCs nominate them actively to be a sustainable, and eco-friendly alternative for OPC [47 and 48].

Generally, the three most common types that belong to MBBs are magnesium oxysulfate cement (MOS), magnesium oxychloride cement (MOC), and magnesium phosphate cement (MPC).

1.3.1 MAGNESIUM OXYCHLORIDE CEMENT (MOC)

Magnesium oxychloride cement (MOC) or Sorel cement is a type of magnesia cement that is formed from the reaction between magnesium oxide (MgO) and a solution of magnesium chloride ($MgCl_2$). At the beginning of the twentieth century, the attention to MOC had increased due to its marble-like appearance, and then it was overlooked due to the availability and the low price of OPC. Recently the interest in MOC has increased due to the less associated carbon dioxide emissions during the manufacturing process.

There are many advantages to MOC compared to OPC including high early strength, high fire resistance, excellent resistance to abrasion, high compatibility with glass fibers due to its high alkalinity, and its ability to be used with a wide range of aggregate types and resources [49].

When MgO dissolves in $MgCl_2$ solution, a homogeneous gel is formed from the precipitation of $MgCl_2$ salts. This gel can produce several crystalline phases depending on the molar ratio between magnesia and magnesium chloride and to the mixing temperature. The main four reaction phases that are responsible for strength and durability of MOC system are $2Mg(OH)_2 \cdot MgCl_2 \cdot 4H_2O$ (phase 214), $3Mg(OH)_2 \cdot MgCl_2 \cdot 8H_2O$ (phase 318), $5Mg(OH)_2 \cdot MgCl_2 \cdot 8H_2O$ (phase 518), and $9Mg(OH)_2 \cdot MgCl_2 \cdot 5H_2O$ (phase 915) [50]. The most

stable one among those phases is phase 518. When phase 518 is formed in the MOC system, better microstructure and mechanical strength will be achieved [51].

There are many factors that can affect the performance of MOC systems such as the curing temperature, magnesia particle size, the molar ratio between magnesia and magnesium chloride ($Mg/MgCl_2$), and the molar ratio between water and magnesium chloride ($W/MgCl_2$). Usually, a high $Mg/MgCl_2$ molar ratio is required to achieve a high-performance MOC paste, while the remaining magnesia (the unreacted magnesia) will work as a filler. In addition to that, a high $W/MgCl_2$ is needed to improve the workability and to ensure the formation of phase 518 [52].

Finally, it is worth noting that despite the many advantages of MOC, its use in multiple applications is limited because of its very poor water resistance capacity [53].

1.3.2 MAGNESIUM OXYSULFATE (MOS) CEMENT

Magnesium oxysulfate (MOS) cement is a type of MBCs, which is produced by the chemical reaction between magnesium oxide (MgO) and magnesium sulfate solution ($MgSO_4$) [54 and 55]. After the global pollution crisis, the attention has begun with such types of cement due to the low emission of carbon dioxide during their manufacture.

MOS has many superior properties such as good fire resistance, lightweight, and good cohesiveness [56]. Furthermore, MOS cement has a good steel-protection property, because of the absence of chloride sources in its gradient [55 and 57]. Therefore, MOS has been used in many civil engineering applications including insulating slabs, refectory structures, and reinforced concrete panels [55]. On the other hand, the use of MOS cement in large-scale applications has been constrained due to its low compressive strength [57].

The mechanical properties of MOS cement is primarily dependent on the phase compositions produced during the hydration reaction. Four crystalline phases exist in the MOS cement system including; $5Mg(OH)_2.MgSO_4.3H_2O$ (5:1:3 phase), $3Mg(OH)_2 .MgSO_4.8H_2O$ (3:1:8 phase), $Mg(OH)_2 .2MgSO_4.3H_2O$ (1:2:3 phase), and $Mg(OH)_2.MgSO_4.5H_2O$ (1:1:5 phase) [58]. All of these crystalline phases are highly dependent on the molar ratio between MgO and $MgSO_4$ ($M/MgSO_4$), the molar ratio between water and $MgSO_4$ ($H_2O/MgSO_4$), and the curing temperature [59]. The reason for the low mechanical strength of MOS cement is the difficulty of obtaining stable crystalline phases at room temperature, e.g., 5.1.3 phase and 1.2.3 phase become stable only if the mixing temperature is more than 48 °C, and 100 °C, respectively [57]. One of great methods to improve the mechanical strength of MOS system is using additives. Many additives have been used over the years by researchers such as phosphoric acid, citric acid, tartaric acid, in the literature it has shown they improved the mechanical strength of MOS cement.

1.3.3 MAGNESIUM PHOSPHATE CEMENT (MPC)

Magnesium phosphate cement (MPC) is a bonding material that belongs to the chemically bonded ceramics (CBCs) [44, 60]. The chemical bonding in MPC is formed by an acid-base reaction between dead burned magnesia and phosphate [61, 62].

Compared to OPC, MPC has many outstanding properties such as rapid setting time, high early strength, very good volume stability, very good durability including chemical attacks, the ability to harden at low temperature (about -20 °C), low drying shrinkage, fire-proof behavior, excellent resistance to abrasion, and excellent bonding to old concrete structures [38, 61]. Therefore, MPC is one of the important promising cement-like materials that can be used in several applications in the field of civil engineering [60,61]. Traditionally, MPC was used as a repair

material including rehabilitation of civil structures, concrete pavement, and damaged runways. Recently, MPC has been used in several applications such as treatment of wastewater [63] and biomedical implants. More Recently, MPC is a high potential candidate for the 3D printing materials for both biomedical implants and complicated building structures [39,40].

As previously mentioned, MPC is produced by mixing dead burnet magnesia and phosphate; the phosphate compounds can be used in several forms such as phosphoric acid, ammonium dihydrogen phosphate, and potassium dihydrogen phosphate. In the last several decades, ammonium dihydrogen phosphate was used to produce MPC [61,62,64, and 65]. The main reaction product is a crystalline structure known as magnesium ammonium phosphate hexahydrate [$MgNH_4PO_4.6H_2O$] or merely the mineral struvite [43]. The main problem with ammonium phosphate is that during the reaction an unpleasant odor is released due to the ammonia gas. Therefore, a new MPC system was proposed to solve this problem, which is to use potassium dihydrogen phosphate (KDP) instead of ammonium dihydrogen phosphate. This new system is better and contains a more suitable phosphate salt for MPC. The main reaction product of the new system has also a crystalline structure known as magnesium potassium phosphate hexahydrate [$MgKPO_4.6H_2O$], or simply K-type struvite. This compound is found to be isostructural with struvite, with the replacement of ammonia ion by the potassium ion [66].

The hydration mechanism of MPC to produce the K-struvite compound can be described by the following equation:

$$MgO + KH_2PO_4 + 5H_2O \longrightarrow MgKPO_4.6H_2O \quad \ldots.(1)$$

The dissolution of MgO in an acid phosphate solution is taking place leading to increasing the solution pH which leads to the K-struvite precipitation [67]. Another formation mechanism of K-struvite crystals was proposed by Qiao [62]. K-struvite crystal formation depends on the

precipitation/dissolution reaction conditions. At first, MgO dissolves through the reaction leading to a continuous increasing pH of the solution. Then a crystalline structure known as phosphorrösslerite ($MgHPO_4 \cdot 7H_2O$) begins to form and dissolves in the solution. After that another crystalline structure ($Mg_2KH(PO_4)_2 \cdot 15H_2O$) starts to appear and dissolves in the solution to produce the K-struvite crystals. Another mechanism was proposed by Ding et al. based on hydrated MPC paste involving two major compounds: K-struvite and unreacted magnesia. The main finding in his research is that the K-Struvite is not necessary to be only in a crystalline form, it can be existing in crystalline and amorphous structures. On the other hand, the unreacted magnesia works as fine aggregates in the hardened matrix leading to better mechanical properties [68]. Fei Qiao et al. explained the mechanism of the exothermic reaction that produces the K-struvite; when water is added to the magnesia and the monopotassium phosphate, phosphates rapidly dissolve in water, leading to form an endothermic valley. Then two exothermic peaks will appear, the first one due to the dissolution of magnesia in the acid solution and the second one due to the formation of the K-struvite [69].

Many previous studies have proved that the fresh and hardened properties of MPC can be affected by the reactivity of the magnesia, magnesia to phosphate molar ratio (M/P), and water to the sold ratio (W/S) [60]. For example, Biwan Xu et al. studied the effect of M/P molar ratios on the behavior and the microstructure of MPC. They found that high M/P ratios can reduce the mechanical strength and decrease the setting reaction. Conversely, using low M/P ratios can produce a denser microstructure and can lead to better crystallization. According to their study, the optimal value of M/P ratio is 4 [60]. Li et al. investigated the influence of different M/P molar ratios ranging from 3 to 6 on the compressive strength of MPC system. They reported that M/P ratio of 4 is the optimal for the compressive strength [61]. Qiao et al. studied the effects of different

M/P ratios ranging from 6 to 12 on the setting behavior and the compressive strength of MPC pastes. The results indicated that setting time decreases by increasing of M/P ratio. Moreover, as M/P ratio increases the compressive strength increases until it reaches a maximum at a ratio of 8, then it decreases with increasing M/P ratio beyond the optimum [62].

There are some studies in the literature which have focused on the relation between M/P ratio and the microstructure of the MPC paste. The microstructure of MPC specimens was investigated by Hongyan et al. They prepared several samples by changing the M/P ratio from 4 to 12. The results showed that the lowest porosity, lowest intrinsic permeability, and the highest compressive strength were obtained when the M/P was 6 [47]. Chau et al. studied the relation between M/P ratio and the microstructure of the MPC paste, starting from phase identification, to morphology examination. According to their study, the final form of K-struvite could be obtained from the growth condition process which is a highly dependent on the M/P ratio. They reported that the mechanical strength of the MPC paste is entirely reliant on the crystallinity of the K-struvite, while the crystallinity of the K-struvite is highly dependent on the M/P ratio. The study proved that the poor crystallinity was observed with low M/P ratio, while the good crystallinity was observed at high M/P ratios. The best crystalline structure and the best mechanical strength were achieved when M/P ratio was 10 [43].

Several studies have demonstrated that the amount of water used is one of the most critical factors that can tailor the MPC properties. Yue et al. studied the influence of W/S ratio for a series of MPC specimens. They reported that the setting time has increased with increasing W/S ratio [70]. Yang and Wu showed that the using high W/S ratio could reduce the compressive strength of MPC paste [71]. Quanbing Yang et al. reported that the fluidity of MPC mortar was increasing rapidly by increasing the W/S ratio. Furthermore, they found that the lower the W/S ratio led to

higher compressive strength [72]. Xiaojie et al. investigated the effects of water content on several MPC properties including temperature evolution, viscosity, and mechanical strength. The results proved that the higher water content, the lower hydration temperature, the higher viscosity values, and the lower mechanical strength [73].

MPC binders are known for their very rapid setting, hence to increase the utilization of this cement alternative fin infrastructure construction applications, there is a pressing need to control and retard the reaction to obtain the required workability. Without the presence of a retarder in the MPC mixes, the setting time is in the range of 30 seconds to 15 minutes. One of the most popular retarders suggested for MPC mixes is borax ($Na_2B_4O_7{\cdot}10H_2O$) besides, there are other compounds which could be used including boric acid (H_3BO_3) and sodium triphosphate ($Na_5P_3O_{10}$).

Halla et al. [74] examined the influence of three different retarders on the setting behavior of the MPC, including sodium triphosphate (STP), boric acid, and borax. The results indicated that a longer setting time could be achieved by using boric acid and borax, while the influence of STP was very limited. On the other hand, Young's modulus and flexural strength decreased using all of these retarders. Moreover, Formosa et al. [75] used the boric acid to improve the setting time of MPC paste. They demonstrated that the using of boric acid as a setting retardant increased the setting time and improved the workability. Lahalle et al. [76] studied the effect of boric acid on the dissolution process of MPC compounds, the results reported that the boric acid did not affect the dissolution process of the major compounds (MgO and KH_2PO_4), but it slowed down the precipitation process of the K-struvite.

The influence of mixing borax and polycarboxylate superplasticizer (PCE) as a hybrid retarder on the rheological properties, flow and setting time, of MPC specimens was studied by Hongo et al. [77]. They reported that the adding PCE in the mixture could delay the chemical

reaction by obstructing the dissolution of MgO and MKP. However, the presence of PCE and borax together in the mix, cannot improve the workability of the system, since the presence of borax prevented the absorption of PCE by MgO particles. Nevertheless, the improvement in the setting time due to the use of borax was not enough to handle the paste for real-life applications the maximum setting time that could be achieved, by using borax compound, is 7 minutes [78].

A series of MPC specimens with different borax contents were studied by Jianming et al. [79], to investigate the influence of borax on the hydration and the rheological properties. Hydration temperature, pH value, fluidity, setting time, and compressive strength measurements were conducted using XRD and SEM. techniques. They concluded that the borax could decrease the hydration rate-or increase the setting time- by forming a thin film onto MgO surface which hinders the dissolution process of these MgO particles. This reduction in the hydration rate can decrease the water consumption by the reactants (MgO and MKP); as a result, the fluidity of the system had increased.

As shown from the literature above, MPC is still facing many unresolved challenges, many researchers are searching for compatible additives to astound these challenges and to improve the overall performance of MPC such as fly ash (FA), silica fume (SF), metakaolin, slag, acetic acid (AA), and graphene oxide (GO) [80-84].

FA was used to improve the compressive and flexural strength of MPC [80]. The reported results showed that the using FA improved the compressive strength, and on the other hand it reduced the flexural strength. Also, the influence of combining FA and SF with MPC produced denser products and improved the mechanical strength of the system and the water resistance. The hypothesis for the combined effect on the results, was (1) Physically; they could work as a filler, so they filled the micropores and improved the mechanical strength, (2) Chemically; the silicon

oxide in the SF could react with MgO particles to form MgSiO3, which improved the bonding strength of the system and enhanced its physical properties [81]. Xu et al. [82] used two different designed methods to incorporate FA in MPC mortars. At first, they used the FA as a filler to replace the solid contents (MgO and KDP), and they used it as a reactive material to replace only the MgO. Using FA as a reactive material was better and led to better fresh properties, denser microstructure and higher compressive strengths.

Other additives such as AA and GO were studied [83-84] to improve the setting time and the microstructure. AA improved the setting time and the microstructure of the system leading to better mechanical strength [83]. The experimental results reported by Lu et al. [84], indicated that GO reduced the setting time and the workability. On the other hand, adding small weight percentages of GO improved the mechanical strength, while using high weight percentages reduced the mechanical strength of the paste.

According the literature provided, there are several factors that can play a significant role in tailoring the mechanical and rheological properties of MPC. These critical factors can include M/P molar ratio, W/S molar ratio, and physical and chemical characteristics of the used retarder. Many contradictions and deficiencies have been found in the literature, starting from understanding the MPC behavior under different conditions, and ending with the influence of various retarders. At first, there is an apparent contradiction in the literature regarding the optimal M/P molar ratio. As some studies have confirmed that the optimal value for M/P ratio is ranging between 4 and 6, others have confirmed that it is more than 10. Also, there were few studies that examined the relationship between the M/P ratio and the workability.

On the other side, it is clear that the MPC system is susceptible to the water content regarding the rheological properties. In some cases, adding or dropping a small amount of water

can make a big difference in terms of initial setting time and flowability which is a great challenge that facing the use of MPC for various applications, especially for AC.

Another drawback that was found from the previous studies is the calculation of the water content ratio for the MPC mixing proportions. The published work primarily uses the mass ratio between the water and the solid content to describe the amount of uses water rather than using a molar ratio between the water and MPC main reactant (MgO or MKP). This expression may cause a misinterpretation of the real impact of water content on the fundamental understanding of the MPC behavior. The rapid setting time of MPC is found to be one of the most significant challenges that are facing its utilization in various applications. However, there are only a few studies that have focused on the impact of several retarders on the performance of MPC. According to the thorough literature we conducted, there is only one study which has discussed the effect of borax in depth. However, there is no published research on the effect of boric acid on the chemical reaction of MPC and its influence on hardened and fresh properties.

Utilizing of MPC for AC application requires specific rheological and hardened properties. The most critical properties that can affect the performance of the AC process are (1) setting time, (2) fluidity, and (3) green strength. These critical features are found to be very correlated to the mix design of MPC paste. Therefore, the used mix design must satisfy the required fresh and hardened properties.

Before adjusting the required properties for AC application, there are many aspects that need to be studied in depth to provide a better understanding of MPC behavior under different conditions. Therefore, a fully experimental program should be established in order to study the effect of different factors on the performance and microstructure of MPC. This experimental

program must satisfy the optimization of MPC paste under different conditions including physical, chemical, mechanical, and electrical characterization.

1.4 ARTIFICIAL NEURAL NETWORKS (ANNS)

Artificial neural network (ANN) is an intelligent artificial system that has been used to solve and analyze a wide variety of mathematical and statistical problems. The idea of using artificial neural networks in various fields came from neural networks in animals and human brains [85]. ANN is very useful when used to create a model for a complex system especially when the relationship between the input and output groups is indirect or incomprehensible. Moreover, the ANN techniques have the ability to describe nonlinear relations between several variables. ANN consists of four main components including (1) neurons, (2) connections, (3) propagation function, and (4) learning rule.

ANN is composed of several processing nodes called neurons. All of these neurons are connected to each other through weighted connection lines to establish an intelligent network that capable of producing the appropriate output. The function of these connection lines is transferring the outputs of several neurons to the input of the other neurons, where the input values are computed by the propagation functions. The learning rule is the used algorithm which adjusts and modifies the connection weights and threshold values during the several iterations.

Based on connection type classification, there are two types of ANNs; feedforward neural networks and feedback neural networks. In the feedforward neural network, each neuron in the same layer is receiving the input from the previous layer and providing the output for the next layer to be used as input again. In the feedforward networks, all the neurons are engaged in a set of layers including inputs layer, middle (hidden) layers, and outputs layer. There are no

connections between the neurons in the same layer. Usually, feedforward neural networks are used for approximations and predictions.

In feedback neural networks, each neuron is receiving the input from all the previous neurons and providing one output for all next neurons to be used as one of their inputs. In other words, if the total number of neurons is n, each neuron should have (n-1) inputs and one output. Usually, feedback neural networks are used as optimization tools.

ANN can be applied to accomplish many tasks in different engineering fields such as designing, forecasting, prediction, statistics, clustering, and classification [86]. In order to get an efficient ANN model, the datasets should be divided into three groups included training, testing, and validation data points [87]. At first, the relationships between each node will be generalized by using the training datasets to achieve the initial estimation for data patterns. Then the testing datasets will be processed to produce approximately correct estimation for the data patterns and to compromise the relations between each node. Finally, the model will be validated using the validation datasets to ensure that the model is effective and can predict accurate outputs.

Recently, ANN has been used widely to model many engineering experiments included concrete and construction areas. Many of these models have been prepared to predict the fresh and hardened properties of cement pastes and mortars [88]. Onal and Ozturk utilized an artificial neural network analysis to find the relationship between microstructural properties and compressive strength values of cement mortar [85]. Lee used the ANN technique to predict the mechanical strength of concrete cubes [89]. In the last few years, the using of ANN technique has gone further. Mohamed et al. utilized an ANN model to predict surface area fraction and phases correlation functions of cement material. Their model proved that ANN techniques are beneficial in predicting SEM images the related correlation functions [90]. Dias and Pooliyadda performed an ANN model

to estimate the mechanical strength and the flowability of high strength concrete blended with chemical admixtures and mineral additives [91].

MPC is very sensitive to the water and magnesia contents, and it can be affected by changing the proportions between MPC components. The hardened and fresh properties of MPC are highly dependent on the M/P ratio, W/P ratio, and boric acid content. Practically, it is very hard to obtain the mechanical and fresh properties for every mixture. Therefore, it is beneficial to perform an ANN model that can predict several MPC properties for different paste mixtures. Moreover, this model will be very efficient to use these mixes for the 3D printer. The inputs of this model will be the required compressive strength, initial setting time, and flow, where the outputs will be the MPC mix proportions including M/P ratio, W/P ratio, and boric acid content (B/M). Thus, all inputs will be adjusted based on 3D printer requirements without wasting any material.

1.5 NEED OF RESEARCH

In the last decade, additive manufacturing (AM) is becoming one of the most promising technologies for all industries. According to several studies, the implementing of AM technologies in construction field has the potential to solve many structural related problems and will reduce cost and time. The potential advantages of applying additive construction (AC) technology are; saving time, decreasing the on-site labor requirements on site, optimizing suitable materials which reduces material waste, improving the high-finishing quality, allowing an increase in the structural geometrical complexity, and reducing the overall construction cost, with the capability of eliminating the presence of traditional formworks.

Despite the fact that the construction industry contributes more than 4% of the US gross domestic product (GDP), but it is still very far from exploiting modern technology in all of its fields. Compared to other industries, construction is the most time-consuming and labor-intensive industry all over the world. Therefore, the researchers are moving toward expanding the use of technology in all aspects of this field. Recently, some new/high-level technologies have been used in order to improve the construction industry such as drone imagery, robotics, and digital project.

From the beginning of the twentieth century until the present time, concrete production has been based on the production of Portland cement (OPC). According to the U.S., Environmental Protection Agency; OPC industries are the third largest source of emitted carbon dioxide in the united states of America [92]. Moreover, some of recent studies have shown that the contribution of cement industries in the emission of carbon dioxide was about 4.8% of the world total [94]. Therefore, the global attention to the global warming, especially after the high concentration of carbon dioxide in the atmosphere, has led many researchers to find an alternative to OPC. Thus, the current trend towards finding less carbon dioxide-emitting cement industries is becoming increasingly desirable and should be accomplished in the next few decades [95].

The idea of finding an alternative to OPC is not new, in recent decades, many cement types have been listed as sustainable cement and can be used as an alternative to OPC including geopolymer cement, calcium aluminate cement, super sulfated cement, and magnesium-based cement [96].

In the last few decades, Magnesium based cements (MBCs) have received significant attention from researchers because it is considered as eco-friendly cement. Compared to OPC, MBCs production is considered to be low energy consumer and low carbon dioxide emitter. From another point of view, MgO can absorb CO_2 from the atmosphere to form hydroxycarbonate. Some

research has shown that during its operation, MBCs can absorb the amount of carbon dioxide equivalent to those emitted during its production [97].

Several studies have been established to investigate the performance of the MPC mixes. From the literature we conducted, it is clear that there is a conflict in understanding and decoding the behavior of MPC. Besides, only few studies have investigated the influence of different retarders/additives on the performance of the MPC. Therefore, it is necessary to go deeper and to understand the behavior of the MPC system under different conditions in order for it to be used it for AC application. The research we are currently conducting is serving multiple transdisciplinary top-notch material design and technological topics. It is a proof of concept of the feasibility of 3D printing ordinary Portland cement (OPC) alternatives such as MPC binders, to be utilized in terrestrial and extraterrestrial construction applications. Fresh and hardened properties for MPC pristine and modified pastes and mortars have been evaluated to meet the additive construction requirements.

In addition, artificial neural networks (ANN) has been utilized in a very emerging technological field, where the potential of connecting a customized material science research to real-world applications is becoming a necessity for real-time correction during a 3D printing process, or to predict performance-based property. Two ANN models have been optimized in this paper, in the first model the input is the MPC paste or mortar ingredients and the output is the predicted performance of interest; in the second model the input is the performance of demand and the output is the mix ingredients. For this study three-layers, feed-forward error backpropagation ANN model is developed utilizing a TR-SEQ1 model. It is expected that the simulated results we have obtained are in a very good agreement with the experimental results conducted. The statistical accuracy measurements of the model indicated that prediction of the compressive strength, flow

and initial setting time using ANNs could be achieved with good accuracy, benefiting the MPC mix design with desirable fresh and hardened properties.

1.6 OBJECTIVES

The primary objective of this research is to utilize MPC for AC applications. The fresh and hardened properties of MPC paste are optimized to meet 3DP requirements. Employing MPC in different applications is facing many challenges, there is a still a necessity of understanding, characterizing and improving the physical, chemical, mechanical, and electrical properties to meet the demands in need. MPC has a high potential to be utilized as an indigenous cement alternative for earth and planetary. The research conducted for this dissertation is expected to broaden the understating of cement alternatives and increase their in-situ utilization capacity in extreme conditions. The main objectives of this research are to an attempt to:

1. Investigating the influence of M/P and W/P ratios on mechanical, physical and thermal properties and the microstructure of the MPC binders.
2. Evaluating the effect of boric acid, acetic acid, and graphene nano platelets (GnP) on the mechanical, physical, thermal, and microstructures of MPC binders.
3. Utilizing X-Ray diffraction (XRD) and Fourier-Transform infrared (FTIR) to chemically characterize the hydrated MPC products, Compressive Strength (CS) to evaluate the mechanical properties, Initial setting time (IST) and flow table tests to evaluate the physical properties of the plastic-state and Transient Plane Source (TPS) to evaluate the thermal conductivity, of the MPC pastes and composites.
4. Decoding the correlation of the boric acid chemo-physical effect on the mechanical and thermal properties of the MPC binders.

5. Decoding the correlation of the GnP chemo-physical effect on the mechanical and thermal properties of the MPC binders.
6. Optimizing the M/P and W/P molar ratios, boric acid and GnP %content, on the MPC composite physical and mechanical properties.
7. Developing artificial neural network (ANN) models to bridge the gap between the binder fresh and hardened properties of the MPC pastes and composites.

1.7 APPROACH

Utilizing of MPC material for AC technology requires adjusting the rheological and hardened properties of MPC to meet the basic requirements of 3DP. The most critical properties that can affect the performance of the AC production are: (1) setting time, (2) fluidity, and (3) compressive strength. These critical features are found to be very correlated to the proportions between major MPC compounds, in addition to the type and content of the used additive/retarder.

In order to achieve the proposed objectives, a fully experimental program has been run in this research. This experimental program includes physical, chemical, mechanical, and thermal characterization of different MPC mixtures. Therefore, several aspects of MPC paste have been studied in depth to provide a better understanding of the MPC behavior.

In this research, three different additives/retarders are used to improve the performance of the MPC system including boric acid, graphene nanoplatelets (GNP), and acetic acid (AA).

1.7.1 MPC PASTE CHARACTERIZATION

The three raw materials that used to prepare the MPC mixtures includes dead-burnt magnesia (MgO) powder, mono-potassium phosphate powder (KDP), and distilled water (H_2O). The MPC system is described by using two parameters including (1) the molar ratio between magnesia and monopotassium phosphate (M/P), (2) the molar ratio between water and monopotassium phosphate (W/P). The main mix designs are divided into three primary groups in order to study the influence of each additive/retarder as follows:

a) Group one: to study the behavior of the MPC paste with the addition of the boric acid.
b) Group two: to study the influence of the GNP on behavior and the microstructure of the MPC paste.
c) Group three: to study the influence of the AA on the performance of the MPC paste.

The physical properties of the MPC mixtures are evaluated by using the initial setting time and fluidity. The initial setting time of the MPC pastes is measured according to ASTM C403 standard and by using the Vicat apparatus and the needle while the fluidity is measured according to ASTM standard C230 and by using the flow table test.

For the mechanical properties, each MPC mixture is placed into standard 2” cubes brass molds to follow the ASTM standards (C109) for compressive strength testing. After 24 hours, all the MPC specimens are de-molded and cured at room temperature for seven days. Then, the compressive strength of each cube is measured by using an 810 Material Testing System (MTS).

The chemical characterization of the MPC pastes is determined by using the X-ray powder diffraction (XRD) technique in order to understand the behavior of the MPC deeply and studying the effect of each MPC parameters/additives. Moreover, the chemical interactions between the

main MPC ingredients and the used additives (boric acid, GNP, and acetic acid) are investigated by the Fourier transform infrared (FTIR). Then, the thermal conductivity of the MPC pastes are determined according to ISO22007-2 specifications and by using the Transient Plane Source method (TPS). Finally, the morphology and the microstructure of the MPC pastes has been identified using the scanning electronic microscopy (SEM).

1.7.2 ANN MODELING

Recently, the artificial neural network (ANN) approach is used in several technological fields to connect the material science knowledge to real-life applications. In this work, two ANN models have been optimized to predict the behavior of the MPC paste under different conditions. For the first model, the input variables are the MPC paste ingredients, and the output variables are the MPC paste properties. For the second model, the input variables are the MPC properties while the output variables are the mix ingredients.

A simple feedforward backpropagation algorithm is applied to determine the best ANN model that can represent the data sets, where the optimum number of hidden nodes is determined by using Najjar et al. procedure [98-100]. Then, the absolute sum of square error (ASE), the main absolute relative error (MARE), and the R square have been calculated for each number of hidden nodes with 20000 iterations. Finally, all the results are collected and sorted based on the calculated ASE values from the lowest to the highest, and the model that has the least ASE is selected and validated.

1.8 DISSERTATION OUTLINE

This dissertation consists of seven chapters. Chapter one presents the introduction and the relevant literature of this work including additive construction, magnesia-based binder, and artificial neural network approach. Also, the chapter presents the need for this research in addition to the objectives and the approach. Chapter two presents the experimental work including the used material, the samples preparation, and the characterization scheme. Chapter three describes the behavior of the MPC paste with boric acid. The chapter gives more insight about the physical, mechanical, thermal, and chemical performance of the MPC paste with the addition of the boric acid. Chapter four gives a detailed description of the MPC behavior manly with the addition of graphene nanoplatelets (GNP). The chapter presents the influence of the GNP on the physical, mechanical, and chemical properties of the MPC paste in addition to the microstructure and thermal conductivity analysis. Chapter five discusses the effect of acetic acid on the physical and mechanical properties of the MPC paste. In chapter six, three-layers, feed-forward error backpropagation ANN models are developed utilizing a TR-SEQ1 model. In this chapter, three databases are used to develop the ANN models. Two ANN models have been optimized for each database, in the first model the input variables are the MPC paste ingredients, and the output variables are the predicted performance of interest; in the second model the input variables are the performance of demand, and the output variables are the mix ingredients. Finally, conclusions and recommendations are reported in chapter seven.

CHAPTER II

MATERIALS AND METHODS

2.1 INTRODUCTION

This chapter presents a brief about all the used materials in this research, in addition to the experimental procedures that used to prepare different types of magnesium phosphate cement (MPC) mixtures. Besides, the chapter gives a brief about the physical, mechanical, chemical, and thermal characterization tests that conducted for the prepared MPC specimens including all the techniques and the procedures.

2.2 MPC MATERIALS

This research aims to study the behavior of the MPC paste under different conditions, and the influence of adding multiple additive materials. The three raw materials that used to prepare the MPC mixtures includes dead-burnt magnesia (MgO) powder, mono-potassium phosphate powder (KDP), and distilled water (H_2O). Since the initial setting time of the MPC paste is very rapid (from 30 seconds and up to 4 minutes), the boric acid (H_3BO_3) is added to slow down the reaction rate and enhance the initial setting time of the pastes. Generally, two main parameters are used to describe the MPC system: (1) the molar ratio between magnesia and monopotassium phosphate (M/P), and (2) the molar ratio between water and monopotassium phosphate (W/P). In order to enhance the performance of the MPC pastes, three different additives/retarders have been

used and evaluated including (1) boric acid (H_3BO_3) as a retarder, (2) graphene nanoplatelets (GnP), and (3) acetic acid (AA). The main mix designs are divided into three primary groups.

For Group one, the MPC specimens are designed and prepared by mixing the four main ingredients including magnesia, mono-potassium phosphate, distilled water, and boric acid, which later for group two and three will be a main ingredient at a fixed percentage. The main purpose of preparing group one is to study the influence of M/P ratio, W/P ratio, and B/M ratio on the physical, chemical, mechanical, and thermal behavior of the MPC paste. For group two, the MPC specimens are prepared to study the influence of the GnP on the behavior of the MPC paste. Therefore, the MPC mixtures are designed by adding several GnP dosages to the main four ingredients that mentioned above and by using two different techniques. In the first technique, the calculated amount of GnP is added to the water and dissolved using a Cole-Parmer Ultrasonic Cleaner, while in the second technique, the polyethyleneimine is introduced as a surfactant and used with the GnP to improve its solubility in the aqueous solution. For the third group, the MPC pastes are prepared to study the impact of the acetic acid on the MPC performance. In this group, the MPC specimens are prepared by adding different rates of the acetic acid concentration to the four main ingredients of the MPC paste.

2.2.1 MAGNESIUM OXIDE (MgO)

The Magnesium oxide (MgO) or magnesia, also known as oxomagnesium, periclase, is one of the main ingredients of the MPC paste. It is odorless white solid minerals that has a molar mass of 40.3044 g/mol. The MgO is produced from magnesium-rich brine and dolomitic lime, that fired in a shaft kiln [101]. Calcining magnesium oxide at different temperatures results in different types

of magnesia. There are three main products of magnesia, that outcome of applying heat for calcining at:

a) High temperature ranges from 1500 to 2000 °C, this reduces the surface area and turns out to dead-burnet magnesia which has low reactivity.
b) Medium temperatures range from 1000 to 1500 °C, this produces hard-burned magnesia, which has limited reactivity.
c) Lower temperature ranges from 700 to1000 °C, that gives light-burned magnesia, which is reactive [102].

Since the MPC paste is known for its very rapid setting time, the MgO type that used in this research is selected to be the dead-burnt magnesia (MgO) that purchased from Martin Marietta Magnesia Specialties, LLC. Figure 1 presents the compound structure of the MgO, while the chemical compositions of the used MgO powder are shown in table 1.

Table 1. Chemical composition of the used MgO powder [103].

Magnesium Oxide (MgO)	Silicon Oxide (SiO_2)	Calcium Oxide (CaO)	Iron Oxide (Fe_2O_3)	Aluminum Oxide (Al_2O_3)
98	0.7	0.95	0.15	0.2

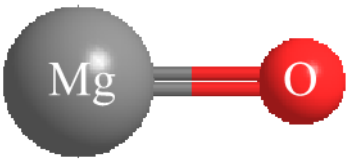

Figure 1. Magnesium oxide compound structure**.**

2.2.2 MONOPOTASSIUM PHOSPHATE (KDP)

The monopotassium phosphates are a soluble salt of potassium dihydrogen phosphate ion, that is used as a food additive, a fungicide, buffering agent and a fertilizer [104]. The monopotassium phosphates are produced by the reaction of potassium carbonate with phosphoric acid. It is also known as monobasic potassium phosphate, monopotassium dihydrogen phosphate, monopotassium monophosphate, or KDP [105].

The monopotassium phosphate is an odorless white powder that can be both, polymorphous or crystals at room temperature or powder that are slightly soluble in water and insoluble in alcohol. The molecular formula of the monopotassium phosphate is H_2KO_4P, with an average mass of 136.085 Da.

The KDP material that used in this research was purchased from Premier Construction Products Group (CPG), LLC. Waynesville, North Carolina, USA. Figure 2 shows the compound structures of the monopotassium phosphate, where the physical and chemical properties of the monopotassium phosphate are shown in table 2.

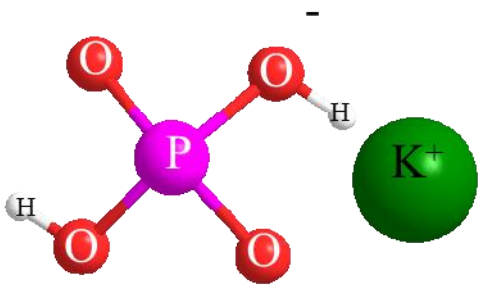

Figure 2. Monopotassium phosphate compound structure.

Table 2. Physical and chemical charactrization of the used monopotasium phosphate [106].

Appearance	White crystalline fine powder
pH range	from 4.2 to 4.8
Solubility in water	25g/100ml
Bulk density	40-50 lb/ft^3

2.2.3 BORIC ACID (H_3BO_3)

The boric acid, also known as orthoboric acid, boracic acid, borofax, and boron hydroxide, is a weakly acidic hydrate of boron with a molecular formula of H_3BO_3 or BH_3O_3 and a molecular weight of 61.831 g/mol. The boric acid is used with the MPC paste to increase its initial setting time and slow down its acid-base reaction. The content of the boric acid in the MPC mixtures is calculated based on the mass ratio between boric acid and magnesia (B/M ratio).

Boric acid plays many roles in chemical reactions due to its antiseptic and antiviral properties. Boric acid is as a flame retardant, a neutron absorber, and a precursor of other chemical compounds. In industry boric acid is mainly used in fiberglass production. It exists in a form of colorless crystals or a white powder that dissolves completely in hot water and partially in cold water. It is found naturally in volcanic districts in a mineral presence, called sassolite. Figure 3 shows the compound structure of the boric acid.

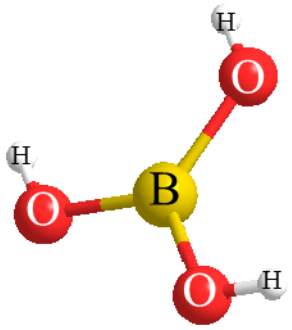

Figure 3. Boric acid compound structure.

In this work, the boric acid is purchased from Duda Energy, LLC, Decatur, AL, USA, with a purity of 99.9%. Table 3 summarizes the physical and chemical properties of the used boric acid powder.

Table 3. Physical and chemical properties of the used boric acid powder [107].

Physical/chemical property	Discerption/Measured value
Appearance	Crystalline, White Solid
pH	5.1 at 1.8 g/l at 25 °C (77 °F)
Melting point	160 °C
Initial boiling point and boiling range	1860°C
Relative density	1.440 g/cm3
Solubility	In Water: 4.7% @ 20°C; 27.5% @ 100°C
Decomposition temperature	169±1 to HBO_2 & -1 1/2 H_20 at 300°C

2.2.4 ACETIC ACID (CH_3COOH)

In this study, the acetic acid is used with the MPC components in order to improve the initial sitting time and enhance the overall performance of the MPC paste.

Acetic acid, also known as ethanoic acid, ethylic acid, and acetic acid glacial, is an organic compound with a chemical formula of CH_3COOH, also written as CH_3CO_2H or $C_2H_4O_2$, and a molecular weight of 60.052 g/mol. Acetic acid is a significant chemical reagent and a useful industrial material that involves in fabricating many artificial fibers and other polymeric materials. The acetic acid compound structure is presented in figure 4

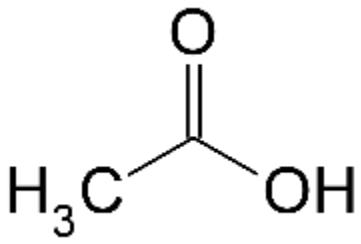

Figure 4. Acetic acid compound structure [108].

2.2.5 GRAPHENE NANOPLATELET (GnP)

Graphene is a crystalline allotrope of carbon with 2-dimensional properties. It is a source of carbon consisting of a single layer of carbon atoms, each carbon atom is linked to another three carbon atoms on a two-dimensional plane that generates hexagonal lattice. The atomic structure of graphene is presented in figure 5.

Graphene is one of the most promising additive material to be embedded with the composite materials in the construction field. Recently, many forms of graphene structures/compounds have been used to improve the material properties such as graphene oxide

(GO) and graphene nanoplatelets (GnP). GnP represents a new form of carbon nanoparticles with multifunctional properties and it consists of small stacks of graphene. It can be used to improve the properties of a wide range of materials due to its exclusive nanoscale size, shape, and material composition. Nowadays, the GnP is highly implemented as a nanoscale additive for cementitious materials to improve its mechanical properties. Besides, the GnP has the potential to enhance other properties such as electrical and thermal conductivity. Figure 6 shows the atomic structure of the GnP.

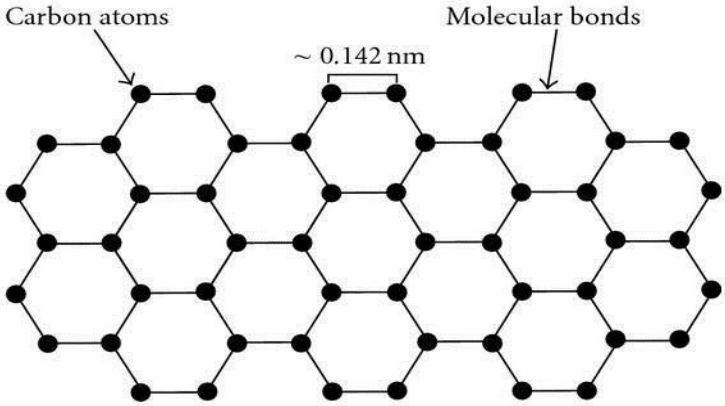

Figure 5. Graphene atomic structure [109].

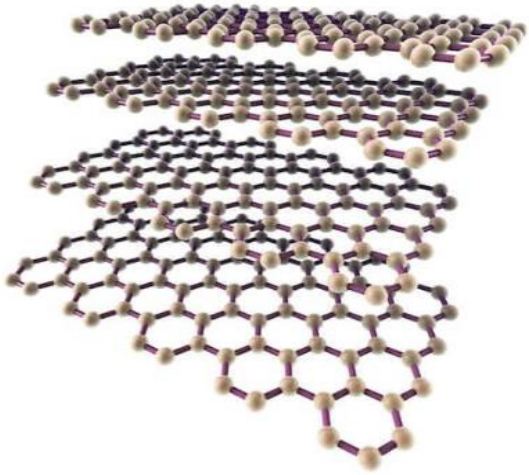

Figure 6. GnP atomic structure [110].

In this research, different dosages of the GnP are used with the MPC paste to improve its properties. The GnP that used in this research has been purchased from XG Sciences, Inc. Lansing, MI 48911 - USA. It is consisting of short stacks of graphene sheets having a platelet shape with a density of 2.2 g/c3, average thickness of approximately 6 to 8 nanometers, typical surface area of 120 -150 m2 /g, and average particle diameters of 50 microns [111]. The thermal, mechanical, and electrical properties of the used GnP are summarized in table 4.

Table 4. Thermal, mechanical, and electrical properties of the used GnP [111].

	Parallel to surface	Perpendicular to surface
Thermal conductivity (W/m.K)	3000	6
Thermal Expansion (m/m/K)	4-6 x 10-6	0.5-1 x 10-6
Tensile modulus (MPa)	1000	NA
Tensile strength (MPa)	5	NA
Electrical conductivity (S/m)	107	102

2.2.6 POLYETHYLENEIMINE (PEL)

In this research, the Polyethyleneimine material is used as a surfactant to enhance the solubility of the graphene and improve the dispersion of the GnP in the GnP mixtures. The Polyethyleneimine material (C_2H_5N) with a molecular weight of 43.069 (g/mol) is provided by Acros Organics, Fisher Scientific, USA.

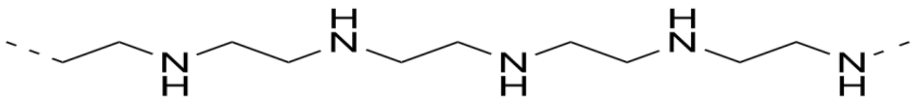

Figure 7. PLE atomic structure [112].

2.3 MIX DESIGN AND SAMPLES PREPARATION

2.3.1 GROUP ONE (BORIC ACID)

As previously mentioned, the behavior of the MPC paste specimens can be driven by three main factors including magnesia to phosphate molar ratio (M/P), water to solid mass ratio (W/S) and boric acid to magnesia mass ratio (B/M). In this paper, the author chose to represent the MPC pastes ingredients in molar ratios rather than the mass ratios terminology to capture the impact of the different MPC mix proportions on the acid-base reaction, in addition to the influence of these factors on physical, mechanical, and thermal properties of the MPC system with the addition of boric acid as a retarder.

The MPC pastes are prepared using the following procedures: (1) the dry powders are weighted and mixed for 2 minutes, (2) the boric acid is dissolved in the distilled water using a Fisher Scientific Thermix Stirrer Model 120s with a speed of 300 RPM for 15 minutes, and finally, (3) the water is added to the mixture, and further mixing is provided for more 2 minutes. Figure 8 presents the mixing procedures of the prepared MPC specimens in this group. The mix proportions of the prepared MPC specimens will be discussed later in chapter III. For each specimen, the MPC mixture is divided into four different parts as follows:

a) The first part is used for the flow table test.
b) The second part is used for the initial setting time test.
c) The third part is placed into standard 2” cubes brass molds to follow the ASTM standards (C109) for compressive strength testing (figure 9). After 24 hours, all the MPC specimens are de-molded and cured at room temperature for seven days.

d) The fourth part is placed into plastic molds and cured for 7 days for the XRD and the FTIR test.

(a) Mixing of the dry powder for 2 minutes.

(b) Dissolving the boric acid by the thermix stirrer with a speed of 300 RPM for 15 minutes

(c) Mixing of the MPC ingredients after the water addition for 2 minutes.

Figure 8. Mixing procedures of the prepared MPC paste for group one.

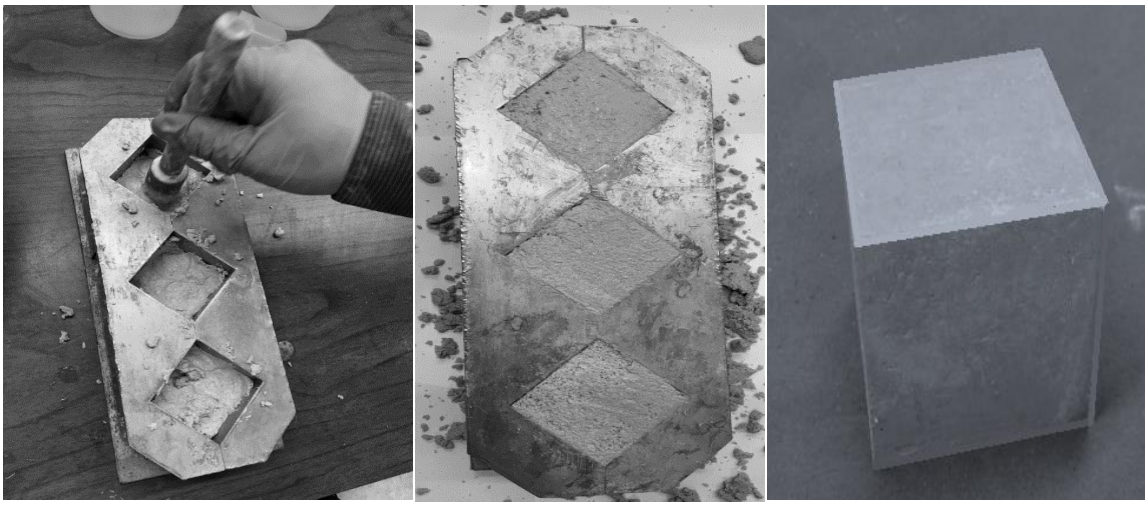

Figure 9. Casting procedures of the prepared MPC cubes.

2.3.2 GROUP TWO (GnP)

In this group, the MPC specimens are designed to study the influence of the GnP. The MPC specimens are prepared by mixing MgO, KDP, boric acid, GnP, polyethyleneimine, and the distilled water. The magnesia to phosphate molar ratio (M/P) has been selected to be 6 while the desired water content is calculated based on the molar ratio between KDP and water (W/P) and

has been selected to be 3.6. This W/P ratio can provide mid-range workability for the paste, and it can guarantee that the available water is enough for the acid-base reaction. Also, the B/M ratio of 5% has been used for all the MPC specimens in this chapter in order to increase the initial setting time.

For the control specimens, without using the GnP or the surfactant, the pastes are prepared using the same procedures that mentioned in the previous section. For the GnP modified MPC specimens, two different techniques are used to add the GnP to the mixture. At first, the desired GNP dosage is calculated based on the weight ratio between GnP and the total solid (MgO + KDP). Then, (2) the calculated amount of GnP is added to the water and dissolved using Cole-Parmer Ultrasonic Cleaner Model 08895-04. The ultrasonic parameters are fixed for all specimens with a power output of 200W and frequency of 20 kHz for 30 minutes. Finally, (3) the water is added to the dry powders, and further mixing is provided for 2 minutes. The sample preparations of the GnP modified MPC are presenting in figure 10.

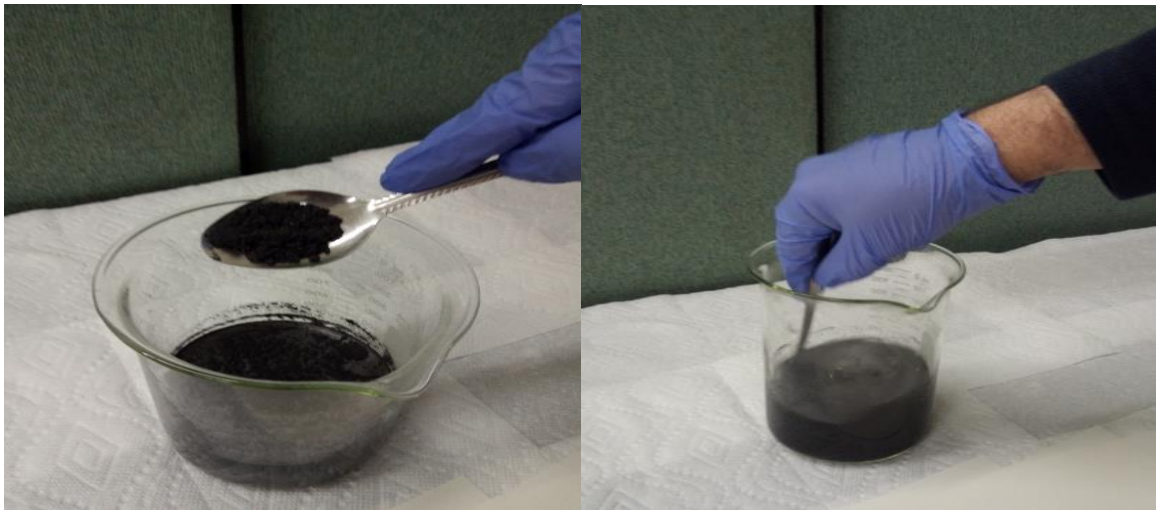

Figure 10. Mixing procedures for GnP modified MPC paste.

Another series of the MPC specimens are prepared using the GnP with the PLE as a surfactant to improve the dispersion of the GnP. The optimum amount of the PLE is found to be 10% by the weight of GnP. For these specimens, the required amount of the surfactant and the GnP are added to the water and mixed mechanically for 2 minutes, and then, they are dissolved using the same ultrasonic procedures that mentioned above. Finally, another series of the MPC specimens are prepared by adding only the PLE in order to study the influence of the surfactant. This series is prepared by following the same procedure that mentioned above. The mix proportions of the GnP modified MPC specimens will be discussed later in chapter IV.

2.3.3 GROUP THREE (ACETIC ACID)

This group is prepared in order to study the influence of the acetic acids on the performance of the MPC paste. Also, preparing this group aims to study the influence of a hybrid retardation system of boric and acetic acids on several MPC properties.

In this group; the MPC specimens are prepared by mixing MgO, KDP, boric acid, acetic acid, and distilled water. Based on the study mentioned in chapter three from this research, the optimum B/M ratio is found to be 5%. Therefore, the B/M ratio of 5% has been used for the hybrid system in order to improve the initial setting time of the system. The amount of acetic acid is calculated based on the concentration of acetic acid in the aqueous solution (AAC).

The MPC specimens are prepared using the following procedures: (1) the dry powders are weighted and mixed for 2 minutes, (2) the boric acid and the acetic acid are dissolved in the distilled water using a Fisher scientific thermix stirrer model 120s with a speed of 300 RPM for 20 minutes, and finally, (3) the water is added to the mixture and further mixing is provided for more 2 minutes. The mix proportions of the MPC specimens with different acetic acid concentrations will be discussed later in chapter V.

2.4 CHARACTERIZATION SCHEME

2.4.1 PHYSICAL CHARACTERIZATION

2.4.1.1 INITIAL SETTING TIME

In this research, the setting time of MPC paste is measured according to the ASTM C403 standard by using the Vicat apparatus with a movable rod that weighs 300 g, and a 1mm-diameter needle. The Vicat needle apparatus is shown in figure 11.

Based on the Vicat needle test, the setting time is defined as the number of minutes elapsed from the start of mixing to the time that the material completely loses its plasticity which that the needle failed to penetrate more than 1 mm into MPC paste. For the MPC paste, the initial setting time is recorded every 30 seconds, due to the rapid plasticity loss. The test is performed at the

room temperature (25 ± 2 C0), while the initial setting time test is conducted by using the following procedures:

a) The MPC paste is prepared as described in the sample preparation section, mix design is calculated to achieve an adequate amount for the volume of the ring of the apparatus.
b) The timing started at the instant when all the material is mixed together.
c) When the ring mold is filled, the paste surface was leveled with the top of the mold. and shacked slightly to drive out the air bubbles.
d) The needle was released and allowed to penetrate the paste surface.
e) This procedure was repeated every 30 seconds, due to the rapid rate of the setting time.
f) When a penetration of 25 mm or less is obtained, the time is recorded as the initial time.

Figure 11. The Vicat needle apparatus.

2.4.1.2 FLOW TEST

Flow test is a method to measure the consistency and workability of fresh cement paste or concrete. The workability is the ease of handling and processing the concrete paste without any segregation. The flow of the materials is measured according to ASTM standard C230 and by using the flow table test. Figure 12 shows the flow table. The flow test has been conducted as follows:

a) The material blend was prepared for each sample as presented before in the sample preparation section.
b) A 25 mm layer thickness of blend which is the half height of the ring mold, was poured and tamped 20 times using a mortar tamping rod.
c) Then the second layer was added and tamped using the same procedure for the first layer.
d) The excess paste was cut off to level it with the mold top surface using a mini straight edge trowel.
e) After that, the mold was lifted away from the paste.
f) The directly started to run rotationally the flow table hand for 25 times in 15s.
g) At this point, the final diameter will be measured which is the same as the diameter of the paste flow circle, in some cases the samples were overflow that means that the paste fell outward the plate during the rotation
h) Finally, the flow for each MPC specimen was calculated using the following equation:

$$Flow = \frac{final\ Diameter - Initial\ Diameter}{Initial\ Diameter} \times 100 = \frac{D_f - 101.6mm}{101.6mm} \times 10 \quad \dots 2.1$$

Where; the initial diameter equals to the diameter of the flow table ring, which is 101.6mm, and the final diameter presents the speeded material after 25 drops of the flow table arm.

Figure 12. The flow table.

2.4.2 MECHANICAL CHARACTERIZATION

The compressive strength for the casted MPC cubes is measured according to ASTM standard C109 and by using an 810 Material Testing System (MTS). Three different 2" cubes are prepared and tested for each MPC mixture. All the MPC specimens in this research are tested after 7-days air curing with a loading rate of 0.001 in/sec. Figure 13 shows an MPC paste under the compression test.

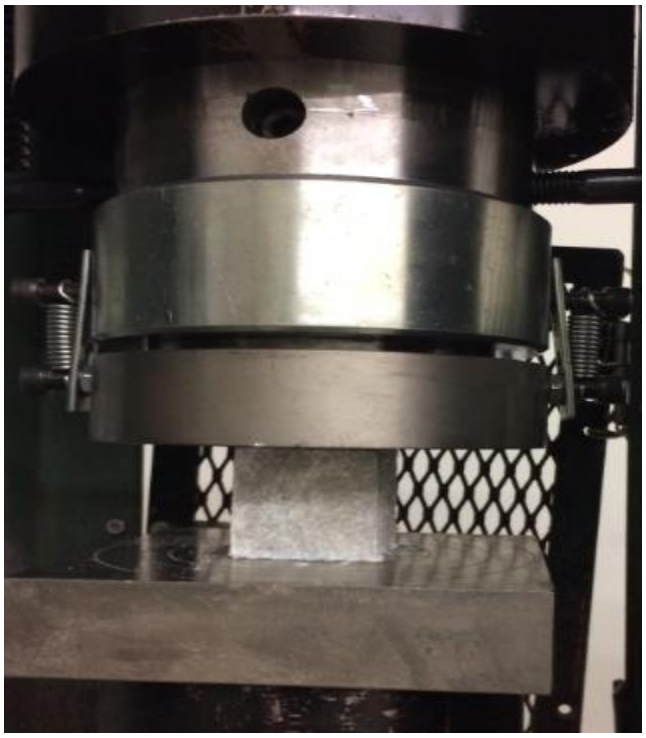

Figure 13. Compression test of an MPC specimen.

2.4.3 X-RAY POWDER DIFFRACTION (XRD)

The phase characterization of the MPC pastes is determined using X-ray powder diffraction (XRD) technique, using Bruker's X-ray Diffraction and Scattering with a scanning rate of 0.2 sec per step, while the 2θ range is from 10 to 70. Figure 14 shows the Bruker's X-ray diffractometer.

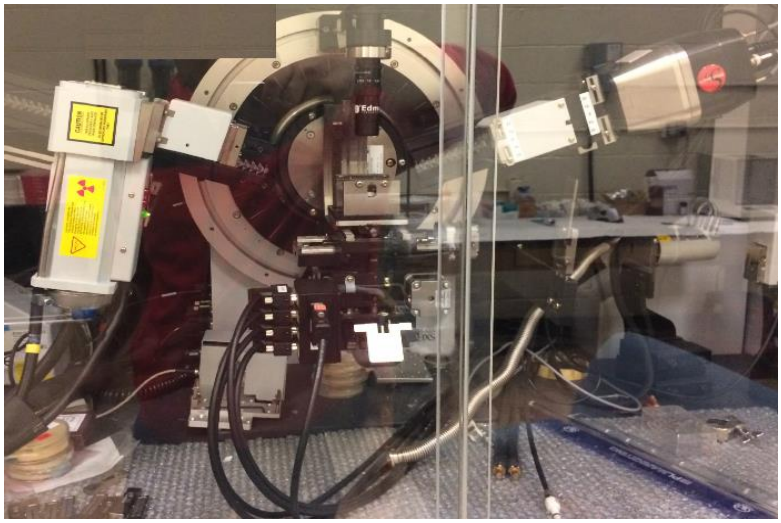

Figure 14. Bruker's X-ray diffractometer.

2.4.4 FOURIER-TRANSFORM INFRARED SPECTROSCOPY (FTIR)

The chemical interactions between the main MPC ingredients and the used additives (boric acid, GnP, and acetic acid) were investigated by the Fourier transform infrared (FTIR) technique. The tested material powders were prepared to be finely ground and homogenized. Then, the FTIR test was conducted using a Cary 630 FTIR machine provided by Agilent Technologies. The wave-number was ranged from 4000 cm-1 to 500 cm-1. Figure 15 shows Cary 630 FTIR machine.

Figure 15. Cary 630 FTIR machine.

2.4.5 SCANNING ELECTRONIC MICROSCOPY (SEM)

The microstructure of the MPC specimens are investigated using the scanning electronic microscopy technique (SEM). A 7-days cured MPC specimens are prepared for the SEM without any polishing or gold coating techniques. The SEM technique is conducted using a Schottky FE-SEM SU5000 that provided by HITACHI with a low kV (from 1 to 5) to avoid charging.

2.4.6 THERMAL CHARACTERIZATION

The thermal conductivity for the MPC specimens is determined using the Transient Plane Source method (TPS), where the thermal conductivity test is conducted according to ISO22007-2 specifications and by using a HotDisk TPS-1500 thermal constant analyzer. The applicable thermal conductivity testing range is 0.01-400 W/m.K. MPC pastes 2" cubes are prepared for the thermal testing, which requires two identical specimens while a hot disk sensor is placed in between them. This thermocouple sensor can work as a heating element and also measures the temperature change. Prior to the thermal conductivity test, all the tested MPC pastes are cured for 7 days and dried in a convection oven for 24 hours to assure dryness, followed by room temperature cooling.

CHAPTER III

OPTIMIZING MAGNESIUM PHOSPHATE CEMENT WITH BORIC ACID: PHYSICAL, MECHANICAL, THERMAL, AND CHEMICAL CHARACTERIZATION

3.1. INTRODUCTION AND LITERATURE REVIEW

As previously mentioned, magnesium phosphate cements (MPCs) are bonding materials that belong to chemically bonded ceramics (CBCs) [44], that is formed by an acid-base reaction between dead burned magnesia and phosphate. The forms of phosphate compounds are: phosphoric acid, ammonium dihydrogen phosphate, and potassium dihydrogen phosphate. In the last several decades, ammonium dihydrogen phosphate is used to produce MPCs [61,62,64 and 65]. The MPC main reaction crystalline product is magnesium ammonium phosphate hexahydrate [$MgNH_4PO_4.6H_2O$]. Also, it is known as the mineral struvite [43]. The main problem associated with ammonium phosphate reaction is the unpleasant odor released due to the ammonia gas. Therefore, a new phosphate compound is proposed to solve this problem, which is the potassium dihydrogen phosphate (KDP) to substitute the ammonium dihydrogen phosphate. This new binder is better in terms of mechanical strength and contains a more suitable phosphate salt for the MPC. The main reaction product of the new system has also a crystalline structure known as magnesium potassium phosphate hexahydrate [$MgKPO_4.6H_2O$], or simply K-type struvite.

The hydration mechanism of MPC to produce the K-struvite compound can be described by the following equation:

$$MgO + KH_2PO_4 + 5H_2O \longrightarrow MgKPO_4.6H_2O \ldots.(1)$$

Some previous studies reported that the K-struvite crystal formation depends on the precipitation/dissolution reaction conditions [62]. Moreover, K-struvite is not necessary to present in a crystalline form; it can exist in amorphous structures as well [68].

Many previous studies have proved that the physical and mechanical properties of the MPC can be affected by magnesia to phosphate molar ratio (M/P), water to the sold ratio (W/S), and physical and chemical characteristics of the used retarder. Biwan Xu et al. [60] found that the high M/P ratios can reduce the mechanical strength and decrease the setting reaction. Conversely, using low M/P ratios can produce denser microstructures and can lead to better crystallization, with an optimal M/P ratio of 4. Also, Li et al. [61] reported that an M/P ratio of 4 is optimal for the compressive strength. Qiao et al. [62] confirmed that the compressive strength increases as the M/P ratio increases with an optimum value of an M/P ratio of 8. Hongyan et al. [47] found that the lowest porosity, lowest intrinsic permeability, and highest compressive strength are obtained at an M/P ratio of 6. Chau et al. [43] suggested that the final form of the K-struvite could be obtained from the growth condition process which is highly dependent on the M/P ratio. The best crystalline structure and the best mechanical strength are achieved when the M/P ratio is 10.

Several researches have studied the amount of effect of W/S on the MPC properties [70-72]. The researchers have reported that while increasing the W/S ratio on the setting time and the fluidity of the MPC mortars increased as well, in which it negatively affected the compressive strength.

MPC binders are known for their very rapid setting which ranges from 30 seconds to 15 minutes, without the addition of any retarder. Hence, in order to increase the utilization of this cement alternative in construction applications, there is a pressing need to control improve its setting time workability. One of the most popular retarders suggested in the literature [75, 76, 78, and 79] for MPC mixes is borax ($Na_2B_4O_7 \cdot 10H_2O$) besides, there are other compounds which could be used including boric acid (H_3BO_3) and sodium triphosphate ($Na_5P_3O_{10}$). Formosa et al. [44] demonstrated that using boric acid as a chemical retardant increased the setting time and improved the workability. Lahalle et al. [76] reported that the boric acid did not affect the dissolution process of the major compounds (MgO and KH_2PO_4), but it rather decelerated the K-struvite precipitation process. Li et al. [78] found the setting time increment due to the use of borax is not enough to handle the paste for real-life applications, the maximum setting time achieved by adding 5% borax is 7 minutes. On the other hand, Jianming et al. [79] concluded that the addition of borax decreases the hydration rate by forming a thin film onto the MgO surface which hinders the dissolution process of these MgO particles. This reduction in the hydration rate can decrease water consumption by the reactants (MgO and MKP); as a result, the fluidity of the system is increased.

According to the literature provided, at first, there is an apparent contradiction in the published research regarding the optimal M/P molar ratio for strength formation. As some studies have confirmed that the optimal value for M/P ratio is ranging between 4 and 6, others have confirmed that it is more than 10. Another drawback that is found from the previous studies is the optimum water content to solid ratio for the MPC mixing proportions. The available literature primarily treated the acid-base cements, such as MPC, as the OPC, in terms of expressing the optimum water content in mass ratio form, rather than using a molar ratio between the water and

MPC main reactant (MgO or MKP), which potentially reduced the sensitivity of the acid-base cement to the mixing water amount and generated a possible misinterpretation of the real impact of water content on the fundamental understanding of the MPC behavior. Moreover, there are only a few studies that have examined the behavior of the MPC cement over a wide range of M/P, W/P, and B/M molar ratios to achieve a full understanding of the MPC paste performance under different parameters/conditions. Finally, there are only a few studies that have focused on the impact of the addition of boric acid on the mechanical behavior of the MPC paste. Moreover, as far the authors are aware to this moment, the effect of the boric acid on thermal properties has not been reported.

This chapter aims to give more insight about the physical, mechanical, thermal, and chemical performance of the MPC paste mainly with the addition of the boric acid for retardation behavior. Therefore, a comprehensive experimental program has been established in order to evaluate the effect of the different factors on the performance and microstructure of the MPC pastes. In the work presented in this paper, due to the sensitivity of the acid-base MPC formation reaction, W/P molar ratio has been used instead of W/S mass ratio to enable a better understanding of the mechanical and physical behavior of this material.

3.2 MIX PROPORTIONS

As previously mentioned, the behavior of the MPC paste specimens can be driven by three main factors including magnesia to phosphate molar ratio (M/P), water to solid mass ratio (W/S) and boric acid to magnesia mass ratio (B/M). In this chapter, the authors chose to represent the MPC pastes ingredients in molar ratios rather than the mass ratios terminology to capture the impact of the different MPC mix proportions (M/P, W/P, and B/M ratios) on the acid-base reaction, in addition to the influence of these factors on physical, mechanical, and thermal properties of the MPC system with the addition of boric acid as a retarder.

In this research, the MPC specimens are named by character numbers. The first number indicates the M/P ratio; the second two numbers refer to the W/P ratio, and the third two numbers indicate the B/M ratio. For example, B32250 sample indicates a specimen with M/P of 3, W/P of 2.2 and B/M of 5%.

A total of 39 MPC specimens are designed and prepared to study the behavior of the MPC paste under different conditions divided into eleven different groups. The first seven groups including (B2-20, B3-18, B3-22, B3-30, B6-30, B6-36, and B6-45) are designed and prepared to study the influence of the boric acid on the MPC pastes. For each group, M/P and W/P molar ratios are kept constant, while the B/M ratio is changed for each specimen. The last 4 groups, including W-4, W-8, W-10, and W-12, are prepared to complete the first seven groups to evaluate the influence of M/P and W/P molar ratio on the optimized pastes. For each one of these four groups, M/P and B/M ratios are kept constant, while the W/P molar ratio is changed for each specimen. Table 5 summarizes the mix proportions of the prepared MPC specimens.

Table 5. Mix proportions of the prepared MPC specimens.

Group	Sample ID	M/P molar ratio	W/P molar ratio	B/M mass ratio (%)
B2-20	B22000	2	2.0	0
	B22050	2	2.0	5
	B220100	2	2.0	10
B3-18	B31800	3	1.8	0
	B31825	3	1.8	2.5
	B31850	3	1.8	5

	B318100	3	1.8	10
B3-22	B32200	3	2.2	0
	B32225	3	2.2	2.5
	B32250	3	2.2	5
	B322100	3	2.2	10
B3-30	B33000	3	3.0	0
	B33050	3	3.0	5
	B330100	3	3.0	10
B6-30	B63000	6	3.0	0
	B63050	6	3.0	5
	B630100	6	3.0	10
B6-36	B63600	6	3.6	0
	B63625	6	3.6	2.5
	B63650	6	3.6	5
	B636100	6	3.6	10
B6-45	B64500	6	4.5	0
	B64525	6	4.5	2.5
	B64550	6	4.5	5
	B645100	6	4.5	10
W-4	B41850	4	1.8	5
	B42050	4	2.0	5
	B42450	4	2.4	5

	B43050	4	3.0	5
	B43450	4	3.4	5
W-8	B83050	8	3.0	5
	B83850	8	3.8	5
	B84650	8	4.6	5
	B86050	8	6.0	5
	B87250	8	7.2	5
W-10	B103850	10	3.8	5
	B104650	10	4.6	5
	B105250	10	5.2	5
W-12	B124650	12	4.6	0.05

3.3 PHYSICAL PROPERTIES OF THE MPC PASTE

3.3.1 INFLUENCE OF BORIC ACID

Figure 16 shows the effect of the boric acid content on the initial setting time for the MPC pastes at different W/P and M/P molar ratios. At constant M/P and W/P ratios, as B/M ratio increases the initial setting time increases until it reaches the maximum of 5% ratio, then it decreases again upon increasing the B/M ratio. The same results are obtained for all M/P molar ratios. For example, for B3-22 group (M/P and W/P molar ratios of 3 and 2.2 respectively), adding 5% of boric acid can increase the initial setting time from 3.5 to 15 minutes. Meanwhile, adding 10 % to the same mix can increase the initial setting time to 9 minutes only. One possible explanation for this retardation mechanism is the ability of the boric acid to form a temporary layer of lunebergite ($Mg_3B_2(PO_4)2(OH)*6H_2O$) which coats the surface of the Mg^{+2} ions and hinder the

dissolution of the magnesium cations. This temporary layer can be destroyed when the amount of the magnesium cations is increasing in the solution leading to continuous dissolution of Mg^{+2} particles again and forming the K-struvite. This temporary layer will be dissolved again in the solution and cannot be found in the reaction products of the system [44-113]. Another possible justification of this retardation that the lunebergite layer is hindering the precipitation process of the final products (K-struvite) rather than the reactant particles (Mg^{+2}) [76].

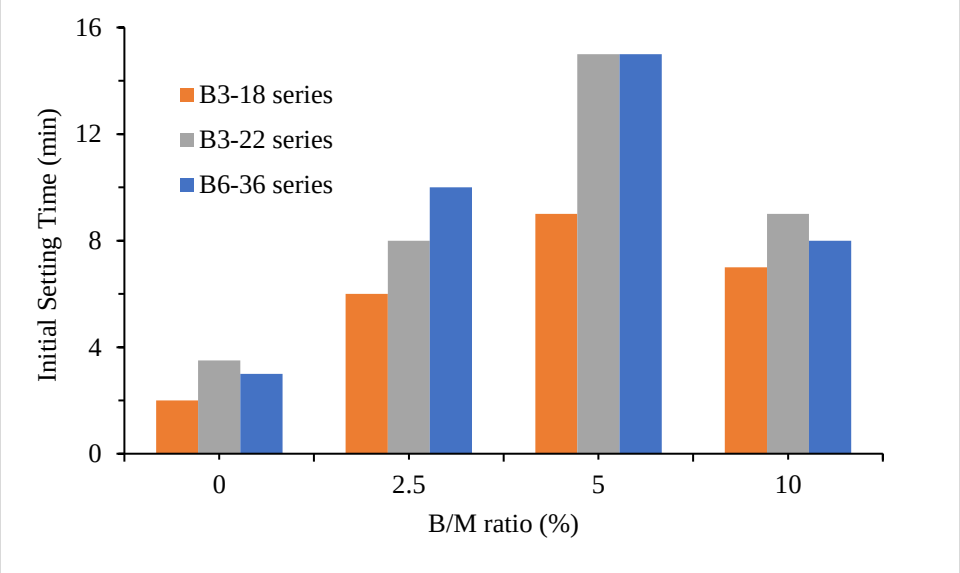

Figure 16. Influence of B/M ratio on the initial setting time of the MPC paste for different W/P and M/P molar ratios.

On the other hand, there is an adverse effect on the initial setting time when the B/M ratio exceeds the 5%, due to the effect of the boric acid on the workability of the system. Table 6 provides the measured flow results of the MPC paste with different B/M ratios. The experimental results demonstrate that using boric acid leads in flowability reduction of the MPC pastes. For example, when the M/P and W/P ratios are 3 and 1.8 respectively, adding 5% of boric acid can reduce the fluidity by 48%. Moreover, using the boric acid can increase the fluidity loss rate over

time. Although the loss of the fluidity over time is not measured, but it was observed during the experiments that the higher the B/M ratio used, the greater the loss of fluidity achieved. This observation can explain why the retardation effect of the B/M ratio of 5% is better than the B/M ratio of 10%. In order to give more insight about the relation between the boric acid content and the fluidity loss of the paste, additional two groups of MPC pastes are prepared (B2-2 and B6-45). These two groups are prepared with a very high-water content to grantee the MPC fluidity will remain very high until the initiation of the sample setting. Figure 17 illustrates the effect of the boric acid content on the initial setting time of overflow MPC pastes. It can be observed that the initial setting time increases when the B/M ratio increases. For instance, using of 2.5 %, 5%, and 10% of boric acid in the case of B6-45 series, can increase the initial setting time by 150%, 350%, and 400% respectively. The reason for the fluidity loss is the negative effect of the boric acid on the dispersion of the Mg^{+2} inside the solution.

Table 6. The flow measurements of the MPC pastes.

Group	Sample ID	Flow (%)
B2-20	N22000	Overflow
	B22050	Overflow
	B220100	Overflow
B3-18	N31800	132
	B31825	70
	B31850	68
	B318100	60

B3-22	N32200	Overflow
	B32225	147
	B32250	116
	B322100	105
B3-30	N33000	Over
	B33050	Over
	B330100	Over
B6-30	N63000	Over
	B63050	82
	B630100	82
B6-36	N63600	Overflow
	B63625	145
	B63650	111
	B636100	111
B6-45	N64500	Overflow
	B64525	Overflow
	B64550	Overflow
	B645100	Overflow

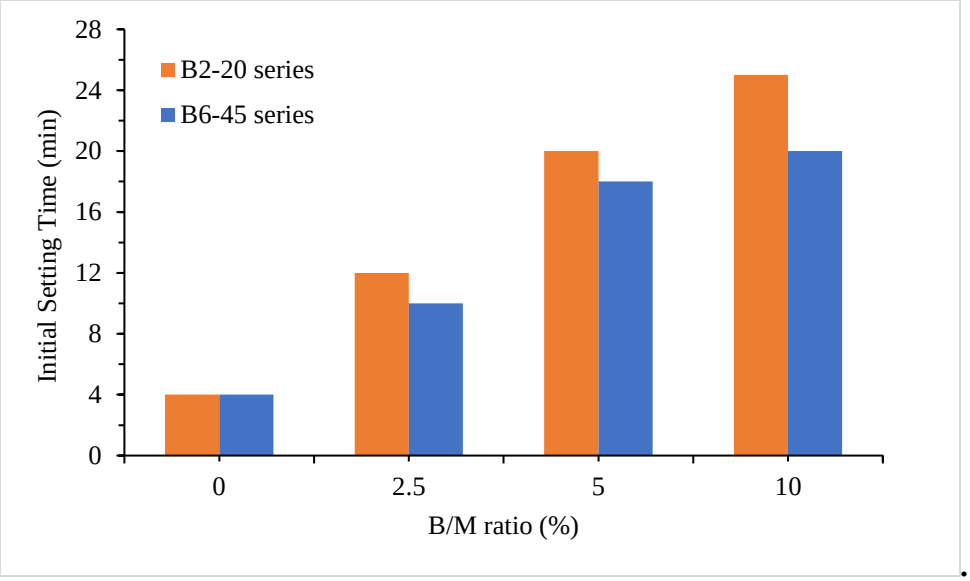

Figure 17. Influence of B/M ratio on the initial setting time of overflow MPC paste.

3.3.2 INFLUENCE OF WATER CONTENT (W/P RATIO)

Compared to ordinary Portland cement (OPC), the initial setting time of the MPC paste is quite shorter. Therefore, the influence of the water content has been studied with the presence of boric acid. The experimental results indicate that the water content is playing a significant role in determining the physical properties of the system. Figures 18 and 19 illustrate the effect of W/P molar ratio on the initial setting time and fluidity respectively. As expected, the initial setting time increases when the W/P molar ratio increases. For example, for M/P ratio of 8, increasing the W/P ratio from 3 to 6 can increase the initial setting time from 5 to 20 minutes. Meanwhile, the flow test indicates that the MPC system is very susceptible to water content. In some cases, adding or dropping a small amount of water can make a big difference in term of fluidity. For example, at M/P molar ratio of 3, changing the W/P molar ratio from 1.8 to 2.2 can

increase the fluidity by more than 70%. These results can indicate that the interparticle lubrication is increased by increasing the water content.

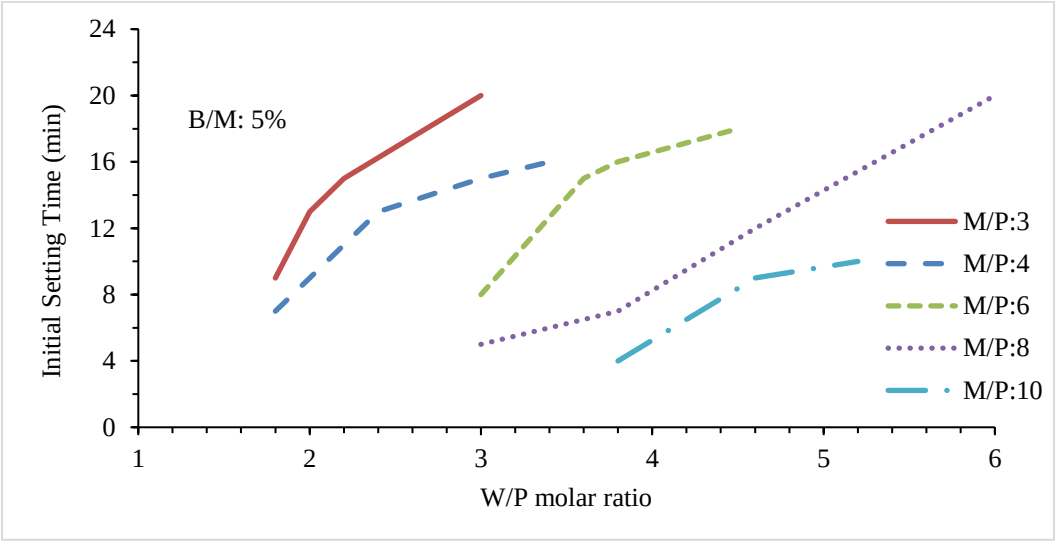

Figure 18. Effect of different W/P molar ratio on the initial setting time of MPC for different M/P molar ratio.

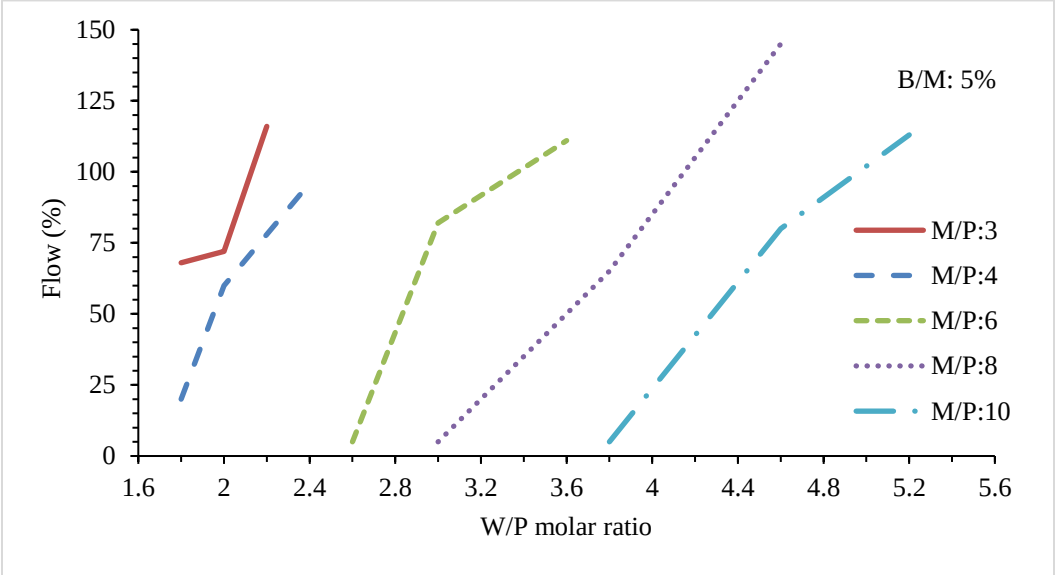

Figure 19. Effect of different W/P molar ratio on the fluidity of MPC for different M/P molar ratio.

3.4 MECHANICAL PROPERTIES OF MPC

3.4.1 INFLUENCE OF BORIC ACID

Boric acid is found to be one of the most critical factors that can affect the compressive strength of the MPC paste. Figure 20 illustrates the influence of the boric acid content on the compressive strength of the MPC paste for different M/P molar ratio. The results indicate that there are two different behaviors of the MPC specimens that contain boric acid. For the MPC specimens that have low M/P ratios (figure 20. a), the compressive strength decreases when the B/M ratio increases. For example, at B3-18 series (M/P of 3 and W/P of 1.8), adding 2.5% 5% and 10% of boric acid leads to reduce the compressive strength by 27%, 47%, and 64% respectively. By adding more water to the MPC mixture, the effect of the boric acid on the compressive strength is becoming slightly lower. For B3-22 series, adding 2.5% 5% and 10% of boric acid leads to reduce the compressive strength by 21%, 34% and 45% respectively. Hence, another MPC series (B3-30) is prepared to investigate whether the presence of the boric acid has the same influence if it used with a very high-water content. The results of this series can demonstrate that the presence of the boric acid is showing the same influence. For B3-30 series (M/P of 3 and W/P of 3), adding 5% and 10% of boric acid can reduce the compressive strength by 35%, 47% respectively.

On the other side, for the MPC specimens that have high M/P ratios (figure 20. b), the experimental results show that the effect of the boric acid is insignificant. When the B/M ratio increases, the compressive strength slightly increases, then it slightly decreases when the B/M ratio is more than the 5%. For B6-36 series, (M/P of 3 and W/P of 3.6), adding 5% of boric acid can improve the compressive strength by 6%. Meanwhile, adding 10% of boric acid to the same mixture can reduce the compressive strength by 4%. Furthermore, the same result is obtained when the boric acid is used with high W/P molar ratios.

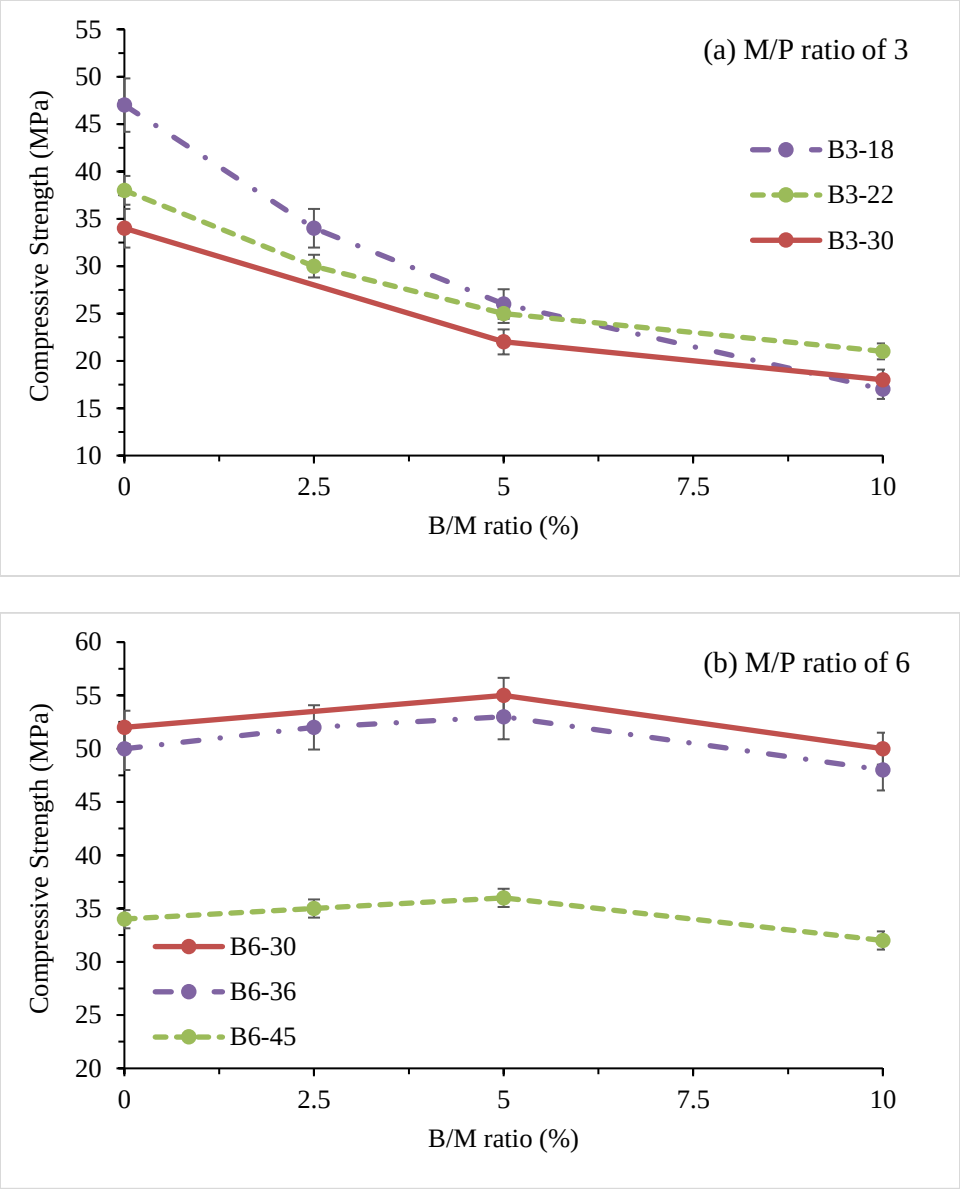

Figure 20. Influence of B/M ratio on the compressive strength of the MPC a) M/P ratio of 3, and b) M/P ratio of 6.

3.4.2 INFLUENCE OF M/P RATIO

The M/P molar ratio has a great influence on the microstructure, the mechanical strength, and the fresh properties of the MPC paste. As previously mentioned, there is an apparent contradiction in the literature regarding the optimal M/P molar ratio. As some studies have

confirmed that the optimal value for M/P ratio is ranging between 4 and 6, others have confirmed that it is more than 10. Figure 21 shows the influence of M/P molar ratio on the mechanical strength of the MPC paste for different W/P molar ratio. It can be observed that for each W/P molar ratio there is an optimal M/P molar ratio. For W/P molar ratio of 3, the experimental results proved that the optimal molar ratio is 6. Meanwhile, the optimal M/P molar ratio is becoming between 6 and 8 if the W/P molar ratio is changed to 3.8. Thus, the optimal M/P molar ratio can be affected by the amount of the used water. For example, the compressive strength of the MPC specimen that has W/P molar ratio of 3 with M/P molar ratio of 3 is found to be very low. This low strength is due to the high-water content which results in a larger spacing of the cement particle. Therefore, when the k-struvite grows, there are too far apart to bind together. Moreover, after casting the cement paste, the excessive amount of water will be squeezed out and evaporated leading to develop a lot of micro- pores/voids inside the casted cement paste. These micro-pores/voids can decrease the density and the compressive strength of MPC paste specimens. By increasing M/P ratio to 6, the amount of used water (W/P ratio of 3) is becoming adequate for the mixture because the additional amount of the magnesia is consuming the excess water and develop more k-struvite which leads to improving the compressive strength. By increasing M/P ratio to 8, the amount of the used water is becoming insufficient for all of these magnesia particles. Thus, the amount of unreacted magnesia particles will be increased, where the amount of the k-struvite will be decreased which leads to reducing the compressive strength of the MPC specimen. Moreover, the low amount of water can reduce the flowability of the system leading to poor compaction and poor compressive strength. As a conclusion, the optimal M/P molar ratio depends on the amount of used water, and this can explain the apparent contradiction that found in the literature. On the other hand, the published work primarily uses the mass ratio between water and solid to describe the

amount of the used water rather than using a molar ratio between water and KDP. This expression may cause a misinterpretation of the real impact of magnesia/water content on the fundamental understanding of the MPC behavior.

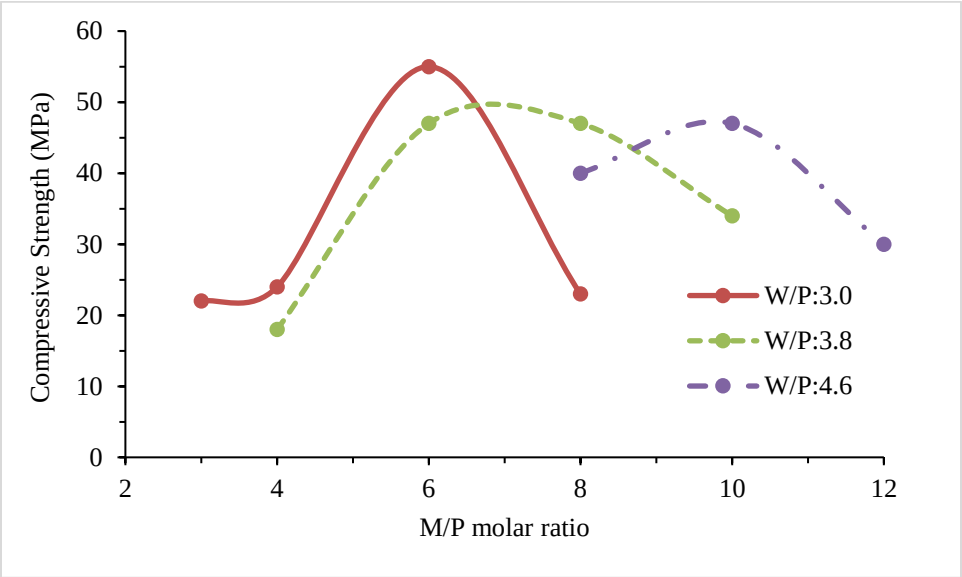

Figure 21. Influence of M/P molar ratio on the compressive strength of MPC paste for different W/P molar ratios.

3.4.3 INFLUENCE OF WATER CONTENT (W/P RATIO)

Figure 22 shows the effect of W/P molar ratio on the compressive strength of the MPC system with the presence of the boric acid. Each curve in figure 22 presents a different M/P molar ratio. It can be observed that there is an optimal water content (W/P molar ratio) for each M/P molar ratio. At first, the compressive strength increases when the W/P molar ratio increases. Then, the compressive strength decreases when the W/P molar ratio increases. This experiment can indicate that the use of a low W/P ratio is not necessarily leading to improve the compressive strength. The compressive strength of the MPC paste is found to be very low when the amount of the used water is limited and may be not sufficient for the acid-base reaction.

On the other side, using a high-water content leads to reduce the compressive strength. For instance, for M/P ratio of 4, the optimal W/P molar ratio is 2.4, while using less or more than this value will reduce the compressive strength of the specimen.

On the other hand, the experimental results indicate that the behavior of the MPC without the presence of boric acid is slightly different. Figure 23 shows the influence of W/P molar ratio on the compressive strength of the MPC past with/without the presence of the boric acid. It can be seen that the reduction in the compressive strength without the presence of the boric acid is much larger. For B/M ratio of 0%, changing W/P ratio from 1.8 to 2.2 can reduce the compressive strength by 19%. Meanwhile, adding 5% of the boric acid to the same mixture can reduce the compressive strength by only 4%. The reason behind this behavior is the negative effect of the boric acid on the fluidity of the system. Table 6 provides the flow results of the MPC specimens. Without using the boric acid, and for W/P ratio of 1.8, the flow of the MPC past is found to be 132%. By increasing W/P ratio to 2.2, the MPC past is becoming too runny, and the flow table test cannot be conducted. As previously mentioned, the high-water content results in a larger spacing of the cement particles and develop a lot of micropores which can decrease the density and the compressive strength of the paste. On the other side, the boric acid has the ability to consume the excess water and reduce the fluidity of the system. For W/P ratio of 1.8, the flow value of the MPC past is found to be 68%. By increasing W/P molar ratio to 2.2, the flow value is increased to 116%. Thus, the reduction in the compressive strength due to the tremendous amount of water is becoming not valid.

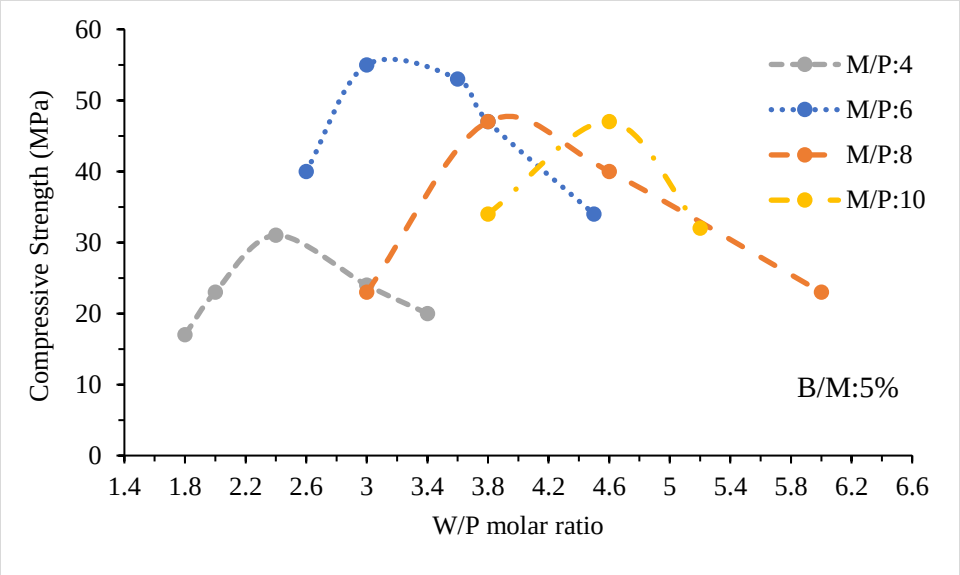

Figure 22. Influence of W/P molar ratio on the compressive strength of the MPC system.

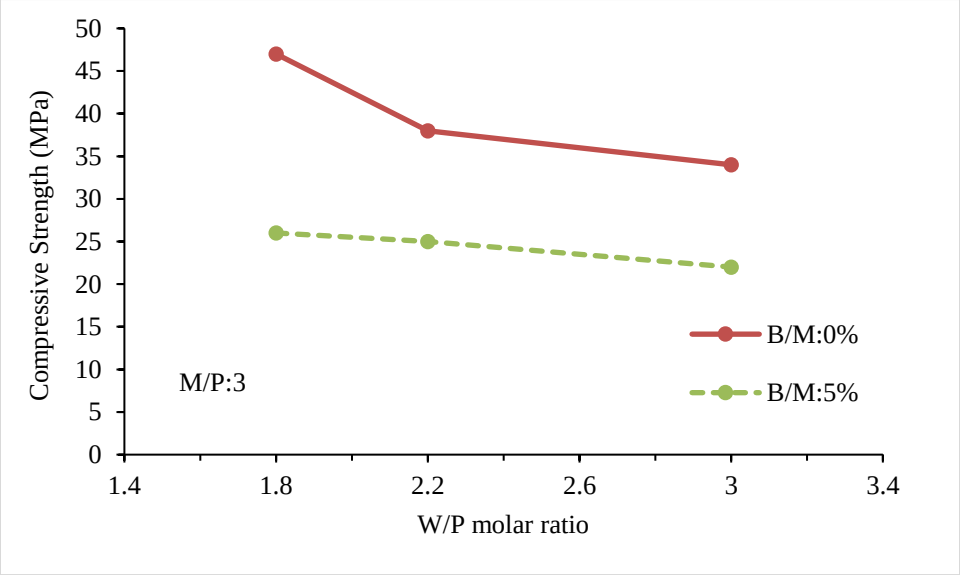

Figure 23. Influence of W/P molar ratio on the compressive strength of the MPC system with/without the presence of boric acid.

3.5 PHASE ANALYSIS

3.5.1 XRD ANALYSIS

The XRD results of the MPC paste specimens are presented in figures 24 and 25. Many of the magnesium phosphate crystalline phases are investigated in this work in addition to all the possible magnesium potassium phosphate minerals. Table 7 summarizes all the magnesium crystalline phases that investigated in this research. The XRD analysis demonstrates that the main reaction product of the MPC system is the well-known K-struvite ($MgKPO_4*6H_2O$), in addition to some unreacted materials including the magnesium oxide (MgO) and the monopotassium phosphate (KDP). Moreover, the only magnesium phosphate crystal that found in the products is the K-struvite, and no any other magnesium phosphate crystalline phases are found in the final product including Cattiite ($H_{44}Mg_3O30P_2$) and Newberyite (H_7MgO_7P) that mentioned in the literature. These crystalline phases could be formed during the hydration processes. Then, they dissolved again before the paste hardening. On the other side, the XRD analysis demonstrates that no boron-containing crystalline phases have appeared in the final products of including Luneburgite $B_2H_{18}Mg_3O_{20}P_2$ and Szaibelyite $BHMgO_3$.

Table 7. Magnesium phosphate/potassium phosphate crystalline phases investigated in this work.

Magnesium phosphate/ potassium phosphate crystalline phases	Formula	Magnesium phosphate/ potassium phosphate crystalline phases	Formula
Hydroxylwagnerite	$H\ Mg_2O_5P$	K-struvite	$H_{12}KMgO_{10}P$

Cattiite	$H_{44}Mg_3O_{30}P_2$	Potassium magnesium catenaphosphate	$KmgO_9P_3$
Newberyite	H_7MgO_7P	Potassium magnesium hydrogendiphosphate dihydrate	$H_5KmgO_9P_2$
Kovdorskite	$H_7Mg_2O_8P$	K Mg0.5 (H_2 P_2 O_7) (H_2 O)	$H_4KMg0.5O8$ P2
Magnesium hydrogen phosphate	$H_4Mg_7O_{24}P_6$	K2 Mg3 (P2 O7)2 (H2 O)10	$H_{20}K_2Mg_3O_{24}$ P_4
Raadeite	$H_8Mg_7O_{16}P_2$	Potassium magnesium hydrogendiphosphate dihydrate	$H_5KmgO_9P_2$
Kovdorskite	$H_7Mg_2O_8P$	Periclase	MgO
Holtedahlite	$H_7Mg_{12}O_{30}P6$	-	$H_{12}Mg_2O_{13}P_2$
-	$H_{13}MgO_9P$	Monopotassium phosphate	H_2 K O_4 P

The XRD analysis for the MPC pastes with low M/P molar ratio are presented in figure 24. All the specimens have the same M/P and W/P molar ratios while the B/M ratios are changed. According to the XRD results, the MPC specimen with no boric acid exhibit more k-struvite characteristic peaks. In other words, some of the k-struvite diffraction peaks are disappeared with the presence of boric acid. For example, the k-struvite peaks that located at about 23.1, 29.3, and 37.9 2θ have appeared with the absence of the boric acid while they are clearly disappeared with the presence of the boric acid. This observation concludes that the existence of the boric acid leads

to poor crystallization growth and maybe less amount of the K-struvite phase. Furthermore, the MPC specimen that includes boric acid exhibits stronger KDP characteristic peak, which indicates that the presence of the boric acid increases the amount of unreacted KDP. There are two possible reasons for this observation. First the presence of the boric acid can prevent the contact between a huge part of the MgO and the KDP particles permanently leading to a poor crystal growth of the K-struvite and maybe reduce its amount. Meanwhile, this suspended/prevented amount of MgO/KDP will not react with the boric acid particles and appeared as unreacted materials in the XRD analysis. Thus, there are no boron-containing crystalline phases in the final products. Second, the boric acid particles have the ability to react with the MgO to form an amorphous boron-magnesium compound.

Figure 25 shows the XRD patterns for MPC paste specimens with high M/P molar ratio. The M/P and W/P molar ratios are fixed to be 6 and 3.6 respectively, while the B/M ratio is changed from 0 to 10%. Based on the shown XRD patterns, the MPC specimens with no boric acid and with 5% of boric acid exhibit stronger and sharper K-struvite characteristic peaks. This observation concludes that the using of moderate amount of boric acid with high M/P molar ratio MPC specimens does not affect the phase composition of the MPC paste. However, using a high boric acid content can apparently affect the crystallinity of the K-struvite and lead to poor crystallization growth. On the other hand, no KDP peaks are found in the final products of all specimens. Besides, the amount of unreacted MgO in the MPC specimen with no boric acid is found to be much higher. These observations can support both hypotheses mentioned above. Hence, the boric acid has the ability to react with the MgO particles to form an amorphous boron-magnesium compound which cannot be seen by the XRD analysis or prevents the reaction between a part of the MgO and the KDP. The reason behind the absence of the unreacted KDP peaks is the using of high M/P molar

ratio. The high M/P molar ratio can provide a considerable amount of MgO particles that can react with the boric acid to form an amorphous boron-magnesium compound, while the residual amount of MgO will be still enough to react with the free KDP particles to form crystal/amorphous K-struvite structures. Moreover, the peaks of the unreacted magnesia are found to be very weak when a high boric acid content is added to the mixture which means that the boric acid can consume the MgO particles in the system. This observation can support the second hypothesis mentioned above.

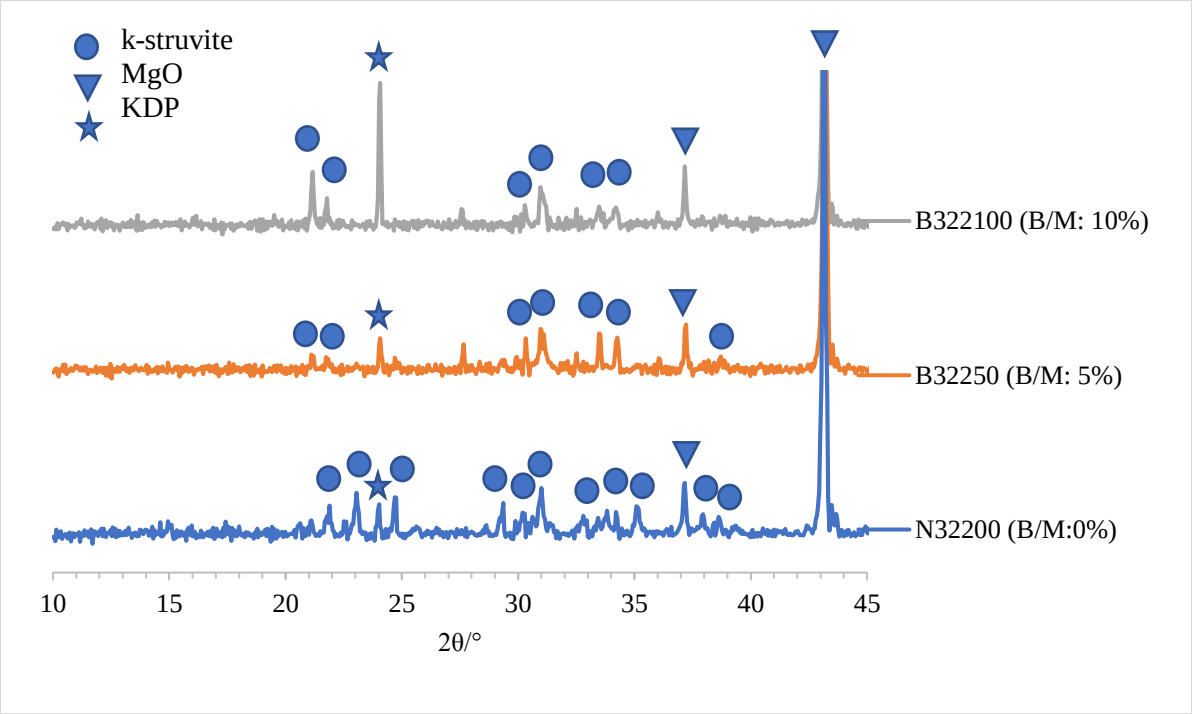

Figure 24. The XRD patterns for MPC paste with low M/P ratio.

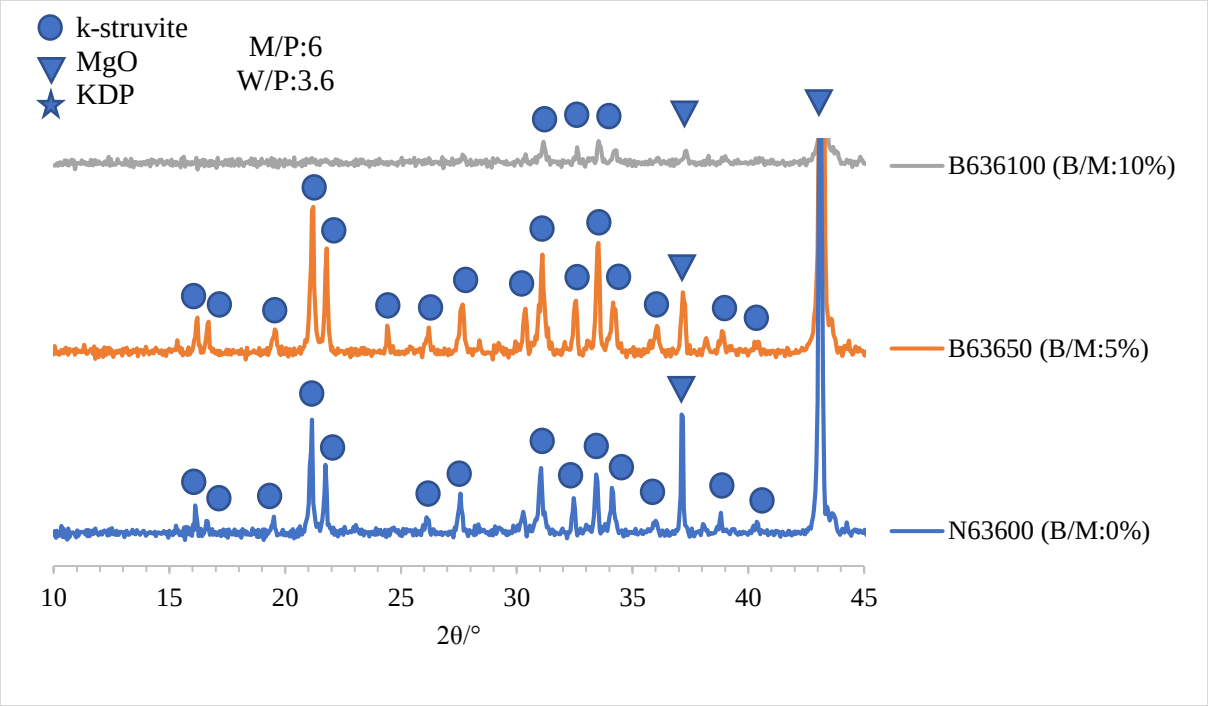

Figure 25. The XRD patterns for MPC paste with high M/P ratio.

3.5.2 FTIR

The FTIR spectra for MPC specimens with different B/M ratios are shown in figure 26; a) for low M/P ratio and b) for high M/P ratio. For both cases, the FTIR spectra reveals a H-O-H stretching vibration at a region of 3670 to 2540 cm^{-1}. This H-O-H stretching vibration modes are related to the presence of the water in the k-struvite crystals. Besides, the analysis shows a bending vibration mode of H-O-H in a range of 2136 to 1966 cm^{-1}. Furthermore, the band that located at about 985 and 667 cm^{-1} indicates a stretching and a binding vibration mode of PO_4^{-3} in the k-struvite crystals respectively. Finally, the results illustrate a possible vibration mode of a metal-oxygen bond at 850 cm^{-1}. The same observations have been reported in previous studies [114 and 115]. In both cases (low and high M/P ratio), no new bonds have been obtained by adding the boric acid to the mixtures. These observations indicate that no boric acid containing crystalline structure has been formed during the reaction process. On the other hand, the results indicate that adding

the boric acid to the MPC mixtures can reduce the intensity of the observed vibration bands which indicates that the amount of these functional groups are decreased by adding the boric acid.

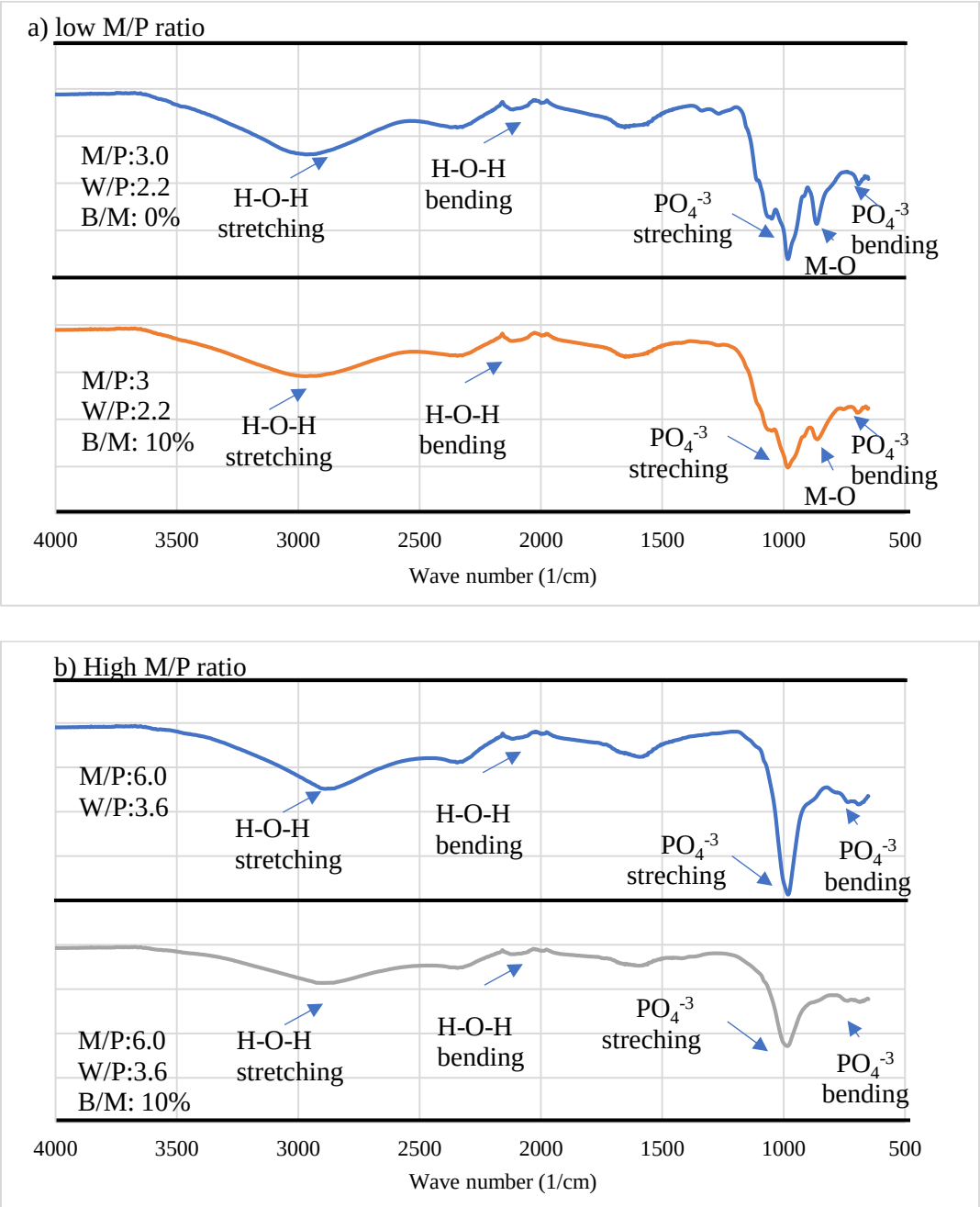

Figure 26. FTIR spectra of MPC paste with different B/M ratios a) low M/P ratio and b) high M/P ratio.

3.6 MICROSTRUCTURE ANALYSIS

The microstructure of the MPC paste with low and high M/P ratio are presented in figure 27 and 28 respectively. For figure 27, the M/P and W/P ratio are fixed to be 3 and 2.2 respectively while the B/M ratio is changed from 0 to 10%. The SEM images of the MPC paste with no boric acid show a dense, mostly crystalline microstructure. Moreover, the shape of the k-struvite crystalline structure is found to be a bladed prism (figure 27. a). After adding the boric acid to the mixture (figure 3.27. b), two types of materials with very different morphology can be observed. The first type, the solid-line rectangle, is a solid material with a smooth and a flat surface while the second type, the dashed-line rectangle, is a low dense needle-like crystalline structure. Adding more boric acid material (figure 27. c) to the MPC mixture can also change the micro-morphology of the studied cement paste. Three different types of material can be observed when the B/M ratio is increased to 10%. As shown in the figure 27. c.1, the first type, the dashed-line rectangle, is a low dense scale-like needle material (figure 27. c.2) while the second type, the solid-line rectangle, is a solid compacted material with no any crystalline shapes (figure 27. c.3), and the third type, the dotted-line rectangle, is a low dense needle-like crystalline material similar to that one that observed in figure 27. c.2.

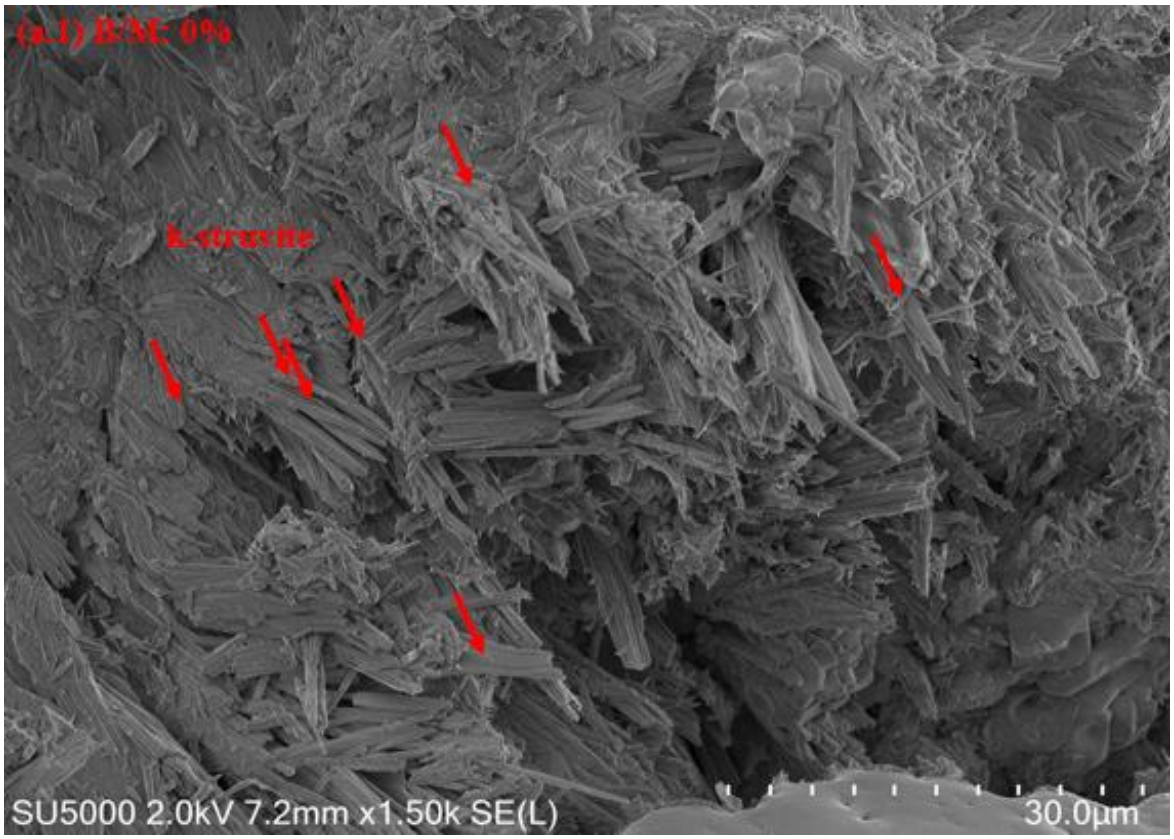
(a.1) B/M: 0%
k-struvite
SU5000 2.0kV 7.2mm x1.50k SE(L)
30.0µm

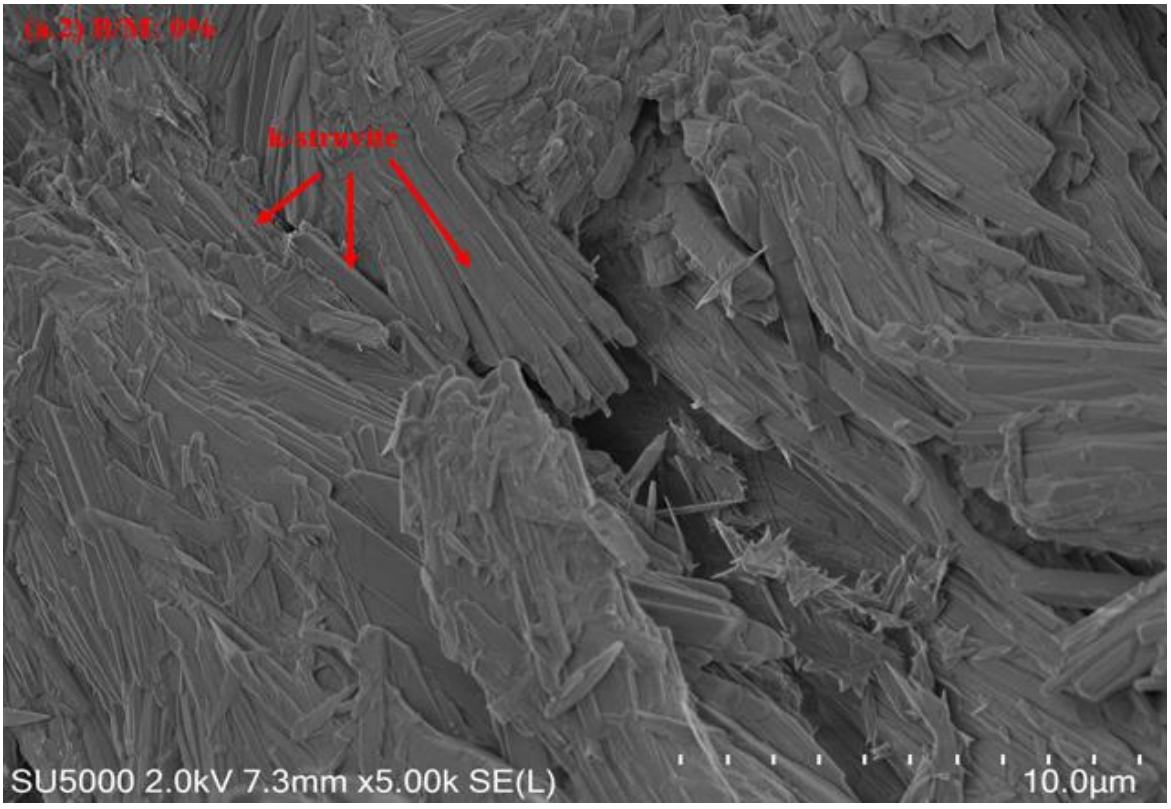
(a.2) B/M: 0%
k-struvite
SU5000 2.0kV 7.3mm x5.00k SE(L)
10.0µm

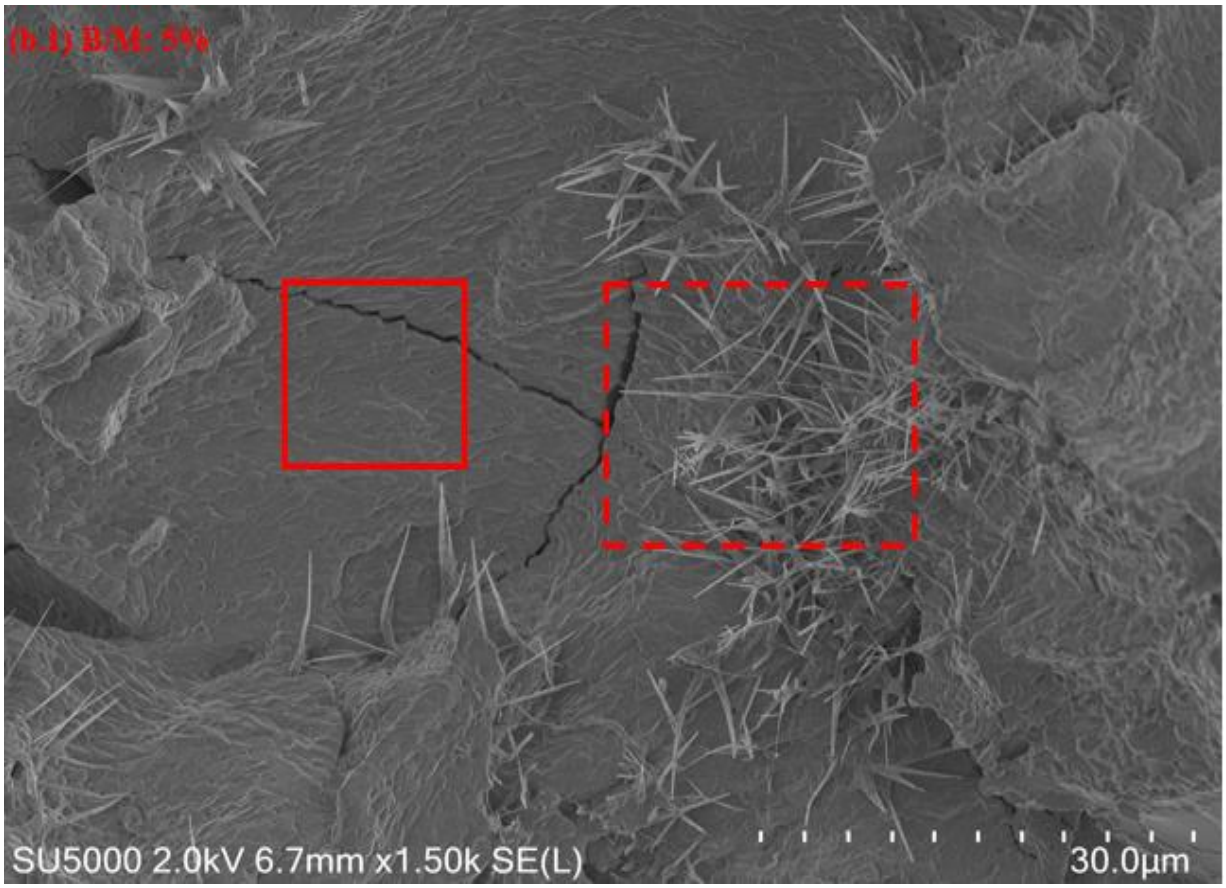
(b.1) B/M: 5%
SU5000 2.0kV 6.7mm x1.50k SE(L)
30.0µm

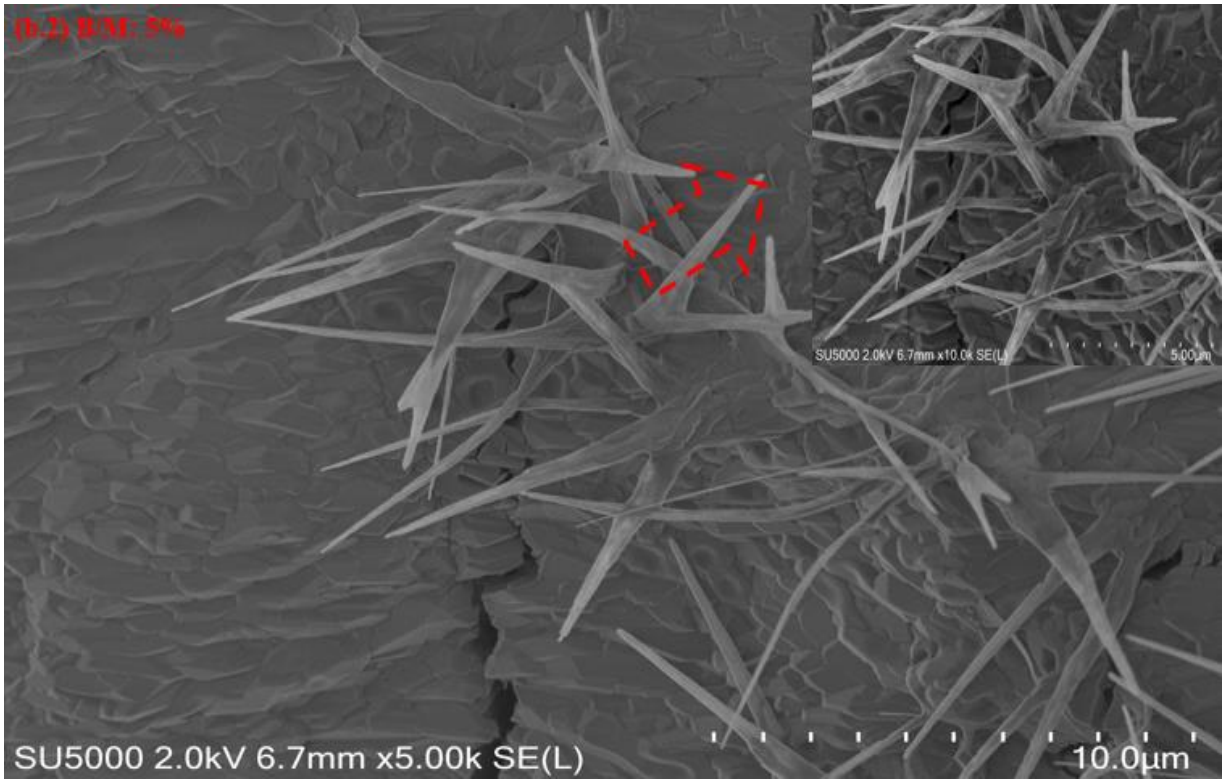
(b.2) B/M: 5%
SU5000 2.0kV 6.7mm x10.0k SE(L)
5.00µm
SU5000 2.0kV 6.7mm x5.00k SE(L)
10.0µm

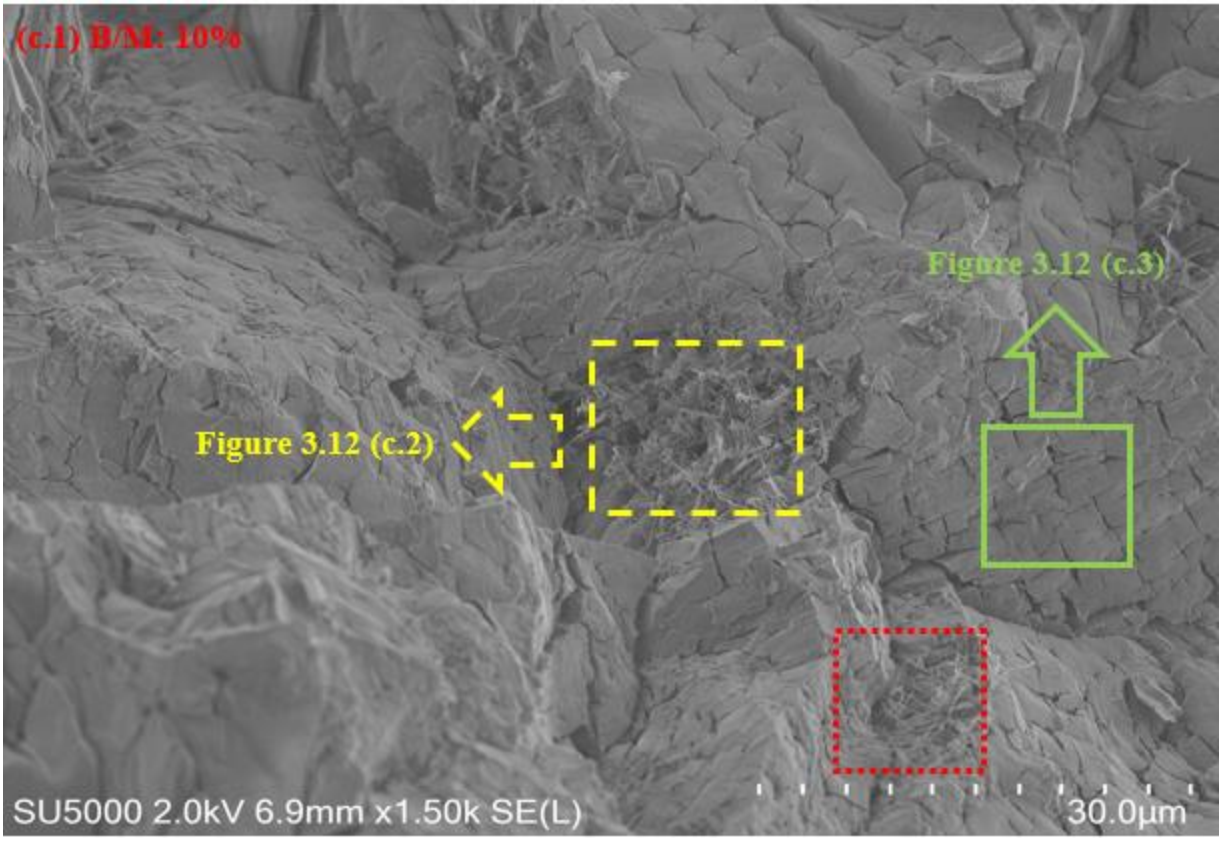
(c.1) B/M: 10%
Figure 3.12 (c.3)
Figure 3.12 (c.2)
SU5000 2.0kV 6.9mm x1.50k SE(L)
30.0µm

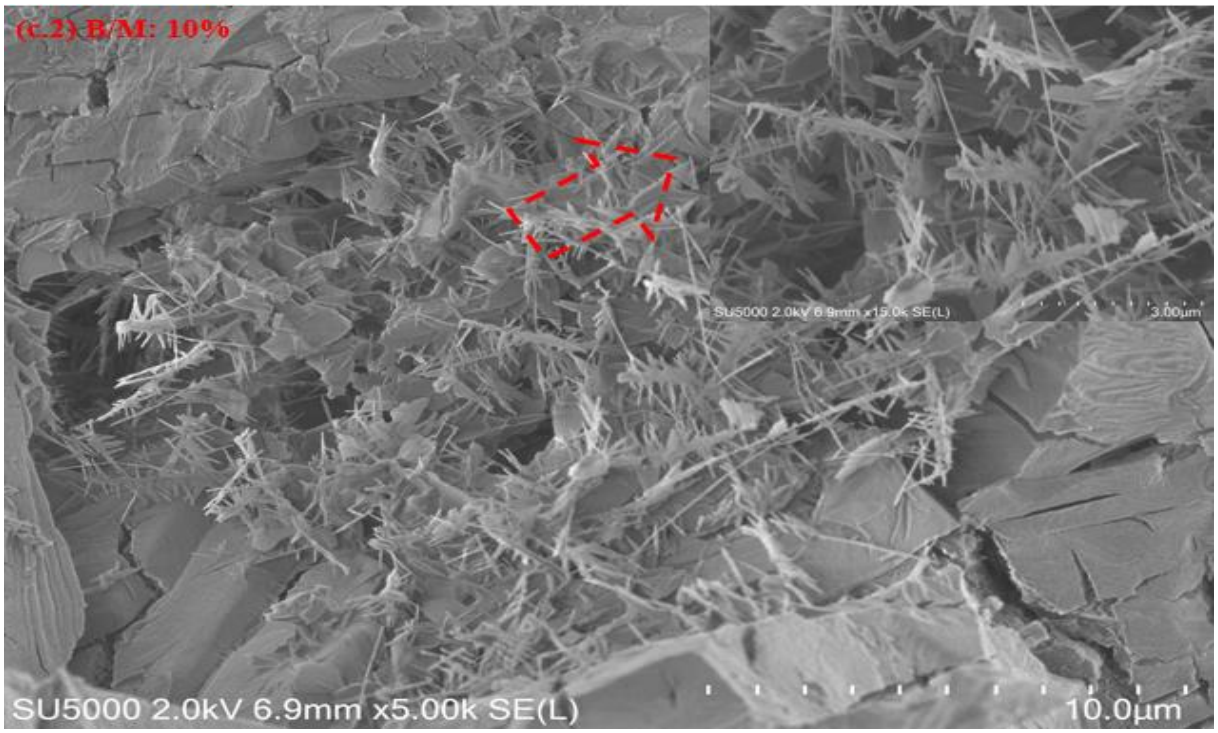
(c.2) B/M: 10%
SU5000 2.0kV 6.9mm x5.00k SE(L)
10.0µm

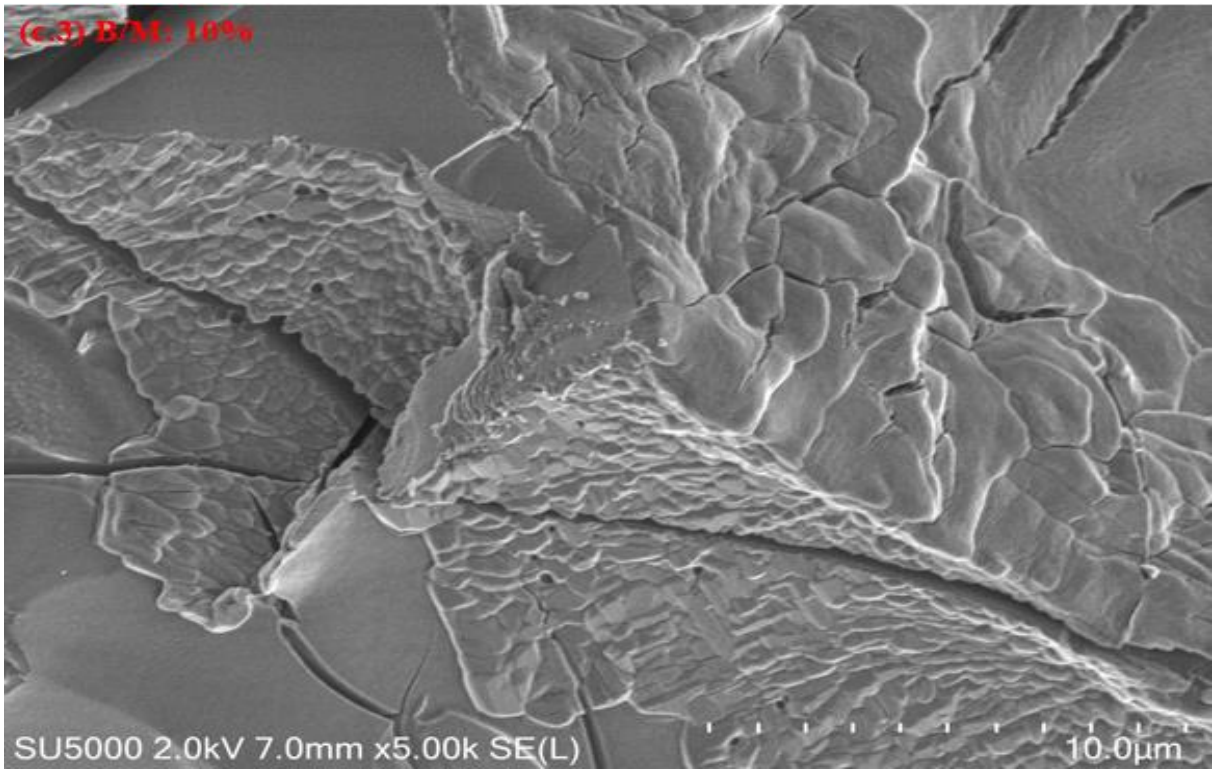

Figure 27. SEM images of MPC paste with low M/P molar ratio; a) B/M ratio of 0%, b) B/M ratio of 5%, and c) B/M ratio of 10%.

Figure 28 presents the SEM images of the MPC paste with high M/P molar ratio. The M/P and W/P molar ratios are fixed to be 6 and 3.6 respectively while the B/M ratio is changed from 0 to 10%. According to the SEM images, the final product of the MPC specimen with no boric acid is a dense short prism-like crystalline structure. This observation can explain the high strength of the B63650 specimen. Also, the k-struvite of the MPC specimen with 5 % of B/M ratio is found to be a prism-like material with a larger size than that specimen with no boric acid (figure 28. b). Finally, the MPC paste with 10% of B/M ratio shows two types of microstructures, the first one, the dashed-line rectangle, is needle shape k-struvite material while the second one, the solid-line rectangle is a plate-like structure with a low density and a smooth surface.

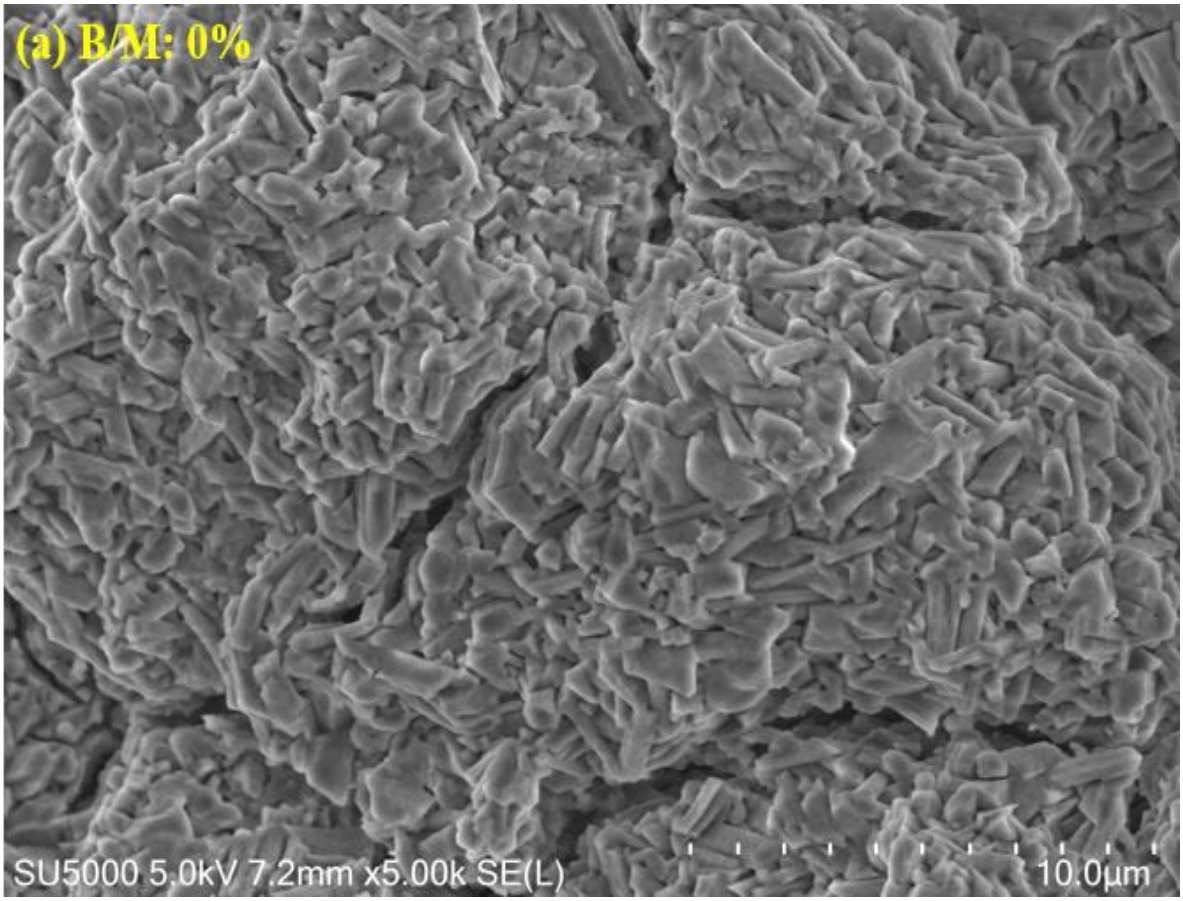
(a) B/M: 0%
SU5000 5.0kV 7.2mm x5.00k SE(L)
10.0µm

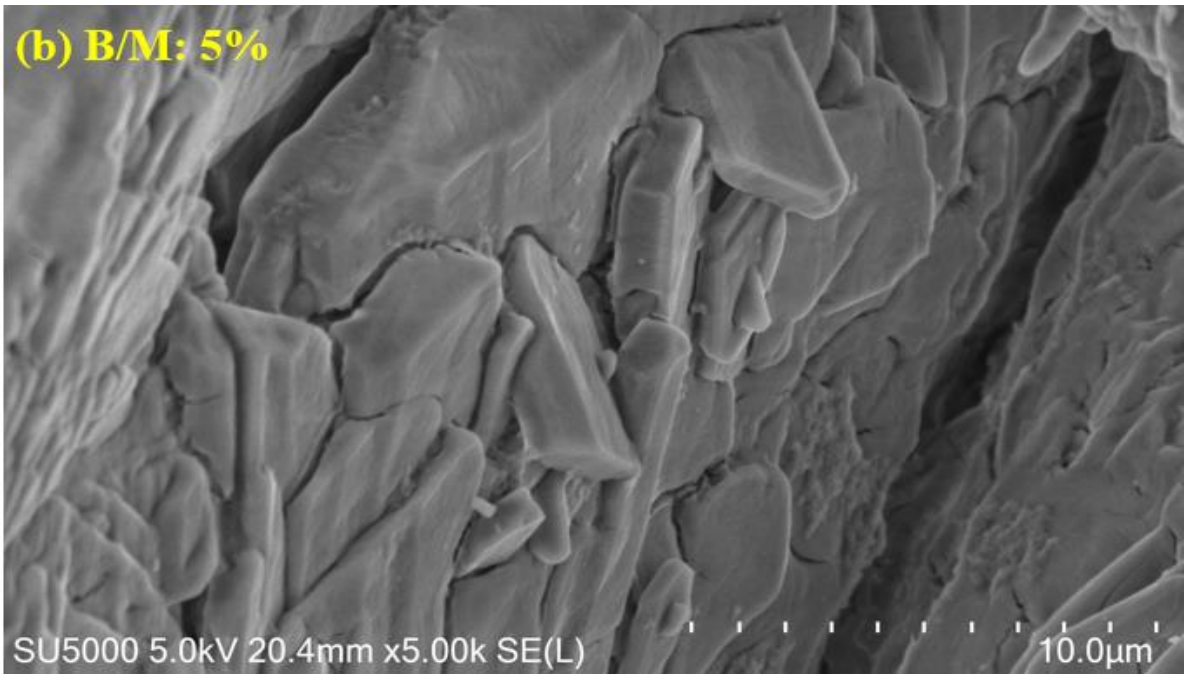
(b) B/M: 5%
SU5000 5.0kV 20.4mm x5.00k SE(L)
10.0µm

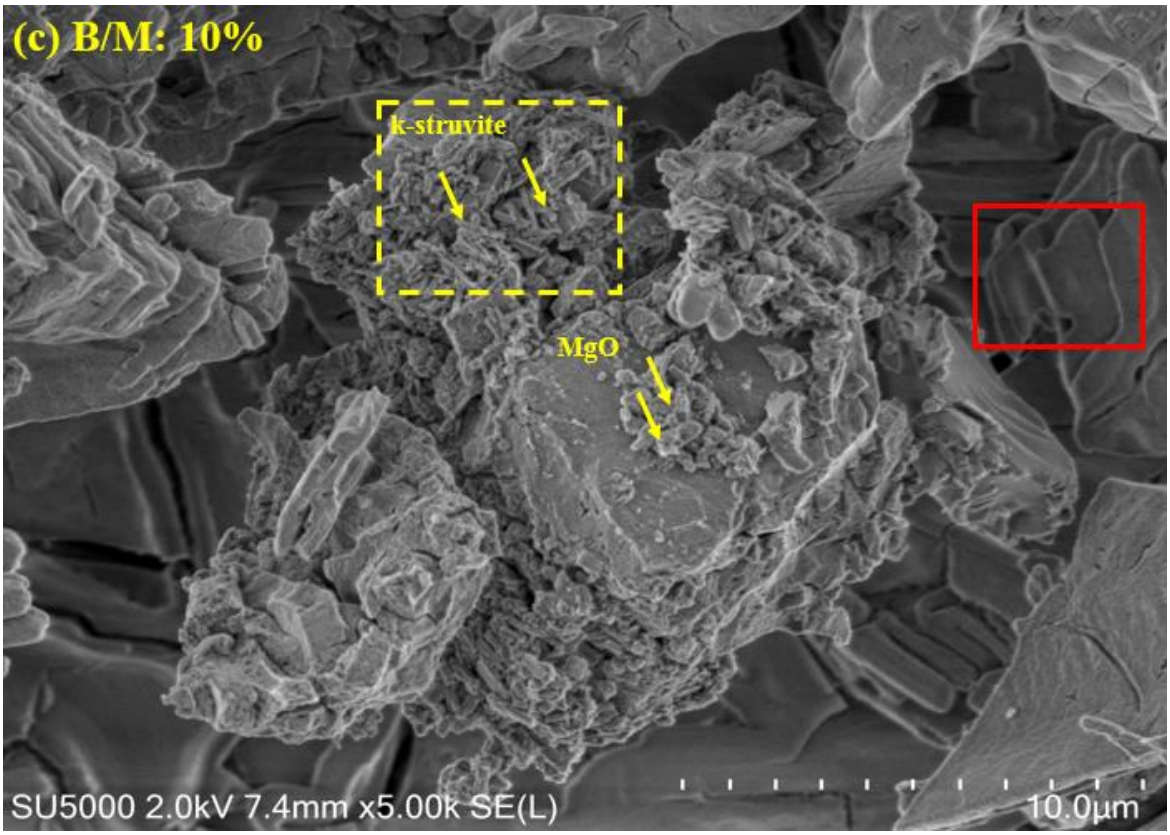

Figure 28. SEM images of MPC paste with high M/P molar ratio; a) B/M ratio of 0%, b) B/M ratio of 5%, and c) B/M ratio of 10%.

The final conclusions from the microstructure analysis can be drawn as follows; the shape of the K-struvite microstructure can be in multiple forms including (1) prism-like structure, (2) needle-like structure, (3) scale-like needle structure, and (4) plate-like structure. The MPC specimens that prepared without using the boric acid are attending to produce a dense prism-like K-struvite structure (figure 27. a and figure 28. a). For low M/P ratio specimens, adding the boric acid is leading to change the morphology of the K-struvite structure due to reducing the amount of the available magnesia. The limited amount of magnesia will produce a needle-like K-struvite structure with a very low density (figure 27. b and c) in addition to a solid compacted smooth surface material that could be a combination of low crystallized/amorphous K-struvite structure

and some unreacted materials (figure 27. c.3). This can explain the weak K-struvite characteristic peaks that obtained when the boric acid is added to a low M/P ratio MPC paste (figure 24) and the low compressive strength of these specimens (figure 20 a). On the other hand, adding a moderate amount (B/M ratio of 5%) of boric acid to a high M/P ratio MPC mixture will not change the shape or the intensity of K-struvite (figure 28. b). However, a larger prism-like crystalline structure is observed. Finally, adding a high amount of boric acid (B/M ratio of 10%) to an MPC mixture with high M/P ratio is leading to change its morphology. Only a few amounts of those prism-like crystals can be observed while the rest of the MPC specimen morphology consists of a plate-like microstructure and a solid compacted material with a smooth surface.

3.7 THERMAL CONDUCTIVITY AND DRY DENSITY

Table 8 summarizes the dry density and the thermal conductivity measurements of MPC specimens with different boric acid dosages. It can be noted that adding boric acid reduces the dry density of the MPC paste due to the porosity increment. For an M/P ratio of 3, adding 5% and 10% of boric acid can reduce the dry density by 2.3% and 5.7% respectively. Also, adding 5% and 10% of boric acid to MPC pastes with an M/P ratio of 6 can reduce the dry density by 4.7% and 7% respectively. Although the phase analysis does not show any crystalline product containing boron (B), the density may indicate that the boric acid can react with one or more of the MPC components to produce a boron-compound which has a lower density than the original MPC reaction products.

Figure 29 shows the thermal conductivity of MPC as a function of boric acid % added for different M/P ratios. It can be observed that the thermal conductivity of the MPC paste decreases when the B/M ratio increases. For M/P ratio of 3, adding 5% of the boric acid does not affect the thermal conductivity, while increasing the boric acid content (B/M ratio of 10%) the thermal

conductivity reduction measured from 1.31 to 1.1 W/mk. Furthermore, increasing M/P molar ratio, increased the MPC specimen's sensitivity to the boric acid addition. For an M/P ratio of 6, adding 5% and 10% of boric acid can reduce the thermal conductivity from 1.93 to 1.78 and 1.6 W/mk respectively.

Table 8. Experimental results for thermal conductivity test of dry MPC paste.

Sample ID	M/P	W/P	B/M (%)	Dry Density (Kg/m^3)	Temperature (ºC)	Thermal Conductivity (W/mk)
N32200	3	2.2	0	2265.5	21.2	1.31
B32250	3	2.2	5	2204.5	21.2	1.31
B322100	3	2.2	10	2135.8	21.2	1.1
N63600	6	3.6	0	2257.9	21.2	1.93
B63650	6	3.6	5	2151.1	21.2	1.78
B636100	6	3.6	10	2097.7	21.2	1.6

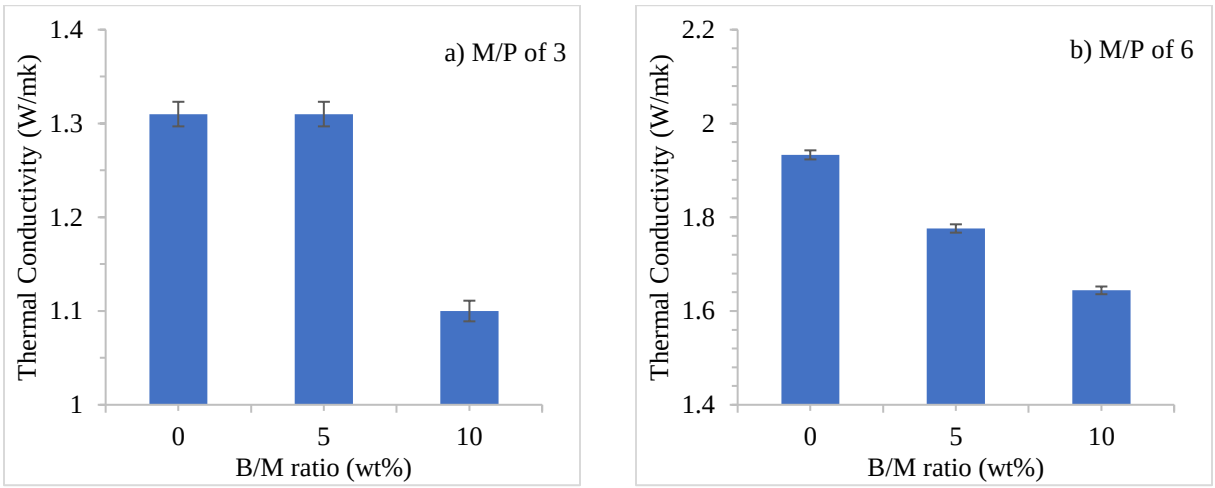

Figure 29. Influence of boric acid content on the thermal conductivity of the MPC paste.

3.8 THE ROLES OF BORIC ACID IN THE MPC PASTE FORMATION

3.8.1 RETARDATION MECHANISM

The findings from this research demonstrate that the initial setting time of the MPC system is highly dependent on the boric acid content. The experimental results approve that the initial setting time of the pastes increases when the B/M ratio increases. The retardation mechanism of the boric acid can be suggested as the following; when the boric acid particles are presenting in the MPC solution, the boric acid dissociates to $B(OH)_4^-$ oxyanions and H^+ ions. Since there is an evidence that the MgO particles have the ability to absorb the $B(OH)_4^-$ oxyanions [116-118], by adding the MgO to the solution, a part of these particles will absorb the $B(OH)_4^-$ oxyanions, while the other parts will dissociate to Mg^{+2} ions and $2OH^-$ anion. Then, the absorbent of the $B(OH)_4^-$ by the MgO particles has the ability to release Mg^{+2} ions leading to increasing the Ph of the solution. As a result, a temporary surface complex ion/compound will be formed by the interaction of MgO, Mg^{+2}, and $B(OH)_4^-$ [118]. This complex compound will dissociate to $MgB(OH)_4^+$ ions which stabilizes the Mg^{+2} particles leading to increase the initial setting time of the MPC system [76]. Another possible reason that found in literature is the ability of boric acid to form a temporary layer of lunebergite ($Mg_3B_2(PO_4)2(OH)*6H_2O$) which can retard the hydration process of the system by ether hindering the contact between the magnesium and monopotassium phosphate particles or slow down the dissolution process of the final product [44-113].

3.8.2 MPC PASTE FORMATION

The authors of this paper have suggested two possible hypotheses that can explain the roles of boric acid in the formation mechanism of the MPC paste.

The first hypothesis indicates that the presence of the boric acid prevents the contact between a considerable part of the MgO particles and the KDP leading to a poor crystallization growth of the K-struvite and maybe reduce its amount. The boric acid can either stabilize the MgO particles by forming the complex ions of $MgB(OH)^{-}_{4}$ or coat the MgO particles by forming a temporary layer of a lunebergite compound. As a result, a huge part of the MgO particles is suspended or inhibited from interacting with phosphate particles while the other part will react with the phosphates to produce the K-struvite. When a low M/P ratio is used to produce the paste, only a few amounts of the magnesium ions will react with the phosphate particles while the others will be suspended/prevented by the boric acid. Then, the exothermic reaction will generate a huge amount of heat/energy and consumes most of the available water in the system, and no further reaction/crystallization growth is possible. The suspended/prevented amount of the MgO particles will not react with the boric acid particles and appeared as unreacted materials in the XRD analysis. Thus, with the presence of the boric acid some of the K-struvite diffraction peaks are disappeared while the intensities of the others are becoming low (figure 24). Furthermore, the KDP diffraction peak intensity of the KDP increases when the boric acid content increases (figure 24) while only a few amounts of the unreacted KDP have appeared with the MPC paste with no boric acid. This observation can indicate that the presence of the boric acid can prevent a massive amount of the MgO from reacting with KDP to produce K-struvite. Therefore, the unreacted KDP peaks can be found when the boric acid is added to the mixture. All of these observations can conclude that the existence of the boric acid leads to poor crystallization growth and maybe less amount of the K-struvite phase.

From the microstructure analysis, the MPC paste with low M/P ratio and no boric acid show a dense prism-like K-struvite structure with no any other compounds (figure 27. a). After

adding the boric acid to the system, a needle-like K-struvite structures with a very low density have been observed (figure 27. b and c) in addition to a solid compacted smooth surface material which could be a combination of low crystallized/amorphous K-struvite and some unreacted materials. Thus, the compressive strength of the MPC pastes with a low M/P ratio is significantly reduced with the presence of the boric acid (figure 20. a). Finally, no boron-containing crystalline phases have been achieved from the XRD or the FTIR analysis (figure 24 and 26. a) which indicates that the boric acid does not react with either the MgO or the KDP particles. On the other side, using a high M/P ratio to produce the MPC paste can provide a considerable amount of the MgO particles in the system. When a moderate amount of the boric acid is added to such system, the boric acid will stabilize/coat a part of the MgO particles while the residual amount of the MgO is still enough to react with the available KDP particles to form crystal/amorphous K-struvite structures. Therefore, the crystallization growth of the K-struvite is not reduced by adding 5% of boric acid to the system (figure 25). Furthermore, no KDP peaks are found in the final products of these specimens (figure 25) which indicates that all the available KDP particles react with the MgO to produce the K-struvite. Thus, there is no reduction in the compressive strength of this specimen (B63650) (figure 20. b). On the other hand, using a high amount of boric acid with a high M/P ratio MPC paste can reduce the crystallinity degree of the K-struvite (figure 25) and can change its morphology. From the SEM images, only a few amounts of the prism-like crystals can be observed when a high boric acid content is added while the majority of the MPC specimen morphology consists of a plate-like microstructure and a solid compacted material with a smooth surface (figure 28). Since the K-struvite can exist in amorphous structures [68], the presence of the boric acid will reduce only the crystallinity degree of the K-struvite and incites the system to produce an amorphous version of the K-struvite. Therefore, the SEM images show another type of

micromorphology consisting of a solid compacted material with a smooth surface (figure 28. c). Thus, the reduction of the compressive strength of this specimen (B636100) is found to be marginal (figure 20. b).

The second hypothesis indicates that the boric acid particles have the ability to react with the MgO to form an amorphous boron-magnesium compound. For the MPC paste with a low magnesia content, the boric acid particles will react with the MgO to form an amorphous boron-magnesium compound. This reaction will consume a lot of MgO leaving the system with a limited amount of the MgO particles. The residual amount of the MgO particles is not enough to react with the all available KDP particles leading to reduce the amount of the K-struvite. Moreover, the presence of the boric acid leads to poor crystal growth of the K-struvite (figure 24 and figure 27). Thus, the XRD analysis shows weaker K-struvite peaks and a stronger unreacted KDP peak after adding the boric acid (figure 24). In this case, the reduction in the K-struvite amount is not because the poor crystallinity of the K-struvite phase, but it is due to the limited amount of the MgO particles after adding the boric acid which is not enough to complete the reaction with all the free KDP particles. Maybe these statements can explain why the MPC paste with no BA has a more compressive strength, and it can explain the reason behind the huge reduction in the compressive strength (-45%) when the boric acid is added (figure 20. a). On the other hand, using a high magnesia content can provide enough amount of magnesia to react with the boric acid in addition to the available KDP particles. Thus, the boric acid will consume many of magnesia particles, but the residual is almost enough to react with the available KDP to produce a high amount of K-struvite compound. Therefore, the unreacted MgO/KDP peaks cannot be found in the high magnesia content MPC final products after adding the boric acid. As a result, the reduction in the compressive strength of the high magnesia content MPC paste is marginal (-4%) when the boric

acid is added. Since no boron-containing magnesium minerals are found in the final products of the MPC paste, the suggested structural form for this compound will be amorphous. Moreover, adding boric acid to the MPC can reduce its density. Although the phase analysis does not show any crystalline product containing boron (B), the density may indicate that the boric acid can react with one or more of the MPC components to produce a boron-compound which has a lower density than the original MPC reaction products. It is worth mentioning that the density of the MgO particles (3.58 g/cm^3) is higher than the K-struvite (1.71 g/cm^3). Finally, if the MgO particles will be prevented from reacting with the KDP and it cannot react with the boric acid, much-unreacted magnesia should appear in the final product. The XRD result indicates that only a few amounts of the unreacted MgO are found when a high amount of boric acid is added to a high M/P MPC paste. As previously mentioned, the high M/P ratio can provide a huge amount of the MgO particles. This amount is much higher than the required amount of all the free KDP particles to complete the reaction. Therefore, all the KDP particles have reacted with the MgO while the boric acid consumes the residual parts to produce the amorphous boron-magnesia compound which cannot be seen by the XRD analysis. This amount should be much higher if the boric acid is preventing the reaction between the MPC main ingredients rather than reacting with the MgO. Table 9 summarizes the shreds of evidence of each proposed hypothesis.

Table 9. The shreds of evidence of the proposed hypotheses.

Characterization scheme	First hypothesis	Second hypothesis
Mechanical characterization	The significant reduction in the compressive strength of the low M/P ratio MPC specimens (figure 20. a)	The significant reduction in the compressive strength of the low M/P ratio MPC specimens (figure 20. a)
Physical characterization	-	The reduction in the fluidly of the MPC paste when the boric acid is added (Table 6)
Chemical characterization	The low crystallinity degree of the K-struvite when the boric acid is used with a low M/P ratio MPC specimens (figure 24)	The low crystallinity degree of the K-struvite when the boric acid is used with a low M/P ratio MPC specimens (figure 24)
	The strong unreacted KDP peaks when the boric acid is used with an MPC spacemen with low M/P ratio (figure 24)	The strong unreacted KDP peaks when the boric acid is used with an MPC spacemen with low M/P ratio (figure 24)
	There are no boron-containing crystalline phases have appeared in the final products of the MPC paste (figure 24, figure 25, and figure 26)	The weak unreacted MgO peaks when a high boric acid content is used with an MPC paste with high M/P ratio (figure 25)

Microstructure analysis	The change in the morphology of the K-struvite when the boric acid is added (figure 27 and figure 28)	The change in the morphology of the K-struvite when the boric acid is added (figure 27 and figure 28)
		The solid compacted material that observed when the boric acid is added (figure 27; b and c and figure 28; b and c)
Density		The reduction in the density when the boric acid is used (Table 8)

CHAPTER IV

INFLUENCE OF GNP ON THE PROPERTIES AND THE MICROSTRUCTURE OF MPC PASTES

4.1 INTRODUCTION AND LITERATURE REVIEW

As previously mentioned, the MPC system is still facing many unresolved challenges such as the very rapid setting time, the high fluidity with a few amounts of water, and the high fluidity loss with time. Many researchers are searching for compatible additives to astound these challenges and to improve the overall performance of MPC such as fly ash (FA), silica fume (SF), metakaolin, slag and acetic acid (AA). [80-83]. The reported results showed that using fly ash (FA) and silica fume (SF) improved the behavior of the MPC cement [80]. Xu et al. [82] used two different designed methods to incorporate FA in MPC mortars. At first, they used the FA as a filler to replace the solid contents (MgO and KDP), and they used it as a reactive material to replace only the MgO. They found that the using of FA as a reactive material was better and led to better fresh properties, denser microstructure, and higher compressive strengths. Zheng et al. [81] demonstrated that using FA and SF together with the MPC system produced denser products and improved the mechanical strength of the system and the water resistance. The hypothesis for the combined effect on the results, was (1) Physically; they could work as a filler, so they filled the micropores and improved the mechanical strength, (2) Chemically; the silicon oxide in the SF could react with MgO particles to form $MgSiO_3$, which improved the bonding strength of the system and enhanced its physical

properties. Jun et al. [83] reported that the used of AA improved the setting time and the microstructure of the system and led to better mechanical strength.

In the last decade, graphene is becoming one of the most promising additive material to be embedded with the composite materials in the construction field due to its outstanding properties. Recently, many forms of graphene structures/compounds have been used to improve the construction material properties including graphene oxide (GO) and graphene nanoplatelets (GnP). GnP represents a new form of carbon nanoparticles with multifunctional properties consisting of small stacks of graphene. GnP has exclusive nanoscale size, shape, and material composition. Therefore, it can be used to improve the properties of a wide range of materials. Recently, the GnP is highly implemented as a nanoscale additive for cementitious materials to improve its mechanical properties. Also, the GnP has the potential to enhance other properties such as electrical and thermal conductivity. Wang et al. [119] reported that the using of 0.05 wt % of GnP with ordinary Portland cement (OPC) can increase the compressive strength by 3%–8% and improve the flexural strength by 15%–24%. Du et al. [120] used a polycarboxylate based superplasticizer as a surfactant to improve the dispersion of GnP. They reported that the optimum dispersion of the GnP could be obtained when the amount of the surfactant is about 15% by weight of GnP. Moreover, they demonstrated that the using of 1 wt% of GnP with the OPC reduced the effective porosity and the critical pore diameter by 37% and 30%, respectively. On the contrary, adding 2 wt% of GnP to the OPC has an adverse effect on both. Tong et al. [121] investigated the effect of GnPs and GONPs on the performance of the OPC. They found that the addition of small dosage of both can increase the compressive strength up to 19.9%. Generally, graphene materials are found to be very useful in enhancing the thermal conductivity of cementitious materials. Sedaghat et al. [122] reported

that the using of graphite can improve the thermal conductivity and reduce the early hydration heat of the OPC. Cui et al. [123] demonstrated that the addition of 5 wt% of GnP to OPC paste increased the thermal conductivity by 77% and reduced the specific heat by 17.7%.

There are only a few studies that have focused on the impact of nanomaterials on the performance of MPC such as carbon nanotube, nano-silica, and graphene. Moreover, the influence of graphene material on the thermal conductivity of the MPC paste has not been reported so far. In 2016, Lu et al. [84] investigated the effect of the graphene oxide (GO) on the behavior of the MPC paste. They reported that the using of GO reduced the setting time and the workability of the paste. Besides, adding small weight percentages of GO can improve the mechanical strength, while using high weight percentages can reduce the mechanical strength of the paste. In 2019, Yue Li et al. [124] studied the effect of carbon nanotubes (CNT) on the mechanical and physical properties of the MPC cement. They used sodium dodecyl sulfate (SDS) in order to improve the dispersion degrees of the CNT. They found that the SDS alone has an adverse effect on the mechanical properties of the MPC. This adverse effect of the SDS could be countered when the CNT is added. Moreover, when the dispersion degrees of the CNT increases, the workability of the system decreases. However, the influence of GNP on the mechanical, physical, and thermal behavior of MPC paste/mortar has not been reported yet.

This chapter aims to understand the behavior of the MPC paste under different GnP dosages including physical behavior, mechanical properties, chemical behavior, and thermal conductivity. Also, the influence of GnP mixing method has been investigated, and the effect of the used surfactant on the performance of MPC specimens has been evaluated.

4.2 MPC MIX PROPORTIONS

As previously noted, the MPC specimens in this chapter are prepared by mixing MgO, KDP, boric acid, GnP, polyethyleneimine (PLE), and distilled water. As noted in chapter 2, the magnesia to phosphate molar ratio (M/P) has been selected to be 6 while the desired water content is calculated based on the molar ratio between KDP and water (W/P) and has been selected to be 3.6. This W/P ratio can provide mid-range workability for the paste, and it can guarantee that the available water is enough for the acid-base reaction. Also, the B/M ratio of 5% has been used for all the MPC specimens in this chapter in order to increase the initial setting time. For the GnP modified MPC specimens, the amount of GnP dosage is calculated based on the weight ratio between GnP and the total solid (GnP/S). Besides, the optimum amount of the surfactant is found to be 10% by the weight of GnP. The mixing procedures and the sample preparations of the MPC pastes were discussed earlier in chapter II.

The prepared MPC specimens in this chapter are divided into four different groups. The first group is prepared as a control specimen (B636) without adding any GnP or PLE. The second group is prepared by adding the GnP to the MPC mixture and without adding any PLE. This group consists of three MPC specimens including GD10, GD25, and GD50. The third group is designed by using the GnP and the PLE consisting of three MPC specimens; GS10, GS25, and GS50. Finally, the fourth group is prepared to study the effect of the PLE on the MPC paste. This group consists of three MPC specimens including SR10, SR20, and SR50. The mix proportions of the MPC pastes are shown in table 10.

Table 10. The mix proportions of the GnP modified MPC specimens.

Sample ID	M/P [a]	W/P [a]	B/M [b] (%)	GnP/S [c] (%)	PLE [d] (%)
B6360	6.0	3.6	5.0	0	0
GD10	6.0	3.6	5.0	0. 1	0
GD25	6.0	3.6	5.0	0.25	0
GD50	6.0	3.6	5.0	0.5	0
GS10	6.0	3.6	5.0	0.1	10
GS25	6.0	3.6	5.0	0.25	10
GS50	6.0	3.6	5.0	0.5	10
SR10	6.0	3.6	5.0	0	0.01 [e]
SR25	6.0	3.6	5.0	0	0.025 [e]
SR50	6.0	3.6	5.0	0	0.05 [e]

[a] molar ratio.

[b] mass ratio between boric acid and MgO.

[c] mass ratio between GnP and total solid.

[d] mass ratio between surfactant and GnP.

[e] mass ratio between surfactant and total solid.

4.3 INFLUENCE OF GNP ON THE SETTING BEHAVIOR AND THE WORKABILITY

Setting time of cement paste is the time when the cement paste starts losing its plasticity. The setting time behavior for any concrete-like material depends on several factors including water content, temperature, salt amounts, type and amount of the used additives, and chemical combinations. By using the Vicat apparatus and the needle, the setting time is measured for

each MPC specimen and compared in figure 30. The experimental results indicate that the addition of the GnP can decrease the initial setting time of the MPC paste. Without using the PLE (Pristine GnP), adding of 0.1 wt%, 0.25 wt% and, 0.5wt% of GnP reduces the initial setting time by 40%, 60%, and 67% respectively. Meanwhile, the effect of the GnP is becoming less when the PLE is added to the mixture due to its ability to cover the GnP particles. Adding 0.1wt%, 0.25 wt% and, 0.5wt% of GnP with the presence of the PLE reduces the initial setting time by 33%, 47%, and 60% respectively.

On the other hand, the experimental results approved that the presence of the GnP can play a significant role in the workability of the system. Figure 31 shows the influence of the GnP content on the fluidity of the MPC paste. It can be observed that adding the GnP to the MPC paste reduces its workability. Adding 0.1wt%, 0.25 wt% and, 0.5wt% of GnP without using the PLE reduces the fluidity of the paste by 4.5%, 18%, and 22.5% respectively. Similarly, the fluidity of the MPC pastes has been reduced by adding the PLE to the mixture. Adding 0.1wt%, 0.25 wt% and, 0.5wt% of GnP with the PLE can reduce the fluidity by 2%, 12%, and 15% respectively. This reduction in the fluidity may be attributed to the presence of the GnP as a hydrophobic material which entraps some water inside the system [125]. Another possible reason for this reduction is the ability of the GnP to absorb water due to its high surface area [84, 126, and 127]. On the other side, using the PLE can reduce the effect of the GnP in the system due to its ability to coat the GnP particles and improving its solubility in the aqueous solvent.

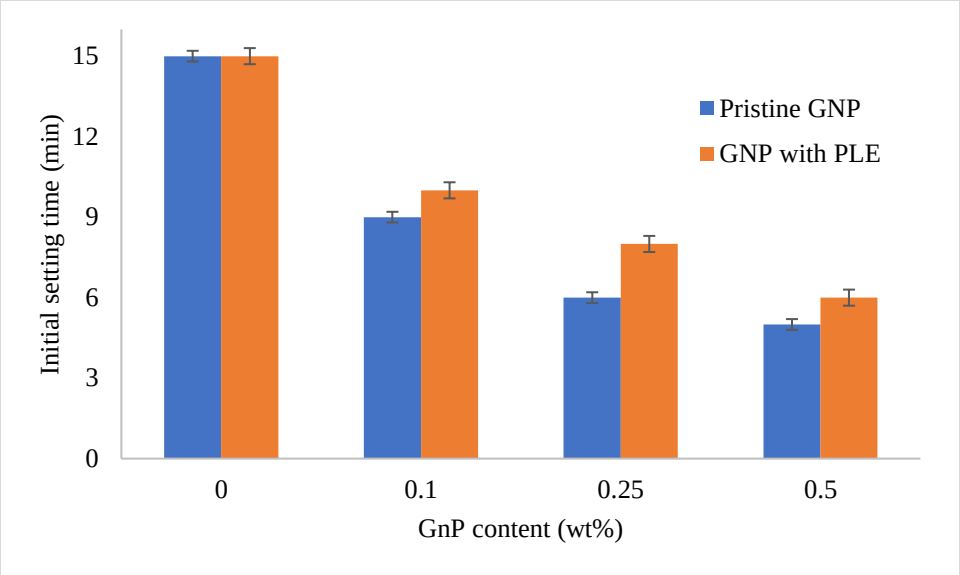

Figure 30. Effect of GnP content on the initial setting time of the MPC paste.

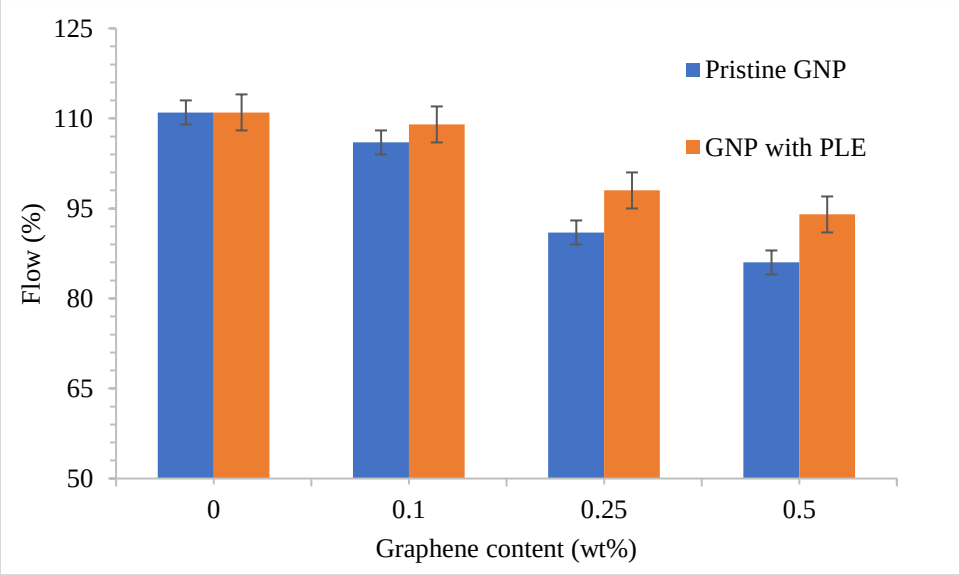

Figure 31. Influence of GnP content on the fluidity of the MPC paste.

4.4 INFLUENCE OF GNP ON THE COMPRESSIVE STRENGTH

Figure 32 shows the effect of the GnP content on the compressive strength of the MPC paste. It can be observed that the compressive strength is decreased with increasing the GnP

content. For example, adding 0.5 wt% of GnP without using the PLE (Pristine GnP) can reduce the compressive strength of paste by 40%. This reduction in the compressive strength can be attributed to the ability of GnP of hindering the reaction between the MgO and the KDP particles. Although there is no evidence of any chemical interaction between graphene and magnesium, there is an evidence of a physical interaction between the surface of graphene and magnesium ions (Mg^{+2}). These types of interactions have been observed recently by using a high-resolution TEM [128]. Thus, the GnP can absorb some of the magnesium ions leading to reduce the amount of reacted magnesia and reduce the amount of the k-struvite in the system. This reduction in the amount of k-struvite can significantly reduce the compressive strength.

Furthermore, the same behavior is found after using the PLE to enhance the dispersion of the GnP powder. As the GnP content increases, the compressive strength decreases. Adding 0.1wt%, 0.25 wt%, and 0.5wt% of GnP with the PLE can reduce the compressive strength by 23%, 36%, and 40% respectively. However, it can be observed that the reduction in the compressive strength was less when the PLE has been used in the system. This observation may be referred to the role of the surfactant in the system. As previously noted, the main role of the surfactant is to improve the solubility of the GnP in the aqueous solvents. The PLE particles have the capacity to be adsorbed onto the carbon surface and prevent graphene-graphene interaction. Thus, the PLE particles can coat the GnP surface and functionalize it noncovalently [129]. This coating of the graphene particles can reduce the amount of adsorbed Mg^{+2} onto the graphene surface and reduce the effect of the GnP on the compressive strength.

Another series of the MPC specimens are prepared by adding the PLE alone in order to investigate the influence of the used surfactant on the compressive strength of the paste. Although the amount of the used surfactant is tiny, the results demonstrate that the addition of the PLE can

impact the mechanical properties of the MPC paste. Figure 33 shows the effect of the PLE content on the compressive strength of the MPC paste. The compressive strength decreases when the PLE content increases. For example, using 0.05 wt% of the PLE which is the required amount to prepare an MPC mixture with 0.5wt % of GnP can reduce the compressive strength by 41%. However, the performance of the MPC specimens prepared by using the PLE and the GnP together is better than those specimens that prepared with the GnP alone. This discrepancy in the results can be explained as follows; the using of GnP powder and without using the PLE can either hinder the reaction by absorbing the Mg^{+2} particles or reduce the amount of the available water which is required to complete the acid-base reaction. Therefore, the amount of the k-struvite will be reduced in both cases leading to a considerable reduction in the compressive strength. Similarly, using the GnP with the PLE has an adverse influence on the compressive strength due to reducing the amount of reacted particles. However, the presence of the PLE can reduce the effect of the graphene by coating the GnP and hindering the physical interaction between the GnP and the Mg^{+2} particles. In the same manner, the presence of the GnP can also reduce the effect of the PLE by its tendency to absorb the PLE particles due to the electrostatic force between them [129]. Thus, adding the PLE with the GnP particles is better than adding the GnP alone or the PLE alone.

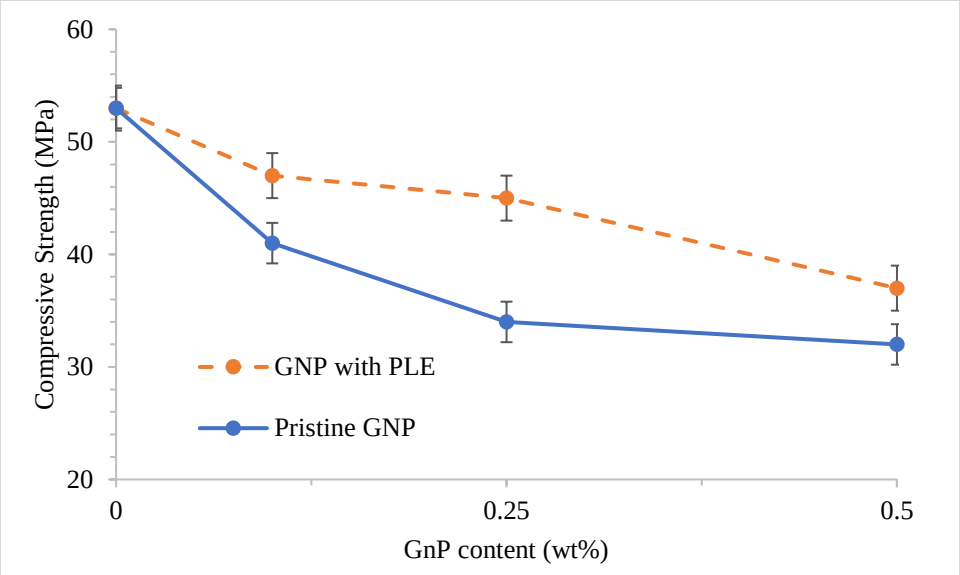

Figure 32. Influence of GnP content on the compressive strength of the MPC paste.

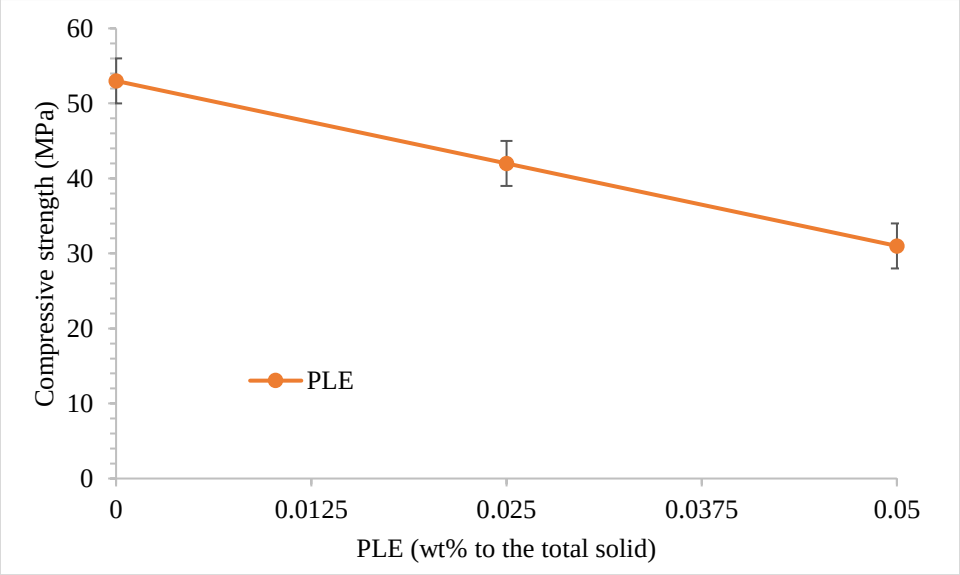

Figure 33. Influence of PLE content on the compressive strength of the MPC paste.

4.5 PHASE ANALYSIS

Figure 34 shows the XRD analysis of the 7-days cured MPC paste with different GnP contents and without using the PLE. All the three specimens have the same M/P, W/P, and B/M ratios while the GnP/S ratio is changed gradually. According to the literature databased for the XRD analysis, the results demonstrate that the main reaction product of the MPC system is the well-known k-struvite ($MgKPO_4*6H_2O$). Also, the XRD patterns show a firm MgO diffraction characteristic peaks which indicates that the MPC system has a high amount of unreacted magnesia content.

It can be seen that the MPC specimen with no GnP content exhibited stronger k-struvite characteristic peaks which indicates that more k-struvite could be formed in this specimen. Maybe this observation can explain why the MPC paste with no GnP has more compressive strength. On the other side, the diffraction peak intensity of k-struvite for 0.025wt% of GNP specimen is weaker than no GnP containing specimen. The amount of crystalline k-struvite, in this case, is much lower. As a result, when the GnP/S ratio increases, the crystallinity of the k-struvite decreases. On the other hand, the amount of unreacted magnesia is found to be much higher for the GnP containing MPC. Therefore, adding the GnP to the MPC paste can reduce the amount of the crystalline k-struvite and change the phase composition leading to a significant reduction in the compressive strength. Although the XRD results demonstrate that there is no any chemical reaction between the graphene and the raw materials of the MPC paste (MgO, KDP, and B), but there is a significant influence of GnP on the phase formation of the MPC system. The presence of GnP can reduce the amount of reacted particles and the amount of the crystalline k-struvite. This reduction in the final product is due to the tendency of the dissolved particles in the MPC system (Mg^{+2} and PO_4^{-3}) to stick with the graphene surface during the hydration process [130 and 131]. This interaction

between the graphene and the MPC ingredients can reduce the amount of the reactant particles and produce less amount of k-struvite. Since the k-struvite is responsible for the strength and the durability of the MPC, the compressive strength also is decreased.

The X-ray diffractograms for another series of MPC paste is presented in figure 35. This series is prepared by adding different percentages of the PLE, and without adding any GnP. All the MPC compound proportions are kept constant while the amount of the PLE is increased gradually. Based on the shown XRD patterns, there is an adverse effect of the PLE on the k-struvite formation. As the PLE content increases, the intensity of the k-struvite characteristic peaks decreases. This observation could explain the low compressive strength of these two specimens.

Moreover, the influence of implementing the GnP with the PLE has been evaluated using the XRD analysis. Figure 36 illustrates the XRD diffractograms of B6360, SR50, and GS50 specimens respectively. The MPC specimen with no GnP/PLE content (B6360) exhibits the strongest k-struvite characteristic peaks. After adding the PLE to the mixture (SR50), the diffraction peaks intensities of the k-struvite have been reduced. When the GnP and the PLE are used together (GS50), the diffraction peaks intensities of the k-struvite are found to be higher. Thus, adding the GnP and the PLE together can lead to a better k-struvite formation and stronger MPC pastes compared to adding the PLE or the GnP alone. This observation is attributed to the fact that the presence of the PLE can reduce the effect of the graphene by coating its particles and hindering the physical interaction between the GnP and the Mg^{+2} particles. In this case, the amount of the absorbed Mg^{+2} particles are becoming less leading to provide more magnesium ions in the system and produce more k-struvite.

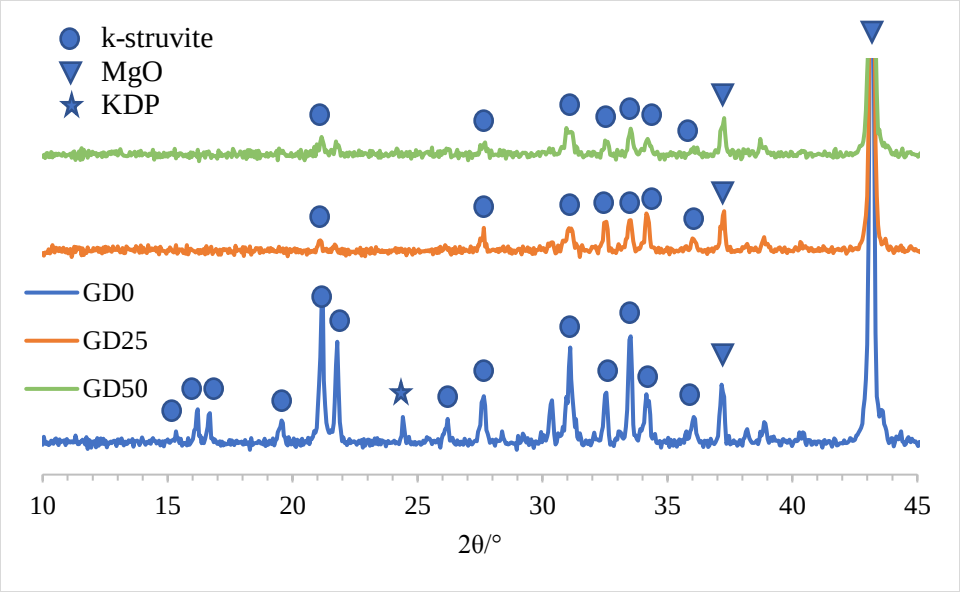

Figure 34. XRD diffractograms of the MPC pastes with different GnP contents and without using the surfactant.

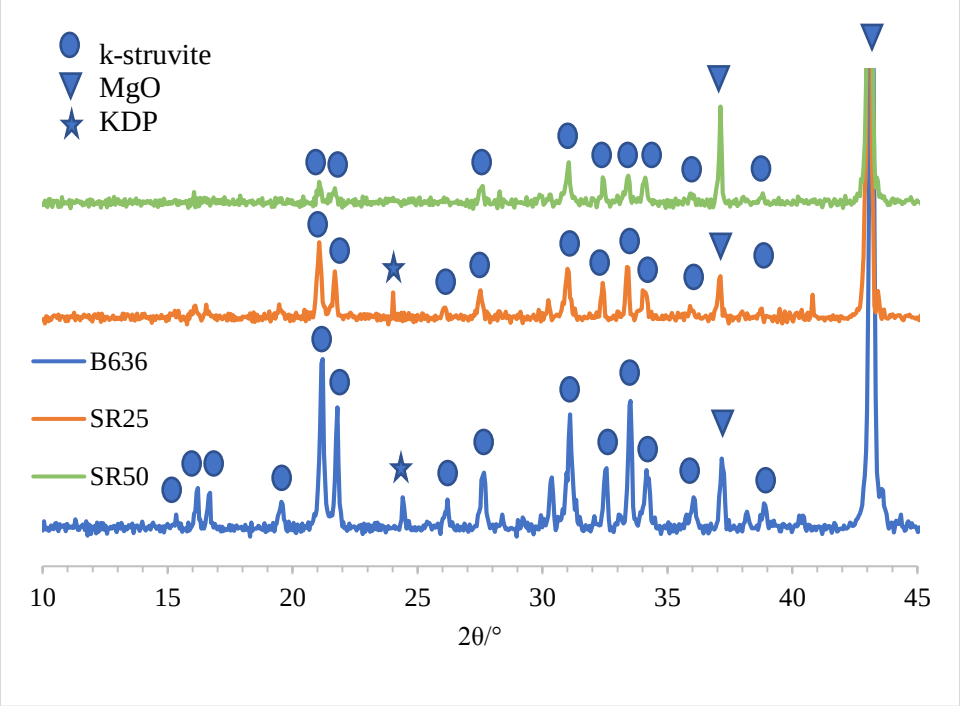

Figure 35. XRD diffractograms of the MPC pastes with different surfactant contents.

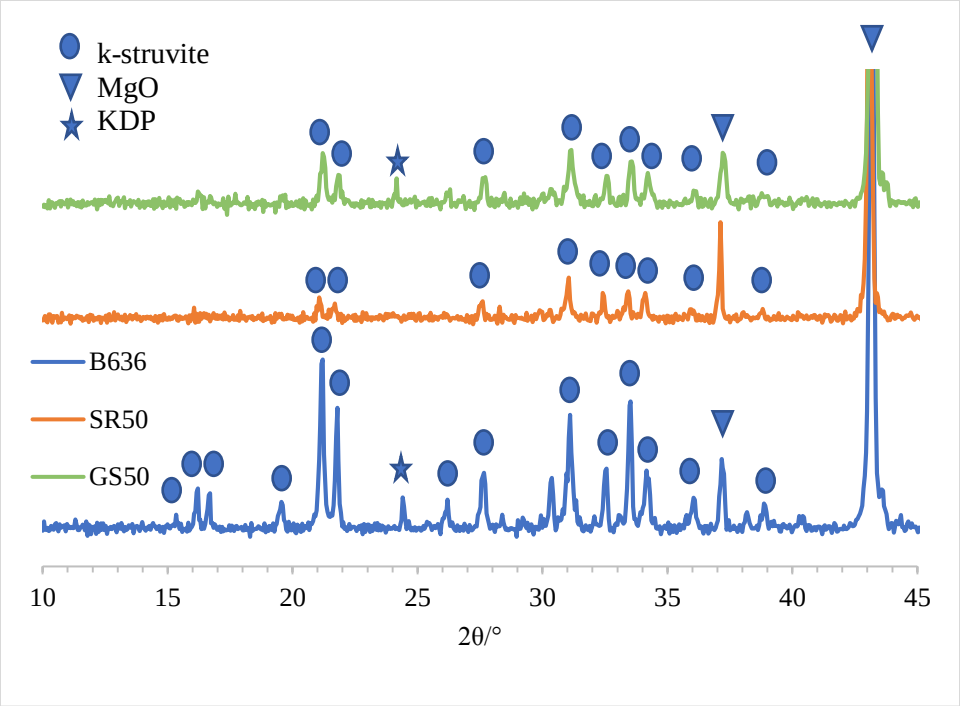

Figure 36. XRD diffractograms of B636, SR25, and GS25 specimens respectively.

4.6 FOURIER-TRANSFORM INFRARED SPECTROSCOPY (FTIR)

The FTIR test has been conducted in order to investigate if there is a chemical interaction between the GnP and the MPC paste ingredients/product. The FTIR spectra for the MPC specimens with different GnP dosages are shown in figure 37. The FTIR spectra illustrate an H-O-H stretching vibration at a region of 3500 to 2500 cm^{-1}. This H-O-H stretching vibration mode is related to the presence of the water in the k-struvite crystals. Besides, the FTIR result shows a bending vibration mode of H-O-H group at about 2100 cm^{-1}. Also, the band that located at about 1000 cm^{-1} indicates a stretching vibration mode of the PO_4^{-3} in the k-struvite crystals while the peak located at about 700 cm^{-1} indicates the binding vibration mode of the PO_4^{-3} [114, and 115].

The same IR characteristic peaks have been obtained after adding the GNP to the MPC mixture. There are no new bands observed when the GNP is added. This observation confirms the

results obtained from the XRD analysis and can demonstrate that there is no any chemical reaction between the GnP and the MPC paste components.

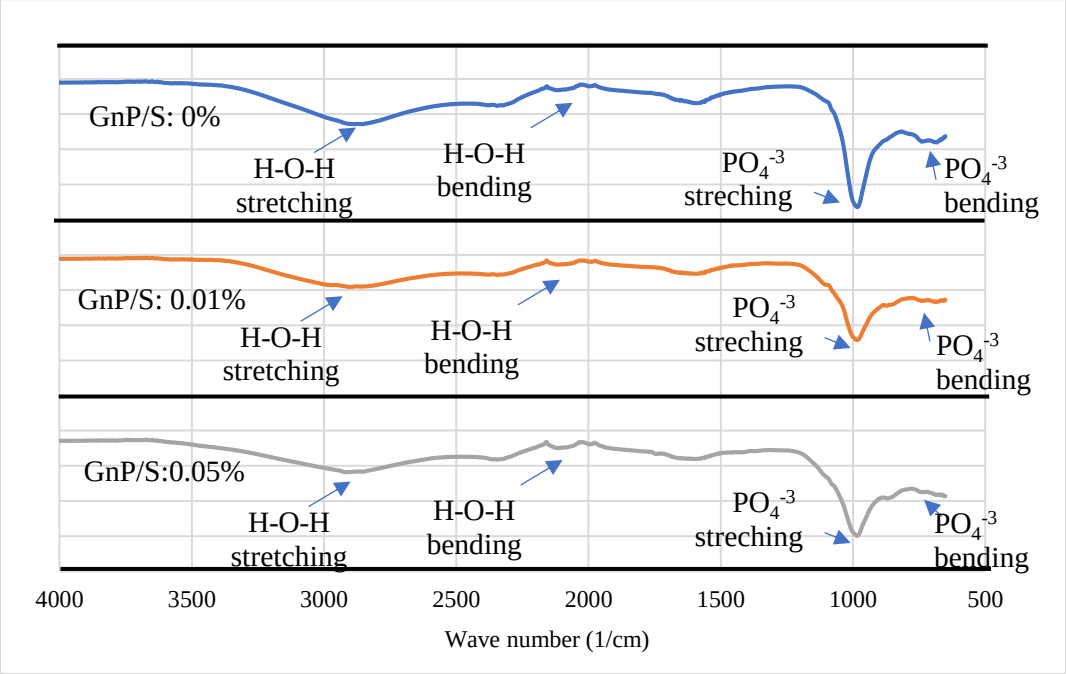

Figure 37. FTIR spectra of MPC paste with GnP content.

4.7 MICROSTRUCTURE ANALYSIS

The microstructure of the GnP modified MPC paste without using the PLE is presented in figure 4.9. The SEM images illustrate that the GnP modified MPC consists of two types of material with very different morphology (figure 38. a). The first type, the dashed-line rectangle, is the GnP while the second type, the solid-line rectangle, is the cementitious material. It can be seen that the morphology of the MPC paste shows a lot of unreacted MgO which covers the k-struvite microstructure (figure 38. b). Furthermore, the SEM images show that the GnP material is located alone without any chemical interaction with the MPC main ingredients (figure 38. c, and d).

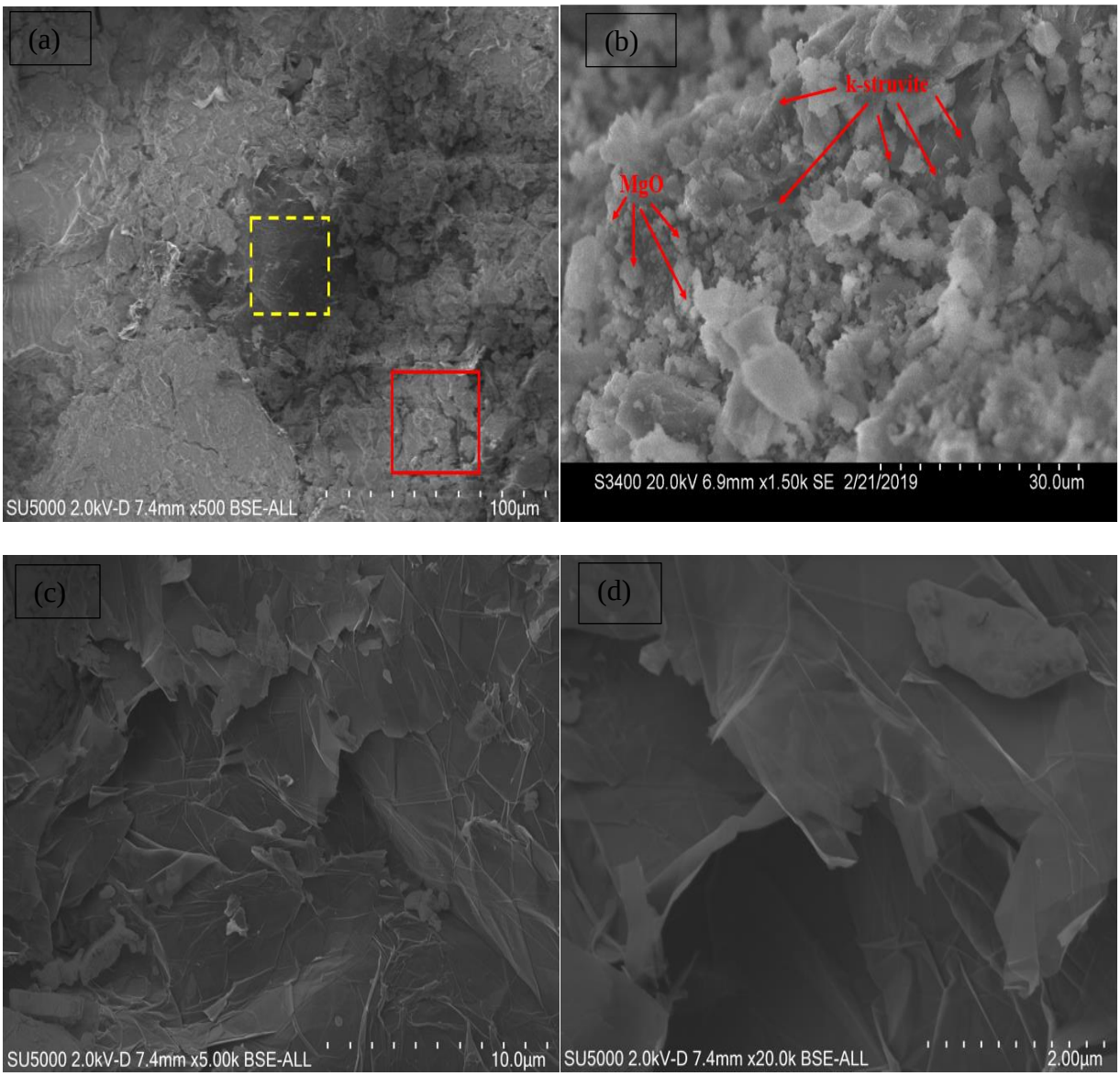

Figure 38. The microstructure of the GnP modified MPC paste without using the PLE.

After the presence of the PLE, The SEM images have not shown any GnP material. Figure 39 shows the microstructure of the GnP modified MPC pastes with the presence of the PLE. Also, two kinds of material have observed using SEM. The first one, the dashed-line rectangle, is the typical cementitious material for the MPC paste while the second one, the solid-line rectangle, is a smooth surface material without any crystalline shape. The SEM analysis shows a prism-like

crystalline structure of k-struvite and some of unreacted MgO (figure 39. b). It should be noted that the prevalence of the unreacted MgO is found to be lower compared to the previous specimen. On the other hand, no any crystalline shapes have been observed for the smooth surface spots (figure 39. c and d). These smooth surface spots could be a coated GnP material by the PLE and a combination of unreacted MgO and amorphous k-struvite.

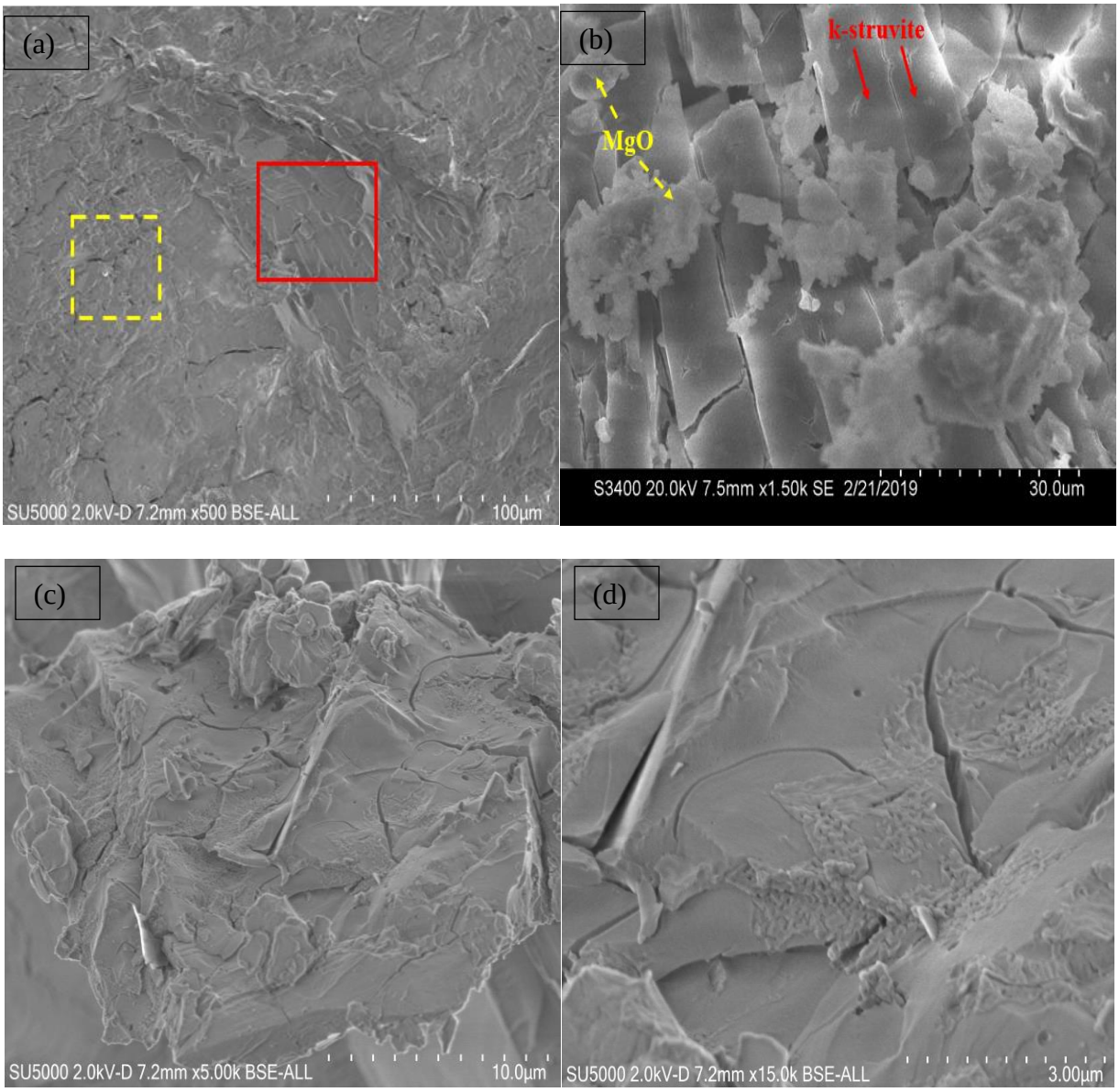

Figure 39. The microstructure of the GnP modified MPC paste with the PLE.

4.8 THERMAL CONDUCTIVITY

The thermal conductivity test was conducted for a series of MPC specimens with different GnP dosages to study the effect of the GnP on the thermal behavior of the MPC paste. Table 11 summarizes the experimental results of the thermal conductivity test where figure 40 presents the thermal conductivity of the MPC as a function of GnP added. It can be observed that the thermal conductivity of the MPC pastes increased with the increasing of GnP content. The addition of 0.1 wt%, 0.25wt%, and 0.5 wt% of GnP improved the thermal conductivity of the pastes by 3%, 12%, and 16% respectively. This enhancement in the thermal conductivity is attributed to the high specific surface area of GnP particles which can fill the nanopores inside the system and improve the thermal conductivity and diffusivity of the MPC system [128].

Table 11. Experimental results for thermal conductivity test of dry MPC paste.

Sample ID	Dry Density (Kg/m^3)	Temperature (^oC)	Thermal Conductivity (W/mk)	Thermal Diffusivity (mm^2/s)	Disk Res. Ω
B6360	2204.475	21.2	1.776	0.689	13.46
GD10	2265.498	21.2	1.824	0.7383	13.49
GD25	2219.73	21.2	1.987	0.7745	13.44
GD50	2250.242	21.2	2.062	0.9248	13.45

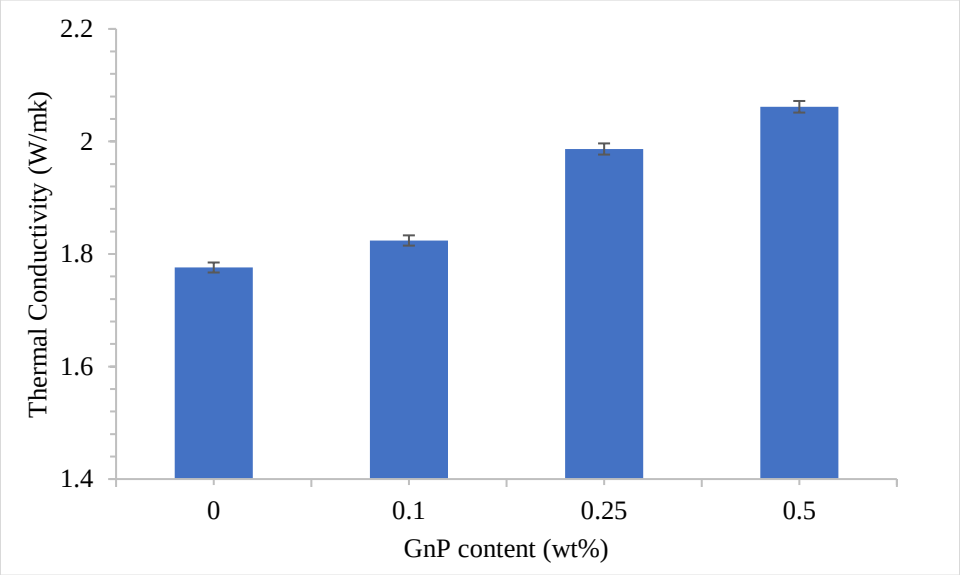

Figure 40. Influence of GnP content on the thermal conductivity of the MPC paste.

CHAPTER V

USING A HYBRID SYSTEM OF BORIC AND ACETIC ACID TO ENHANCE THE INITIAL SETTING TIME OF THE MPC PASTE.

5.1 INTRODUCTION AND LITERATURE REVIEW

In the last few decades, magnesium phosphate cement (MPC) was known for rapid rehabilitation of the concrete structures [62]. Traditionally, MPC was used as a repair material including rehabilitation of civil structures, concrete pavement, and damaged runways. This because the MPC has very rapid setting time in addition to its computability with a wide range of construction material [38]. For instance, the MPC material is known for its excellent bonding to old concrete structures [46].

As previously mentioned, the setting time of the MPC system is very rapid. Usually, the MPC paste/mortar cannot be used without a retarder. This because the maximum initial setting time that can be obtained for an MPC mixture with an adequate flowability is not more than 4 minutes. The most popular retarders suggested for MPC mixes is the boron compounds including borax ($Na_2B_4O_7 \cdot 10H_2O$) and boric acid (H_3BO_3). Occasionally, even with the use of a retarder, the setting time of the MPC paste may not enough to use the paste in the various applications. Based on the study that mentioned in chapter three from this research, by using the boric acid, the maximum setting time for the MPC paste with an adequate flowability and acceptable compressive strength is in a range of 15 to 18 minutes. Furthermore, a similar result has been achieved when the borax is used to retard the MPC paste. Li et al. [78] found that the improvement in the setting

time due to the use of borax was not enough to handle the paste for real-life applications the maximum setting time that could be achieved, by using borax compound, is 7 minutes. Thus, searching for new compatible additives/retarder to control and retard the reaction without affecting the other properties is still desperately needed.

There are only a few studies that have focused on the impact of new additives/retarders on the initial setting time of the MPC paste. Tan et al [77]. used a hybrid system of borax and polycarboxylate superplasticizer (PCE) to improve the fluidity loss and increase the setting time of the MCP paste. They reported that the PCE can delay the reaction of the MPC by improving the stability of the magnesium-based borate layer which can prevent the dissolution of the MPC ions. Jun et al. [83] reported that the used of acetic and boric acid together improved the setting time and the microstructure of the system and leaded to better mechanical strength.

In this chapter, the acetic acid is used with the boric acid to enhance the initial setting time of the MPC system. At first, the acetic acid is used alone to investigate its influence on the MPC paste behavior. Then, a hybrid system of acetic and boric acids is used with different MPC mixtures to improve the setting behavior of the MPC. The study includes physical, mechanical, chemical, and thermal characterization of the MPC paste with different acetic acid dosages in addition to its microstructure.

5.2 SPECIMENS PREPARATION

In this chapter, the MPC specimens are prepared by mixing MgO, KDP, boric acid, acetic acid, and distilled water. Based on the study mentioned in chapter three from this research, the optimum B/M ratio is found to be 5%. Therefore, the B/M ratio of 5% has been used for the hybrid system in order to improve the initial setting time of the system. The amount of acetic acid is

calculated based on the concentration of acetic acid in the aqueous solution (AAC). Three different series of MPC paste are designed and prepared to study the influence of acetic acid. For each series, the M/P, W/P, and B/M ratios are kept constant, while the acetic acid concentration is changed for each specimen. The first series (A3) is prepared to investigate the influence of using acetic acid alone on the MPC paste behavior. In this series, no boric acid is used with the MPC paste while the AAC is increased gradually from 0 to 7.5%. The second and the third series (AB3-22 and AB6-36) are used to investigate the influence of the hybrid system on low and high M/P ratio MPC specimens. In the second series; the M/P, W/P, and B/M ratios are selected to be 3, 2.2, and 5% respectively while the AAC is changed from 0 to 7.5%. In the third series; the M/P, W/P, and B/M ratios are selected to be 6, 3.6, and 5% respectively and the ACC in increased gradually from 0 to 7.5%. By selecting these W/P molar ratios, both series are having almost the same fluidity. The mix proportions of the acetic acid modified MPC specimens are shown in table 12.

Table 12. The mix proportions of the acetic acid modified MPC specimens.

MPC-Series	Sample ID	M/P [a]	W/P [a]	B/M [b] (%)	AAC [c] (%)	Flow
A3-22	A32200	3	2.2	0	0	Over
	A32225	3	2.2	0	2.5	Over
	A32250	3	2.2	0	5	Over
	A32275	3	2.2	0	7.5	Over
AB3-22	AB3225000	3	2.2	5%	0	116
	AB3225025	3	2.2	5%	2.5	116
	AB3225050	3	2.2	5%	5	110

	AB3225075	3	2.2	5%	7.5	109
AB6-36	AB6365000	6	3.6	5%	0	111
	AB6365025	6	3.6	5%	2.5	109
	AB6365050	6	3.6	5%	5	106
	AB6365075	6	3.6	5%	7.5	106

- [a] molar ratio.
- [b] mass ratio between boric acid and MgO.
- [c] acetic acid concentration in the aqueous solution.

5.3 INFLUENCE OF ACETIC ACID ON THE MPC SETTING BEHAVIOR

Figure 41 shows the influence of using acetic acid with/without the presence of boric acid on the initial setting time of the MPC paste. At first, the acetic acid is used alone in order to investigate its influence on the initial setting time. It can be seen, that the addition of the acetic acid can increase the initial setting time of the pastes. The setting time test indicates that the initial setting time of the pastes increases by increasing the concentration of the acetic acid. For example, using an acetic acid concentration of 5% can increase the initial setting time of the paste from 3 minutes to 12 minutes. On the other hand, the addition of the acetic acid alone has the ability to increase the volumetric expansion/cracks of the MPC specimens during the curing process. Figure 42 shows the MPC cube specimens prepared with different acetic acid concentrations. As shown in the figure, when the AAC increases, the expansion cracks of the cube surfaces increase. Moreover, it can be observed that using 7.5% of AAC can cause a high volumetric expansion of the paste during the curing process leading to early failure of the MPC specimen. On the contrary, adding the boric acid to the same mixtures can prevent these

expansion cracks. Figure 43 shows the MPC cube surfaces of an MPC specimen with 7.5% of acetic acid and 5% of the boric acid. It can be observed that the volumetric expansion cracks are disappeared when the boric acid is added.

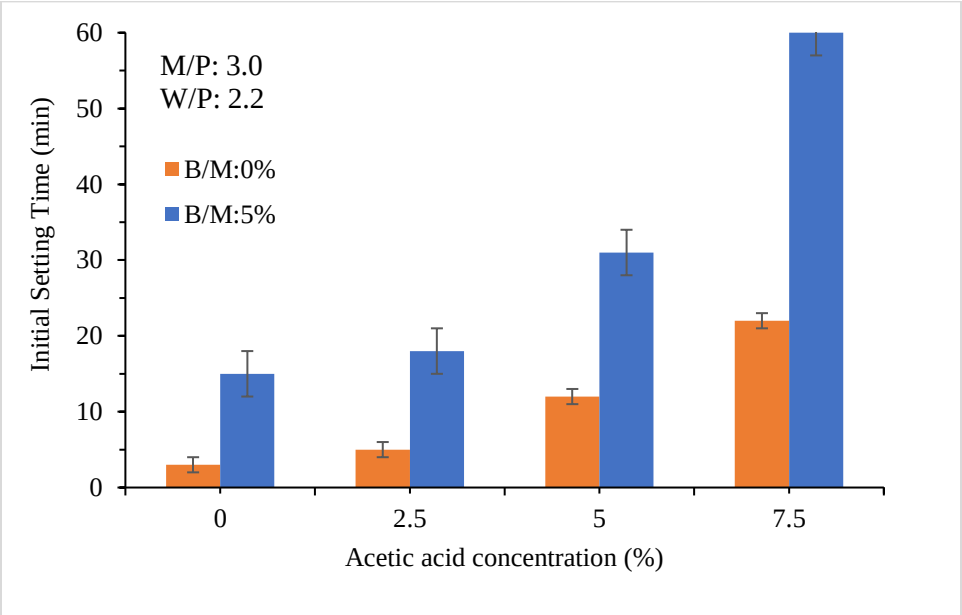

Figure 41. Influence of using acetic acid with/without the presence of boric acid on the initial setting time of the MPC paste.

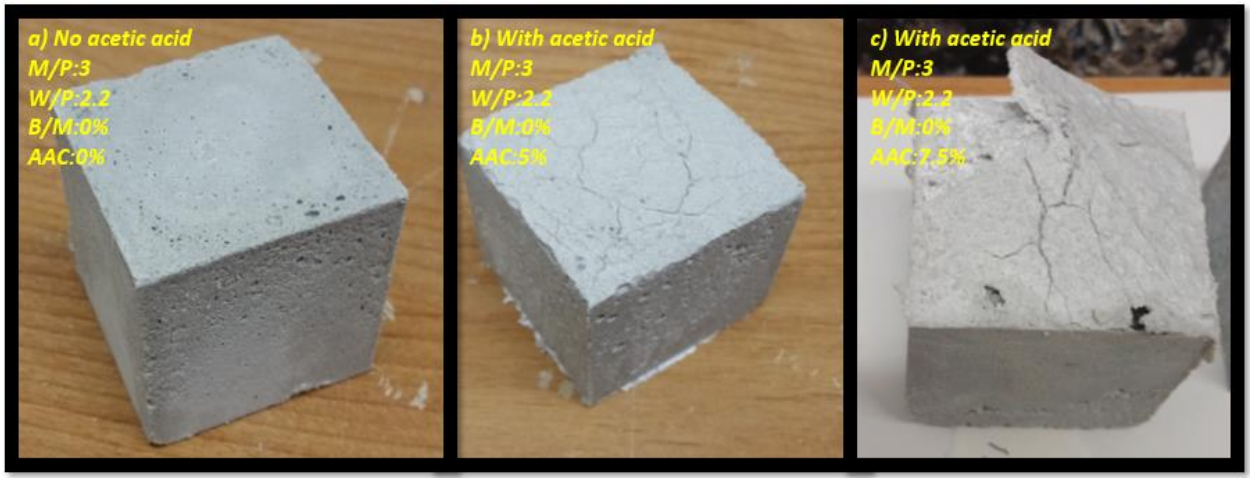

Figure 42. Expansion cracks of MPC specimens with different AAC.

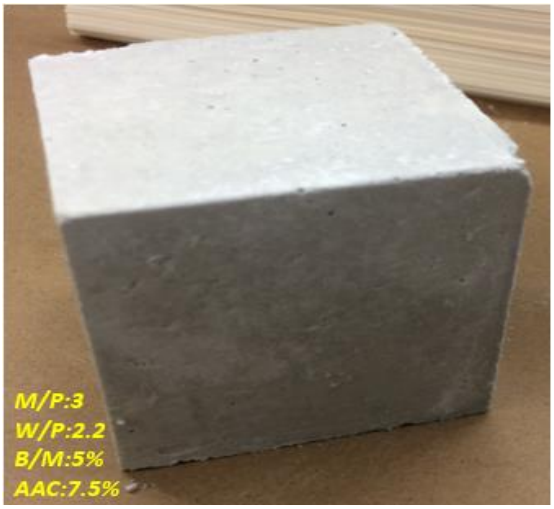

Figure 43. MPC paste with 5% of B/M ratio and 7.5% of ACC.

After achieving these observations, only the hybrid system is used to retard the MPC paste. Moreover, the using of both acids to retard the MPC system is found to be more efficient. For example, at M/P and W/P ratios of 3 and 2.2 respectively, using an AAC of 5% can increase the initial setting time from 3.5 to 12 minutes, while adding 5% of boric acid to the same mixture can increase the initial setting time from 12 to 31 minutes. Thus, using a hybrid system of both acids is found to be more efficient regarding the initial setting time. Furthermore, the hybrid system of both acids is evaluated with a high M/P ratio MPC paste. Figure 44 illustrates the influence of AAC on the initial setting time of a high M/P ratio MPC paste with the presence of the boric acid. Based on the experimental results, the hybrid retardation system is found to be very active to improve the setting behavior of an MPC paste with high M/P ratio. For example, the initial setting time of the paste has increased from 15 minutes to 45 minutes by adding 7.5 % of acetic acid and 5% of boric acid to the mixture.

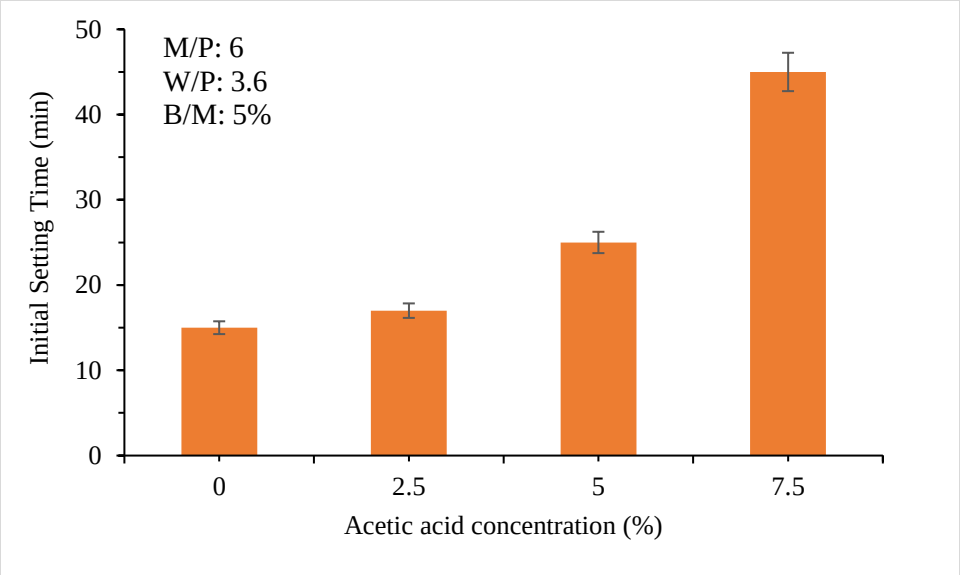

Figure 44. Influence of using acetic acid with boric acid on the initial setting time of the MPC paste.

5.4 COMPRESSIVE STRENGTH

Since the using of both acids can prevent the volumetric expansion cracks and increase the initial setting time efficiently, only the influence of the hybrid system on the compressive strength of the MPC paste has been studied and illustrated in this research. As previously mentioned, the optimal B/M ratio of 5 % is used with different AAC while the influence of the hybrid system has been studied with low and high M/P ratio MPC paste (AB3-22 and AB6-36 series respectively).

Figure 45 show the influence of the hybrid retardation system on the compressive strength of AB3-22 and AB6-36 series respectively. For both series, the compression test illustrates that the compressive strength of the MPC paste decreases when the AAC increases. Moreover, increasing the AAC can decrease the initial stiffness and the toughness of the MPC specimens. For B3-22 series, adding 2.5%, 5% and 7.5% of AAC can decrease the compressive strength by 2%, 60%, and 87% respectively. For AB6-36 series, adding 2.5%, 5% and 7.5% of AAC can decrease

the compressive strength by 35%, 45, and 53% respectively. Thus, the influence of the acetic acid on the compressive is much higher with these MPC specimens that has low M/P ratio. Therefore, the using of the acetic acid is more suitable with high M/P molar ratio. For example, adding 5% of AAC with M/P, W/P, and B/M ratios of 6, 3.6, and 5% respectively can increase the initial setting time to 25 minutes and reduce the compressive strength to 31 MPa which can meet the requirement to use the MPC paste for a wide range of real-life applications.

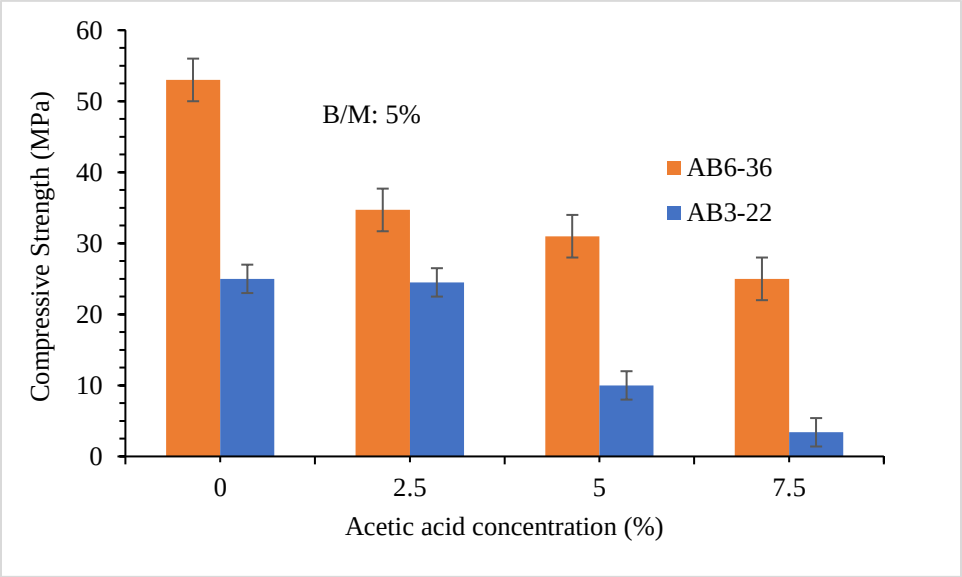

Figure 45. Influence of acetic acid concentration on the compressive strength of the MPC paste with the presence of the boric acid.

5.5 PHASE ANALYSIS

Figure 46 show the XRD results for MPC specimens with no acetic acid, 2.5% of AAC, and 7.5 % of AAC respectively. All the presented MPC specimens in this figure has low M/P ratio and B/M ratio of 5%. The XRD results demonstrate that the main reaction product of the acid-base reaction is the k-struvite (MKP). Moreover, the XRD patterns show strong MgO diffraction

characteristic peaks which indicates that a lot of unreacted magnesia has been existed in the MPC pastes. On the other hand, the XRD analysis demonstrates that no acetate-containing crystalline phases have formed during the reaction process. However, the using of the acetic acid can change the phase compositions of the MPC paste specimens. It can be seen that the MPC specimen with no acetic acid exhibit stronger k-struvite characteristic peaks. Furthermore, some of the k-struvite diffraction peaks are disappeared when the boric acid is added. For example, the k-struvite peaks that located at about 21.2, 27.6, 33.5, and 34.3 2θ are disappeared when the AAC is 7.5%. This observation concludes that the existence of the acetic acid leads to poor crystal growth and maybe less amount of the K-struvite phase. On the other side, the MPC specimen that has high AAC exhibits stronger KDP characteristic peak which indicates that the presence of the acetic acid increases the amount of unreacted KDP. With increasing the AAC, the amount of the unreacted MgO and KDP increase where the amount of the K-struvite decreases. Thus, the using of the acetic acid can prevent the contact between the MgO and KDP particles leading to reduce the amount of the K-struvite. Since the K-struvite is responsible for the strength and durability of the MPC paste, reducing the amount of the K-struvite will reduce the compressive strength of the MPC specimens.

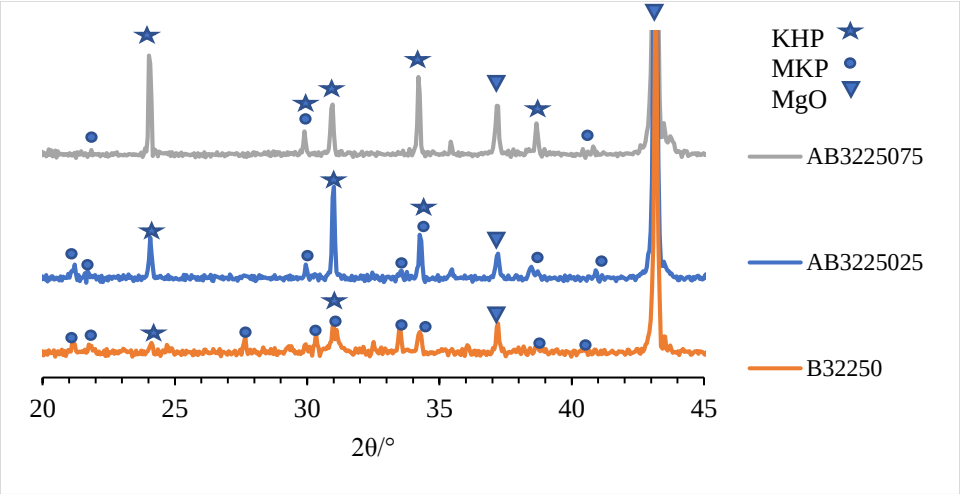

Figure 46. The XRD patterns for MPC paste with low M/P ratio.

5.6 THERMAL CONDUCTIVITY

Thermal conductivity test is conducted for different MPC specimens in order to study the influence of the acetic acid on the thermal behavior of the MPC paste. Table 13 summarize the results of the thermal conductivity test of the MPC paste with different AAC where figure 47 presents the thermal conductivity and diffusivity of the MPC paste as a function of acitic acid added. The experimental results indicate that the thermal conductivity of the MPC paste decreases when the AAC increases. The addition of 2.5% and 7.5 % of AAC can decrease the thermal conductivity from 1.31 to 1.29 and from 1.31 to 0.96 W/mk respectively. Besides, the thermal diffusivity decreases by 28% when the AAC is 7.5%. This reduction in the thermal behavior may be attributed to the effect of the acetic acid on the dry density of the MPC paste. The dry density of the tested MPC specimens are shown in table 13. It is clear that the using of the acetic acid can decrease the dry density of the MPC specimens by increasing the internal voids. One possible reason of this reduction is the high thermal expansion of the acetic acid-containing specimens which can provide more voids in the paste and decrease its density. For example, adding 7.5% of AAC can reduce the dry density of the paste by 9%.

Table 13. Experimental results for thermal conductivity test of dry MPC paste.

Sample ID	Dry Density (Kg/m^3)	Temperature (ºC)	Thermal Conductivity (W/mk)	Thermal Diffusivity (mm^2/s)
B32250	2204.48	21.2	1.31	0.727
AB3225025	2135.82	21.2	1.29	0.610
AB3225075	2013.78	21.2	0.96	0.523

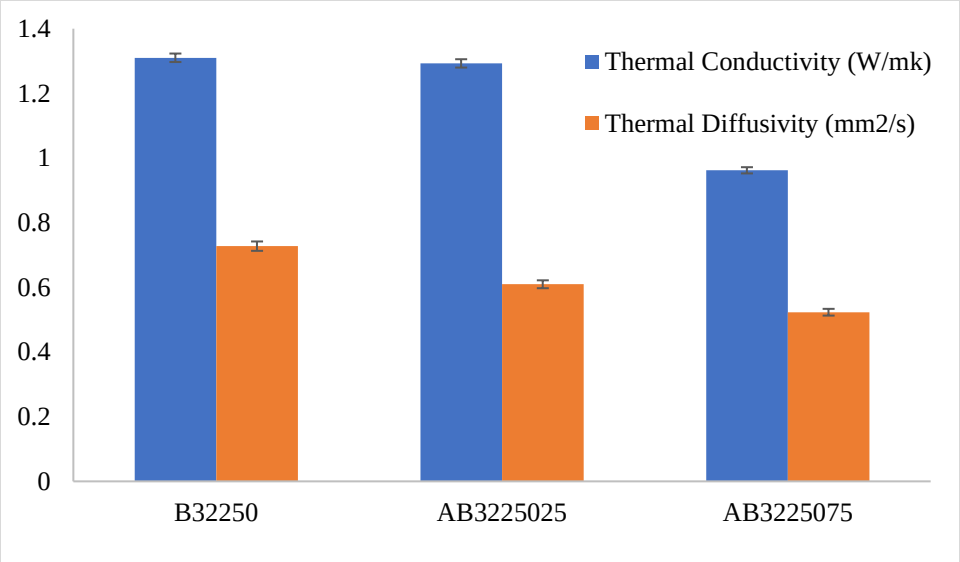

Figure 47. Influence of acetic acid concentration on the thermal conductivity of the MPC paste.

CHAPTER VI

ARTIFICIAL NEURAL NETWORKS (ANNS)

6.1 INTRODUCTION AND LITERATURE REVIEW

Artificial neural network (ANN) is an intelligent artificial system that has been used to solve and analyze a wide variety of mathematical and statistical problems. The idea of using artificial neural networks in various fields came from neural networks in animals and human brains [85]. ANN is very useful when used to create a model for a complex system especially when the relationship between the input and output groups is indirect or incomprehensible. Moreover, the ANN techniques have the ability to describe nonlinear relations between several variables. ANN consists of four main components including (1) neurons, (2) connections, (3) propagation function, and (4) learning rule.

ANN is composed of several processing nodes called neurons. All of these neurons are connected to each other through weighted connection lines to establish an intelligent network that capable of predicting the appropriate output. The function of these connection lines is transferring the outputs of several neurons to the input of the other neurons, where the input values are computed by the propagation functions. The learning rule is the used algorithm which adjusts and modifies the connection weights and threshold values during the several iterations.

Based on connection type classification, there are two types of ANNs; feedforward neural networks and feedback neural networks. In the feedforward neural network, each neuron in the same layer is receiving the input from the previous layer and providing the output for the next

layer to be used as input again. In the feedforward networks, all the neurons are engaged in a set of layers including inputs layer, middle (hidden) layers, and outputs layer. There are no connections between the neurons in the same layer. Usually, feedforward neural networks are used for approximations and predictions. In feedback neural networks, each neuron is receiving the input from all the previous neurons and providing one output for all next neurons to be used as one of their inputs. In other words, if the total number of neurons is n, each neuron should have (n-1) inputs and one output. Usually, feedback neural networks are used as optimization tools. ANN can be applied to accomplish many tasks in different engineering fields such as designing, forecasting, prediction, statistics, clustering, and classification [86]. In order to get an efficient ANN model, the datasets should be divided into three groups included training, testing, and validation data points [87]. At first, the relationships between each node will be generalized by using the training datasets to achieve the initial estimation for data patterns. Then the testing datasets will be processed to produce approximately correct estimation for the data patterns and to compromise the relations between each node. Finally, the model will be validated using the validation datasets to ensure that the model is effective and can predict accurate outputs.

Recently, ANN has been used widely to model many engineering experiments included concrete and construction areas. Many of these models have been prepared to predict the fresh and hardened properties of cement pastes and mortars [88]. Onal and Ozturk utilized an artificial neural network analysis to find the relationship between microstructural properties and compressive strength values of cement mortar [85]. Lee used the ANN technique to predict the mechanical strength of concrete cubes [89]. Alilou et al. used the ANN technique to predict the compressive strength of concrete after 28 days by using the third day compressive strength as an input [132]. Chopra et al. developed an ANN model to predict the compressive strength of concrete. They

reported that the using of ‘Levenberg-Marquardt’ algorithms to predict the concrete compressive strength can provide more than 95% accuracy [133]. Alshihri et al. evaluated the accuracy of predicting the compressive strength of lightweight concrete (LWC) using the ANN technique. They reported that the ANN technique is a sufficient tool for predicting the compressive strength of LWC [134]. In the last few years, the using of ANN technique has gone further. Dias and Pooliyadda developed an ANN model to estimate the mechanical strength and the flowability of high strength concrete blended with chemical admixtures and mineral additives [91]. Mohamed et al. utilized an ANN model to predict the surface area fraction and the phases correlation functions of cement material. Their model proved that the ANN techniques are beneficial in predicting the SEM images and the related correlation functions [90]. However, there is no mathematical/statistical model is found in the literature which describes the physical and the mechanical behavior of the MPC material.

MPC is very sensitive to the water and magnesia contents, and it can be affected by changing the proportions between MPC components. The hardened and fresh properties of MPC are highly dependent on the M/P ratio, W/P ratio, and B/M ratio. Moreover, these properties can be highly affected by using one or more of the compatible additives. On the other side, artificial neural network (ANN) has been utilized in a very emerging technological field, where the potential of connecting a customized material science research to real-world applications is becoming a necessity.

In this chapter, three databases have been used to develop the ANN models. For each database, two ANN models have been optimized, in the first model the input is the MPC paste or mortar ingredients, and the output is the predicted performance of interest; in the second model

the input is the performance of demand, and the output is the mix ingredients. For this study three-layers, feed-forward error backpropagation ANN model is developed utilizing a TR-SEQ1 model.

6.2 EXPERIMENTAL PROGRAM

As previously mentioned, the behavior of the MPC paste specimens can be driven by three main factors including magnesia to phosphate molar ratio (M/P), water to solid mass ratio (W/S) and boric acid to magnesia mass ratio (B/M). In this paper, the authors chose to represent the MPC pastes ingredients in molar ratios rather than the mass ratios terminology to capture the impact of the different MPC mix proportions (M/P and W/P ratios) on the acid-base reaction.

The selected MPC specimens for the ANN models are prepared using different proportions of the MPC main ingredients including magnesia to phosphate molar ratio (M/P), water to phosphate ratio (W/P), and boric acid to magnesia ratio (B/M). Moreover, two different additives are used to improve the performance of the MPC system including graphene nanoplatelets (GnP), and acetic acid (AA). The content of each additive is calculated based on different criteria such as; GnP to total solid ratio (GnP/S), and AA concentration (AAC) in the aqueous solvent. For each MPC specimen, one of the proportions between the main MPC ingredients/additives is changed while all the others are kept constant in order to investigate the influence of that proportion on the physical and mechanical properties of the MPC paste.

The mechanical and physical properties of several MPC paste mixtures are measured and recorded by following a comprehensive experimental program. The measured physical properties are: (1) the workability; which measured by the flow table test, and (2) the initial setting time of the fresh mixtures which measured by the Vicat approach. The mechanical properties of the MPC pastes are represented by the compressive strength of the 2" cube specimens which measured by

the 810 Material Testing System (MTS). Figure 48 shows the three testing machines for the prepared MPC specimens.

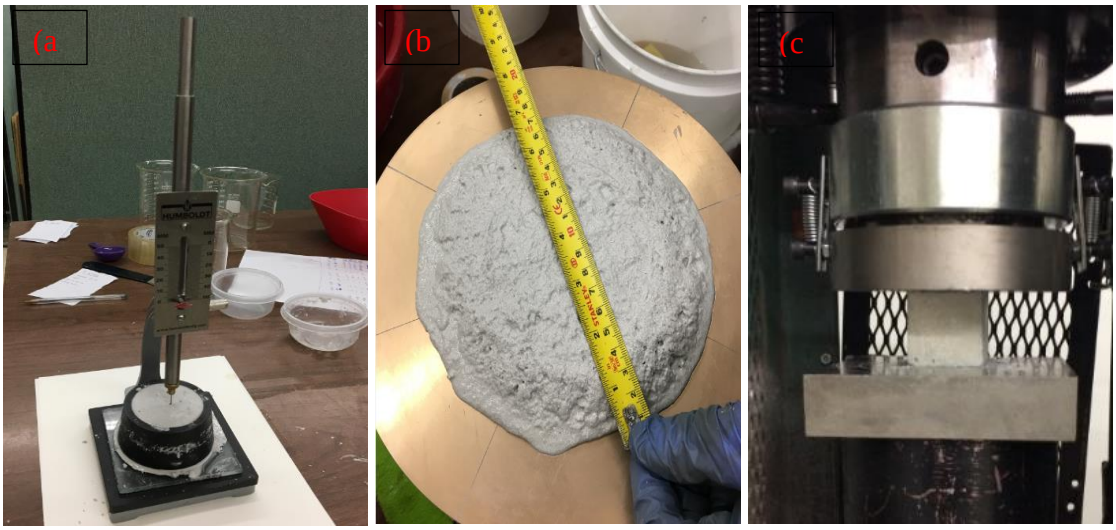

Figure 48. MPC testing program; a) Initial setting time test, b) flow table test, and c) compression test.

6.3 DATABASE DESCRIPTION

Since the mechanical and the physical properties are measured for three times of every MPC mixture, a total of 138 data sets are collected and used to develop the ANN models. Each data set consists of 8 different parameters/properties including (1) M/P molar ratio, (2) W/P molar ratio, (3) B/M mass ratio, (4) AAC, (5) GnP/S ratio, (6) flow, (7) initial setting time, and (8) compressive strength. If one or more additives are not used in any data set, a value of 0% would be reported. The 138 data sets can be classified based on the used additives as follows: (1) 72 data sets with different B/M ratios, (3) 42 data sets with different AAC and 5% of B/M ratios, and (4)

24 data sets with different GnP/S and 5% of B/M ratios. Table 14 summarizes the range of each MPC parameters/properties.

Table 14. The ANN modeling range of each MPC parameters/properties.

	M/P ratio	W/P ratio	B/M Ratio (%)	AAC (%)	GnP/S ratio (%)	Flow (%)	Initial setting time (min)	Compressive strength (MPa)
Minimum value	2	1.5	0	0	0	10	1	3.4
Maximum value	10	5.2	10	7.5	0.5	150	60	55

In this work, three different databases are used to develop the ANN models. In the first database (database # 1), each physical or mechanical MPC property is the average of three different measurements for the same MPC mixture. As a result, the 138 data sets are shortened to become 46. Then, the 46 data sets are divided into three different groups including training, testing, and validation data sets. The 46 data sets can be classified based on the used additives as follows (1) 42 data sets with different B/M ratios, (2) 14 data sets with different AAC, and (3) 8 data sets with different GnP/S ratios. In the second database (database # 2), the available 46 data sets have been manipulated to overcome the lack of sufficient data that represents the influence of the used additives. In other words, there is not enough data to describe the MPC behavior when the acetic acid or the GnP is added. For example, there are only 14 data sets available to describe the MPC behavior using acetic acid and only 8 data sets available to describe the influence of the GnP.

Therefore, all the data sets are divided based on the additive's classification. Then, some of the data sets are repeated in order to increase their weight and let the neural network understand their influence. These new data sets have been built as follows:

(1) The 24 data sets for different B/M ratios have been repeated for two times.

(2) The 14 data sets for different acetic acid concentrations have been repeated for three times.

(3) The 8 data sets for different GnP/S ratios have been repeated for three times.

As a result, a total of 114 data sets are achieved and used to develop another two ANN models. In the third database (database #3), all the available 138 data sets are sorted and used to develop the ANN models.

After sorting and classifying the data sets, two ANN models are developed and presented for each database. In the first models (ANN1-1, ANN2-1, and ANN3-1 for database #1, 2, and 3 respectively) the input variables are the MPC paste ingredients while the output variables are the predicted performance of interest. In the second models (ANN1-2, ANN2-2, and ANN3-2 for database #1, 2, and 3 respectively) the input variables are the performance of demand and the output variables are the mix ingredients. Table 15 summarizes the input and the outputs of ANN1-1, ANN2-1, and ANN3-1 models while table 16 summarizes the input and the outputs of ANN2-2, ANN2-2, and ANN3-2 models.

Table 15. Input/outputs of ANN1-1, ANN2-1, and ANN3-1 models.

Input	Outputs
M/P molar ratio	Flow (%)
W/P molar ratio	Initial setting time (min)
B/M ratio (%)	Compressive strength (MPa)
AAC (%)	-
GnP/S ratio (%)	-

Table 16. Input/outputs of ANN1-2, ANN2-2, and ANN3-2 models.

Input	Outputs
Flow (%)	M/P molar ratio
Initial setting time (min)	W/P molar ratio
Compressive strength (MPa)	B/M ratio (%)
-	AAC (%)
-	GnP/S ratio (%)

6.3 REGRESSION MODELS

In this work, a set of linear regression models are developed using Excel application in order to evaluate the efficiency of the used data sets in predicting the behavior of the MPC paste. Furthermore, this model can be used as a reference to evaluate the efficiency and the performance of the developed ANN models. Since a developing of one linear regression model to predict multi-outputs is not possible, one linear regression model is developed for each output. The same 47 data

sets that used for the ANN models are used to develop the linear regression prediction models. The developed regression models are divided into two main groups. In the first group, a total of three regression models are developed to predict the mechanical and the physical properties of the MPC pastes using the MPC paste ingredients as an input. Table 17 shows the input and the outputs of the developed regression models in the first group. In the second group, a total of 5 regression models are developed to predict the mix ingredients and by using the MPC properties as an input. Table 18 shows the input and the outputs of the developed regression models of the second group.

Table 17. Input/output variables of the first group regressions models.

Model ID	Input					Outputs
LN1	M/P ratio (%)	W/P ratio (%)	B/M ratio (%)	AAC (%)	GnP/S ratio (%)	Flow (%)
LN2	M/P ratio (%)	W/P ratio (%)	B/M ratio (%)	AAC (%)	GnP/S ratio (%)	Initial setting time (min)
LN3	M/P ratio (%)	W/P ratio (%)	B/M ratio (%)	AAC (%)	GnP/S ratio (%)	Compressive strength (MPa)

Table 18. Input/output variables of the second group regressions models.

Model ID	Input			Outputs
LI1	Flow (%)	Initial setting time (min)	Compressive strength (MPa)	M/P ratio (%)
LI2	Flow (%)	Initial setting time (min)	Compressive strength (MPa)	W/P ratio (%)
LI3	Flow (%)	Initial setting time (min)	Compressive strength (MPa)	B/M ratio (%)
LI4	Flow (%)	Initial setting time (min)	Compressive strength (MPa)	AAC (%)
LI5	Flow (%)	Initial setting time (min)	Compressive strength (MPa)	GnP/S ratio (%)

Table 19 summarizes the statistical measurements of the developed regressions models. The statistical analysis indicates that the available data cannot be represented using a set of linear regression models. Generally, the prediction of the physical and mechanical properties of MPC by using a set of regression models is not accurate. At first, the ANOVA test indicates that these three regression moles are significant. The significance F values are calculated to be $2.9x10^{-10}$, $6.3x10^{-13}$, and 4.9x10-^{06} for LN1, LN2, and LN3 models respectively. These low values indicate that the models are significant in term of predicting experimental data sets.

On the other hand, these models are not accurate in predicting the required output; and especially for the compressive strength. The R^2 is calculated to be 0.69, 0.77, and 0.49 for LN1, LN2, and LN3 models respectively. On the other hand, predicting the mix proportions of the MPC

paste by using its properties cannot be performed by using the regression models. From the conducted ANOVA test, all the regression models of the second group have very high significance F values. These high values indicate that the developed models are not significant in term of predicting the required output. Moreover, the R^2 of these five models is very low. For the second group models, the R^2 is calculated to be 0.07, 0.16, 0.01, 0.74, and 0.02 for LI1, LI2, LI3, LI4, and LI5 respectively.

Table 19. Statistical measurements of the developed regressions models.

Model ID	R^2	Standard Error	Significance F
LN1	0.69	17.908	$2.9x10^{-10}$
LN2	0.77	5.292	$6.3x10^{-13}$
LN3	0.49	9.043	$4.9x10^{-06}$
LI1	0.07	2.408	0.109
LI2	0.16	1.020	0.016
LI3	0.01	1.939	0.473
LI4	0.74	1.266	$3.9x10^{-13}$
LI5	0.02	0.013	0.230

6.4 ANN MODEL DEVELOPMENT

In this research, the different ANN models are developed and evaluated by using four different steps. In the first step, the available data sets are sorted based on the maximum and the minimum values for each parameter, and classified into three different groups including training,

testing, and validation. Then, the maximum number of hidden nodes (HN) is calculated using the following equation:

$$Max.\#\ of\ HN = \frac{\#\ of\ training\ data + \#\ of\ testing\ data - \#\ of\ outputs}{\#\ of\ inputs + \#\ of\ outputs + 1} \quad \text{.... Eq (2)}$$

this equation can provide a good estimation of the maximum number of hidden nodes ± 1 in order to afford a stopping criterion regarding the maximum number of hidden nodes for each ANN model. In the second step, the feed-forward back-propagation algorithm is applied, and the optimum number of the hidden nodes are determined by using Najjar et al. procedure [98-100]. This step includes three different stages as follows: (1) the neural network is trained and tested using the selected data sets, while the number of the hidden nodes is changing from 1 to the calculated maximum number of hidden nodes ± 1 for each network, (2) the performance of each network is investigated based on the statistical measurements including the average of the square error (ASE), the main absolute relative error (MARE), and the coefficient of determination (R^2), and (3) all the nural networks are collected and sorted based on the calculated ASE value from the lowest to the highest and the neural network that has the least ASE value is selected. In the third step, the selected neural network is validated using the validation data sets. In the fourth step, all the available data sets are used to train the model (training all) to improve the accuracy of the predicted value [98-100].

6.5 ANN NETWORK DEVELOPMENT OF DATABASE #1

A total of 47 data sets are used to develop the first two ANN models (ANN1-1 and ANN1-2). As previously noted, the 48 data sets are sorted based on the maximum and the minimum values for each parameter and divided into three groups as follows; (1) 24 data sets as a training, (2) 12 data sets as a testing, and (3) 10 data sets as a validation data set. By using the Eq (2), the maximum

number of hidden nodes is calculated to be 3.67. Since the Eq (2) provide an estimation value, the maximum number of hidden nodes is selected to be 5. Finally, the adaptive technique is used to find the optimum number of hidden nodes, and the best network is selected to represent the data.

6.5.1 ANN1-1 MODEL

ANN1-1 model is developed to predict the fresh and the hardened properties of the MPC pastes including flow, initial setting time, and compressive strength. The input and the outputs of this model are summarized in table 15. All the data sets are normalized and scaled in a range of 0-1 due to using of the sigmoidal function. Moreover, the data sets that contain the maximum or the minimum of each variable have been included in the training data. The ANN model procedures for training and testing data sets have been run for five times by changing the number of initial nodes from one to five. Then, the best ANN model is selected based on the ASE value of testing data sets. The optimum number of HN is found to be five, and it is calibrated after 20000 iterations. As a result, the selected ANN model consists of five input nodes in the input layer, five nodes in the hidden layer, and three output nodes in the output layer. The corresponding statistical measurements for this model are ASEts of 0.0129, R^2ts of 0.84, and MAREts of 31.88 for testing data sets; and ASEtr of 0.0025, R^2tr of 0.93, and MAREtr of 15.85 for training data sets. Then, the model is validated and the statistical measurements for the validation data sets are calculated to be ASEval of 0.013, R^2val of 0.77, and MAREval of 23.6. Table 20 shows the statistical measurements of the ANN1-1 model.

Table 20. Statistical measurements of ANN1-1 model.

Model	ANN Structure	MARE tr	MARE ts/val	R^2 tr	R^2 ts/val	ASE tr	ASE Ts/val	ASE Com.
Training-testing	5-5-3 With 20000 iterations	15.85	31.88	0.93	0.84	0.0025	0.0129	0.0154
Training-validation		15.85	23.6	0.93	0.77	0.0025	0.0130	0.0155
Training all		17.28	NA	0.89	NA	0.0042	NA	NA

Figure 49 shows a comparison between the actual and the predicted data sets of ANN1-1 model for the flow, the initial setting time, and the compressive strength respectively. The graphical accuracy shows that the ANN1-1 model is accurate in predicting the different MPC properties. The low scatter of data points around the equality line indicates that the ANN1-1 model is capable of predicting the physical and the mechanical properties of the MPC pastes. For the initial setting time prediction, the reason for the points gathering in a range of 0 to 15 minutes is the nature of the available data sets. The MPC paste is known for its rapid setting time. Therefore, most of the data sets have shown short initial setting time. Furthermore, the graphical accuracy figures show a good agreement between the actual and the predicted values of the validation data sets. On the other hand, the training all technique is applied to improve the accuracy of the selected ANN model. In this technique, all the available data sets are used to train the model while no testing or validation data is presented. The ANN results approved that the training all techniques

is able to improve the efficiency of the selected model and enhance the overall performance. The corresponding statistical measurements for the training all network are $ASE_{(trall)}$ of 0.0042, $R^2_{(trall)}$ of 0.89, and $MARE_{(trall)}$ of 17.28. The graphical accuracy of the training all network is shown in figure 50.

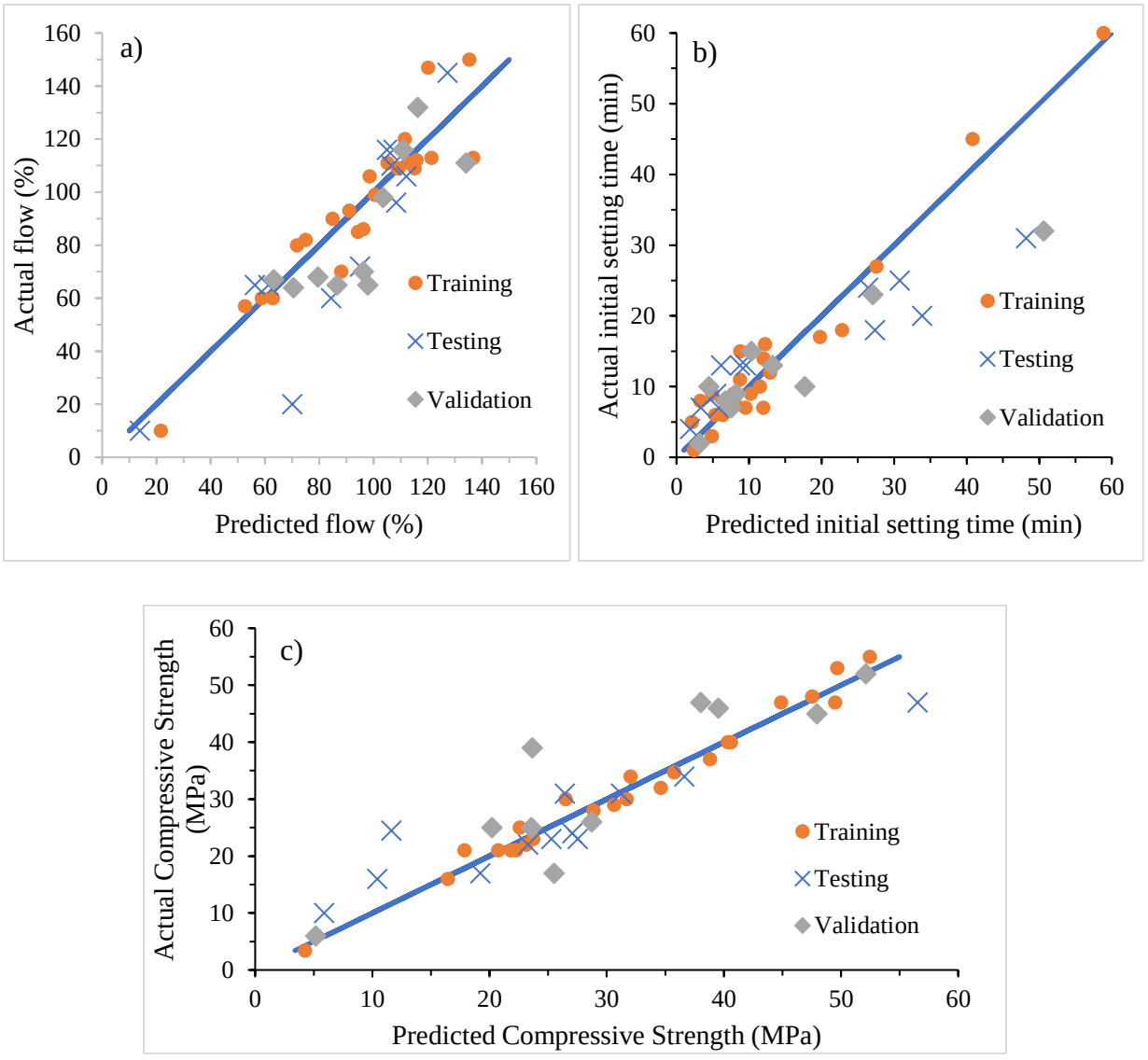

Figure 49. ANN1-$1_{(tr\text{-}ts\text{-}val)}$ model predictions accuracy for a) flow (%), b) initial setting time (min), and c) compressive strength (MPa).

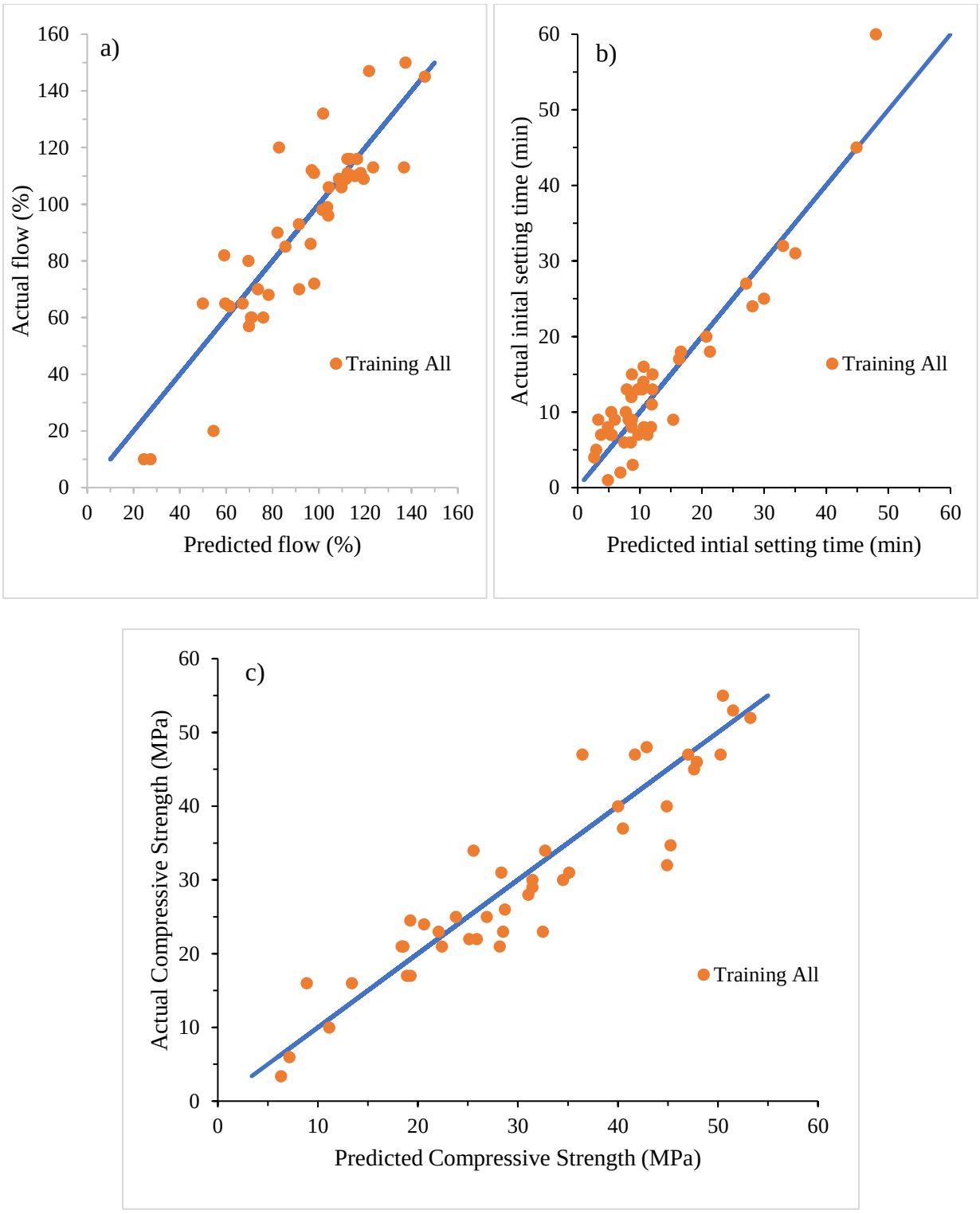

Figure 50. ANN1-1($_{\text{training-all}}$) model predictions accuracy for a) flow (%), b) initial setting time (min), and c) compressive strength (MPa).

6.5.2 ANN1-2 Model

ANN1-2 model is developed to predict the mix proportions between different MPC paste components in addition to three different retarder/additives. The input of this model is the MPC physical and mechanical properties including (1) flow (%), (2) initial setting time (min), and (3) compressive strength (MPa), where the outputs are: (1) M/P molar ratio, (2) W/P molar ratio, (3) B/M ratio (%), (4) AAC (%), and (5) GnP/S ratio (%). The input and the outputs of this model are summarized in table 16. The optimum number of HN is found to be 2, and it is calibrated after 200 iterations. The corresponding statistical measurements for ANN1-2 model approved that the ANN technique is not capable to predict the desired outputs of this model. For example, the statistical measurements of the training data are ASEtr of 0.064, R^2tr of 0.24, and MAREtr of 349.0. For testing data sets, the statistical measurements are ASEts of 0.031, R^2ts of 0.35, and MAREts of 335.73. The reason behind these results is attributed to the fact that each material property could be achieved by using multiple mix proportions. This non-uniqueness in the data sets can affect the efficiency of the neural networks. Furthermore, training the best ANN model using all the available data sets cannot improve the accuracy of the selected model. The statistical measurements of the training all network are calculated to be as follows: ASE(trall) of 0.043, R^2(trall) of 0.28 and MARE(trall) of 336.46. Table 21 shows the statistical measurements of the ANN1-2 model.

Table 21. Statistical measurements of the ANN1-2 model.

Model	ANN Structure	MARE tr	MARE ts/val	R^2 tr	R^2 ts/val	ASE tr	ASE Ts/val	ASE Com.
Training-testing	3-2-5 With 200 iterations	349.00	335.73	0.24	0.35	0.064	0.031	0.095
Training-validation		349.00	323.27	0.24	0.34	0.064	0.032	0.096
Training all		336.46	NA	0.28	NA	0.043	NA	NA

Figure 51 shows a comparison between the actual and the predicted data sets of ANN1-2 model for M/P, W/P, B/M, AAC, and GnP/S respectively. The graphical accuracy shows that the ANN1-2 model is inaccurate in predicting the mix proportions of the MPC paste ingredients. For example, for predicting M/P molar ratio, most of the predicted data points are in a range of 4 to 6. This wrong prediction is attributed to the fact that most of the available data sets have this range of M/P ratio while only a few data sets with M/P ratio of less or more than these values are available. Thus, training the model with a few data sets is not enough to let the network understand the real impact of each variables. Furthermore, there is no significant enhancement has been observed in the model accuracy after using the training all technique.

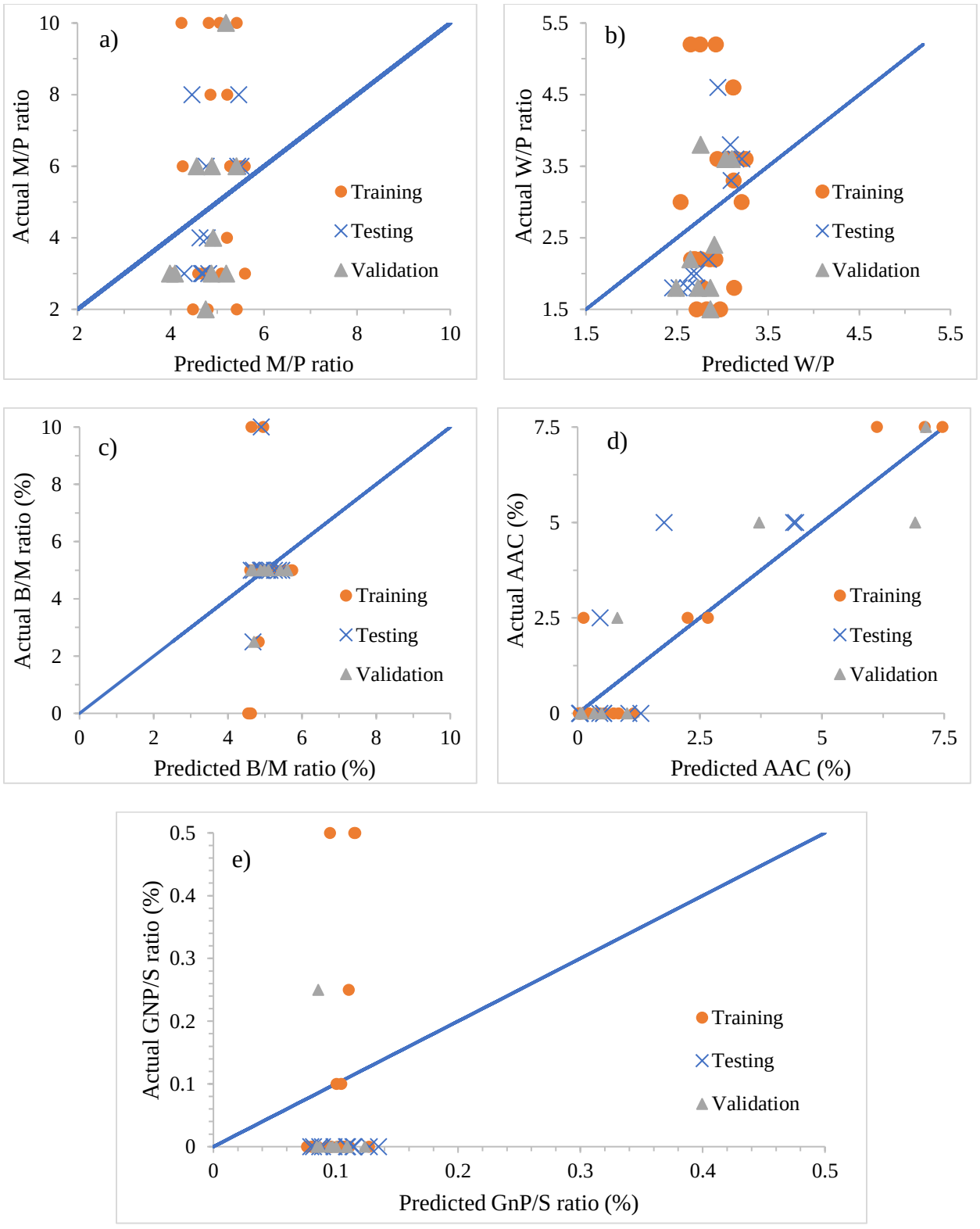

Figure 51. ANN1-1($_{tr\text{-}ts\text{-}val}$) model predictions accuracy for a) M/P ratio (%), b) W/P ratio (%), c) B/M ratio (%), d) AAC (%), and e) GnP/S ratio (%).

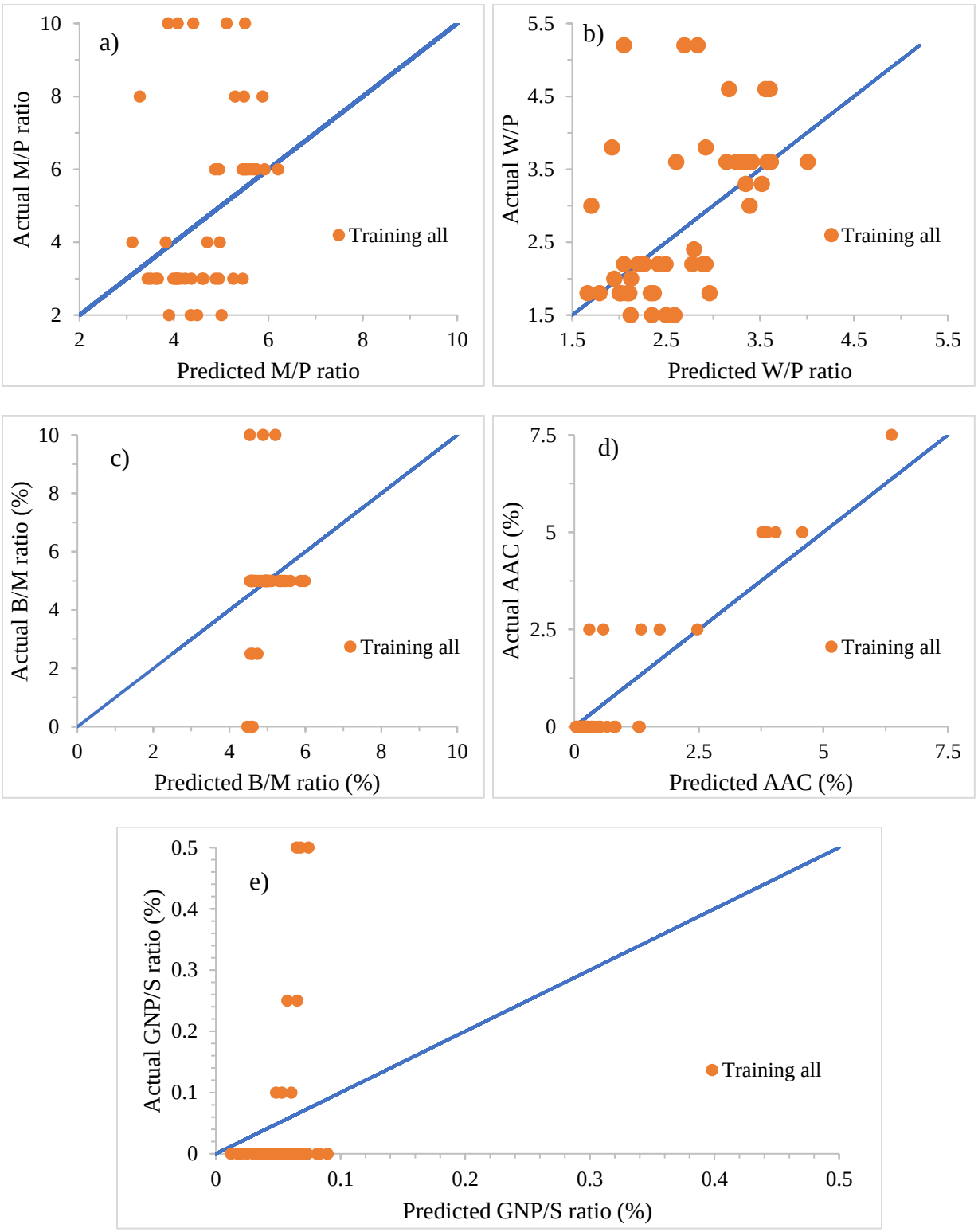

Figure 52. ANN1-1($_{\text{training all}}$) model predictions accuracy for a) M/P ratio (%), b) W/P ratio (%), c) B/M ratio (%), d) AAC (%), and e) GnP/S ratio (%).

6.6 ANN NETWORK DEVELOPMENT OF DATABASE #2

As previously mentioned, database #2 has been built by repeating some of the data sets to give it more weight in the neural network process. All the data sets in this database are sorted based on the maximum and the minimum values for each parameter and divided into three groups including 69, 25, and 20 data sets as training, testing, and validation respectively. By using the Eq (2), the maximum number of hidden nodes is calculated to be 10.1. Since the Eq (2) provide an estimation value, the maximum number of hidden nodes is selected to be 11. Then, the optimum number of hidden nodes are determined using the adaptive technique and the best network which can represent the data has been selected based on the statistical measurements.

6.6.1 ANN2-1 MODEL

ANN2-1 model has been optimized to predict the physical and mechanical properties of the MPC paste by using the MPC ingredients as inputs. Table 15 shows the inputs and the outputs of the ANN2-1 model. The ANN model procedures for training and testing data sets have been run for 11 times by changing the number of initial nodes from 1 to 11. Then, the best ANN model has been selected based on the ASE value of the testing data sets. The optimum number of HN is found to be 11, and it is calibrated after 20000 iterations. The neural network for testing data sets yields an ASEts of 0.0087, R^2ts of 0.88, and MAREts of 27.96. Similarly, the statistical measurements of the training data sets are calculated to be ASEtr of 0.0008, R^2tr of 0.97, and MAREtr of 5.4. After obtaining these results, the model has been validated using the validation data sets, and the statistical measurements are found to be as ASEval of 0.0086, R^2val of 0.85, and MAREval of 25.14. All the statistical measurements of training, testing, and validation of ANN2-1 model are summarized in table 22.

Table 22. Statistical measurements of the ANN2-1 model.

Model	ANN Structure	MARE tr	MARE ts/val	R^2 tr	R^2 ts/val	ASE tr	ASE Ts/val	ASE Com.
Training-testing	5-11-3 With 20000 iterations	5.4	27.96	0.97	0.88	0.0008	0.0087	0.0095
Training-validation		5.4	25.14	0.97	0.85	0.0008	0.0086	0.0094
Training all		6.735	NA	0.98	NA	0.0007	NA	NA

Figure 53 shows the graphical comparison of the predicted data sets for flow, initial setting time, and compressive strength of ANN2-1 model respectively. The graphical accuracy shows a good agreement between the actual and the predicted values for all the outputs. Moreover, The ANN2-1 model is found to be very accurate in predicting the different MPC properties. The low scatter of data points around the equality line indicates that the ANN1-1 model is able to predict the physical and the mechanical properties of the MPC pastes. On the other hand, the training all technique is applied for this database to improve the accuracy of the selected model. As previously mentioned, all the available data sets are used to train the model while no testing or validation data is presented. The ANN for training all process yields an $ASE_{(trall)}$ of 0.0007, $R^2_{(trall)}$ of 0.98, and $MARE_{(trall)}$ of 6.735. The graphical comparisons of the predicted data sets for training all network are shown in figure 54. As shown in the graphical accuracy figures using of the raining all

technique has improved the accuracy of the model. For example, all the predicted data for the compressive strength are closer to the equality line when the training all technique is used.

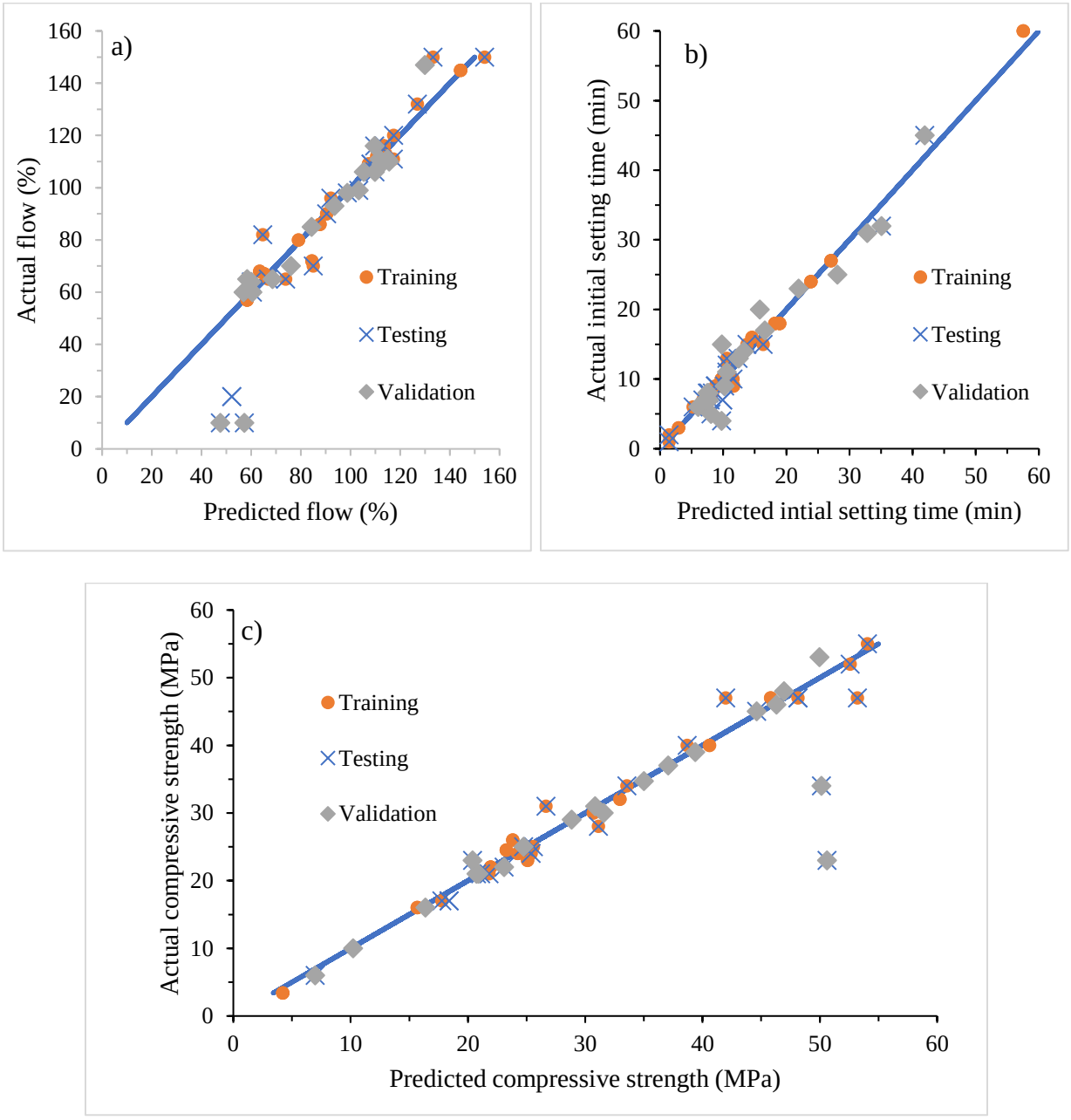

Figure 53. ANN2-1($_{tr\text{-}ts\text{-}val}$) model predictions accuracy for a) flow (%), b) initial setting time (min), and c) compressive strength (MPa).

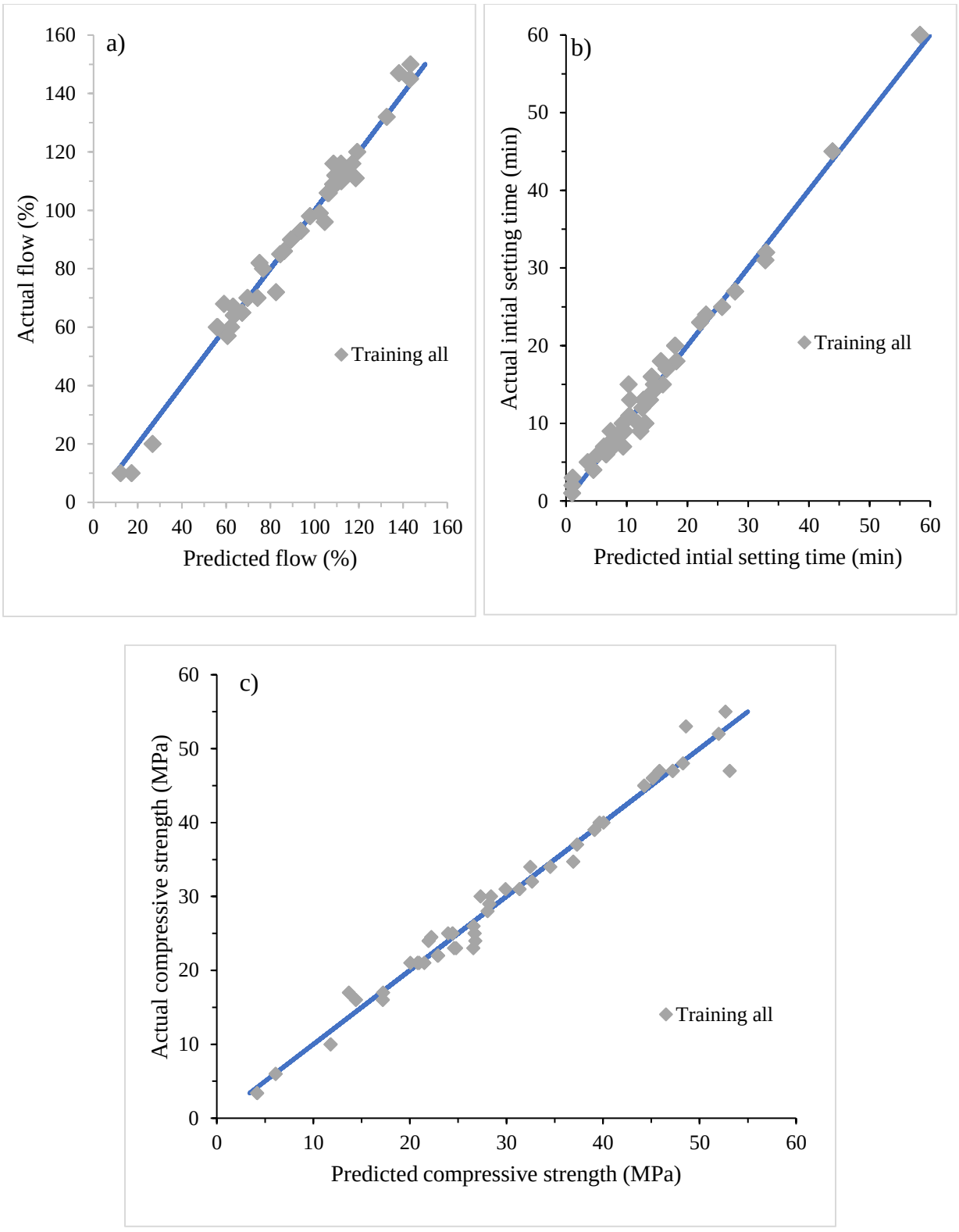

Figure 54. ANN2-1($_{\text{training all}}$) model predictions accuracy for a) flow (%), b) initial setting time (min), and c) compressive strength (MPa).

6.6.2 ANN2-2 MODEL

ANN2-2 model is developed to predict the mix proportions between different MPC paste components by using the measured MPC properties as inputs. Table 16 summarizes all inputs and outputs of this model. The optimum number of HN is found to be 11, and it is calibrated after 20000 iterations. As a result, the selected ANN model consists of 3 input nodes in the input layer, 11 nodes in the hidden layer, and 3 output nodes in the output layer.

The ANN2-2 model shows a better performance than the ANN1-2 model. The corresponding statistical measurements for ANN2-2 model are ASEts of 0.006, R^2ts of 0.9, and MAREts of 305.4 for testing data sets, and ASEtr of 0.0038 R^2tr of 0.89, and MAREtr of 323.13 for training data sets. Although, the both models (ANN1-2 and ANN2-2) are having the same inputs/outputs, but the using of database #2 to develop the ANN2-2 model improves the prediction accuracy. The reason behind these results is attributed to replicating the acetic acid and the GnP data sets. These replications can modify the weight of these data sets and supply more information to the used algorithm. For example, both of R^2tr and R^2ts are increased from 0.35 and 0.24 to 0.9 and 0.89 respectively when database #2 has been used. Besides, the statistical measurements of the validation data sets in this model are becoming much better. Table 23 summarizes the statistical measurements of the ANN2-2 model while figure 55 shows its graphical accuracy. The graphical accuracy shows a good agreement between the actual and the predicted values for most of the outputs, and the low scatters of the data points around the equality line indicates that the ANN2-1 model is able to predict the proportions between different MPC components/additives by using the fresh and hardened properties. However, the model is not much accurate in predicting the high and low B/M ratio. One possible reason for that is the lake of the data sets that have high and low percentage of B/M ratio. On the other hand, training all technique is used to improve the accuracy

of the model. The statistical measurements indicate that using all the data to train the ANN model can improve its accuracy. The statistical measurements of the training all model are ASE(trall) of 0.0035, R_2(trall) of 0.91 and MARE(trall) of 304.4. Figure 56 shows a comparison between the actual and the predicted parameters for ANN2-2$_{\text{(training all)}}$

Table 23. Statistical measurements of the ANN2-2 model.

Model	ANN Structure	MARE tr	MARE ts/val	R^2 tr	R^2 ts/val	ASE tr	ASE ts/val	ASE Com.
Training-testing	3-11-5 With 20000 iterations	305.4	323.13	0.89	0.90	0.0038	0.006	0.009
Training-validation		305.4	271.8	0.89	0.82	0.0038	0.0038	0.003
Training all		303.4	NA	0.92	NA	0.0035	NA	NA

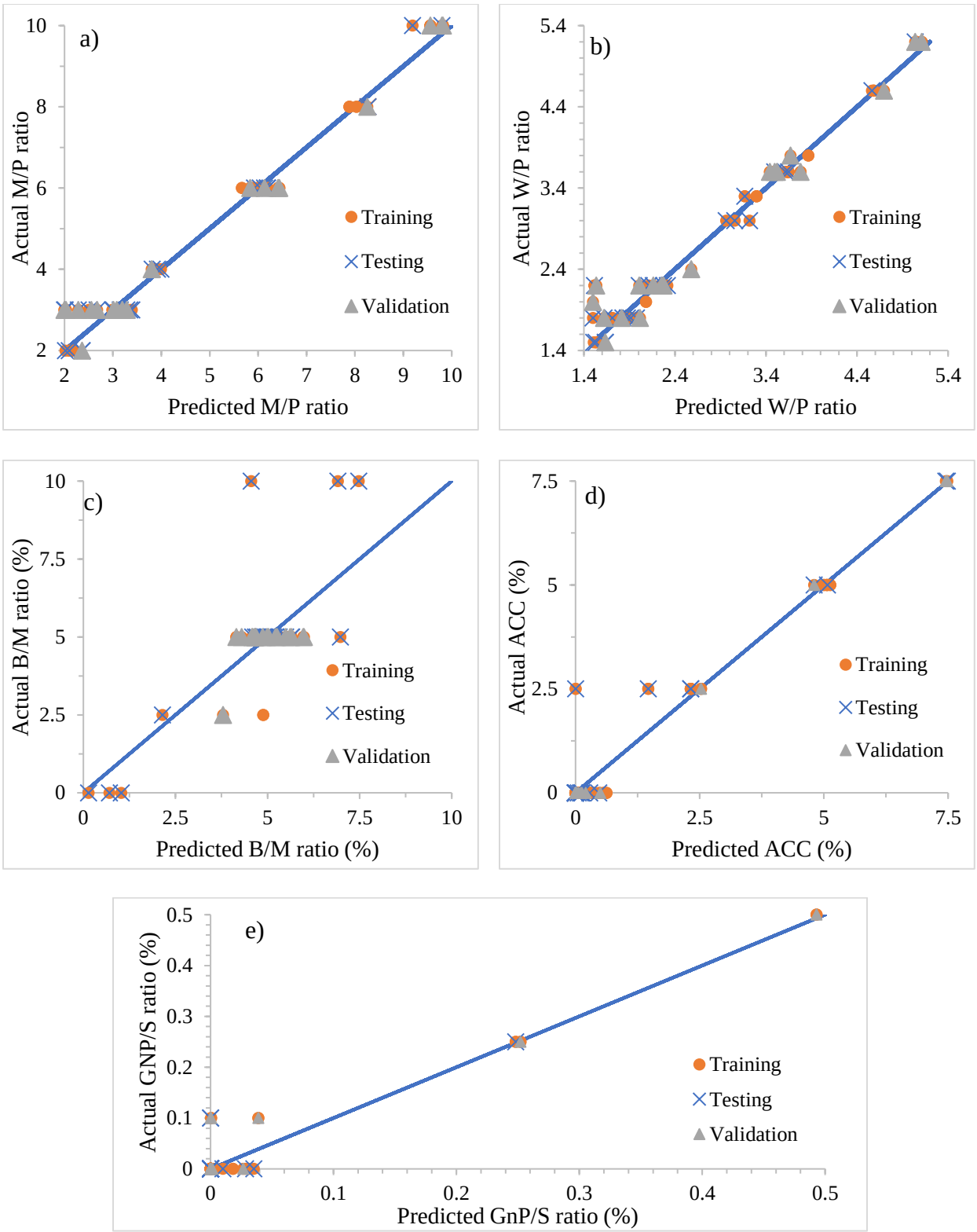

Figure 55. ANN2-2($_{tr\text{-}ts\text{-}val}$) model predictions accuracy for a) M/P ratio, b) W/P ratio, and c) B/M ratio, d) AAC ratio, and e) GnP/S ratio.

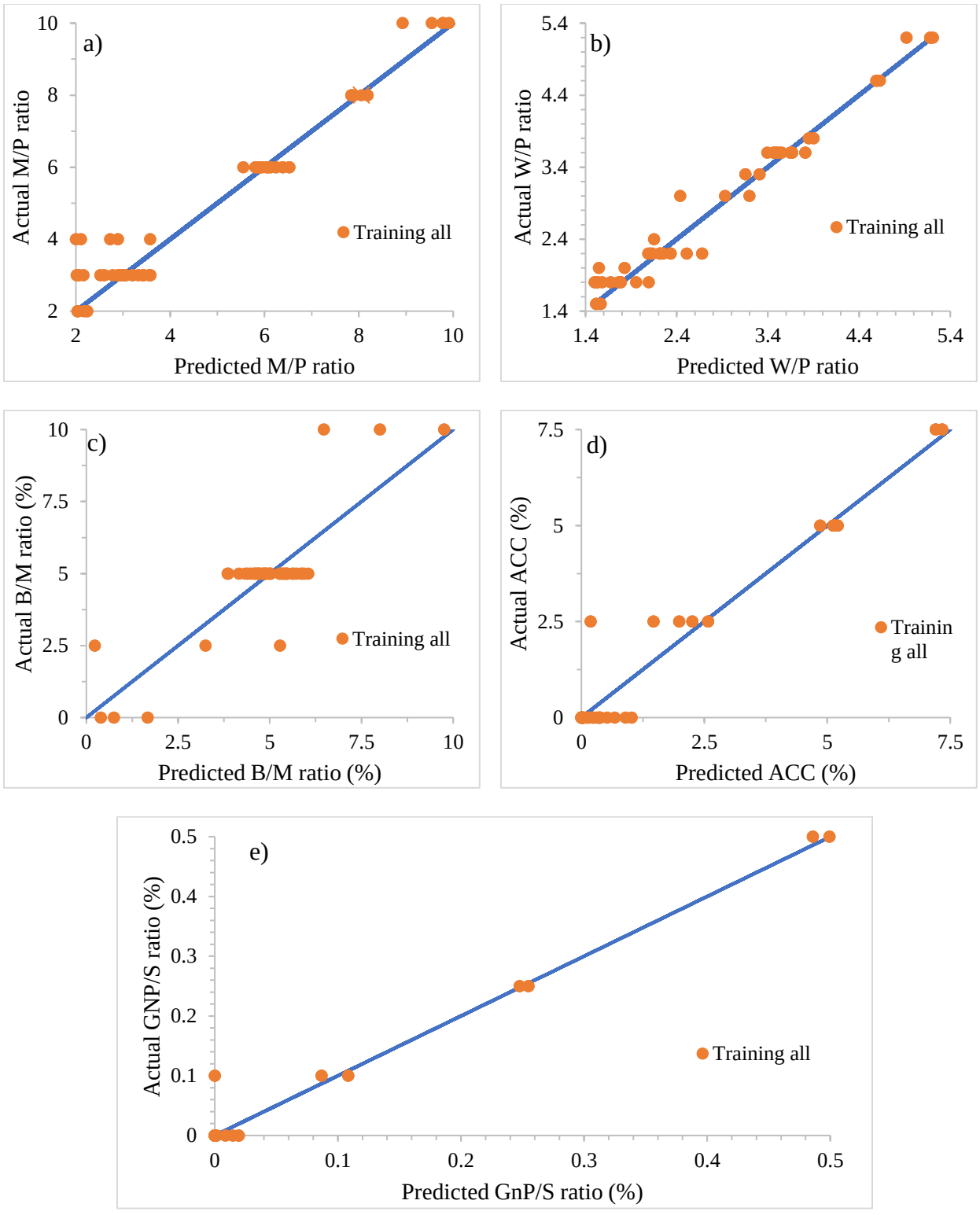

Figure 56. ANN2-2($_{\text{training all}}$) model predictions accuracy for a) M/P ratio, b) W/P ratio, and c) B/M ratio, d) AAC ratio, and e) GnP/S ratio.

6.7 ANN NETWORK DEVELOPMENT OF DATABASE #3

Database #3 consists of 138 data sets; each three data sets represent three different measurements of the MPC properties for the same mixture. As a result, a total of 138 data sets are collected and sorted based on the maximum and the minimum values for each variable and divided into three groups including 83 data sets for training, 31 data sets for testing, and 24 data sets for validation. The maximum number of hidden nodes is calculated to be 12.3; therefore, the maximum number of hidden nodes is selected to be 13. Then, the optimum number of hidden nodes is determined using the adaptive technique.

6.7.1 ANN3-1 MODEL

ANN3-1 model has been developed to predict the fresh and the hardened properties of different MPC mixtures by using the MPC mix proportions as inputs. All the inputs and the outputs of this model are summarized in Table 15. In order to determine the best ANN model, the neural network is trained and tested for 13 different times. Then, the best network is selected based on the ASE value of the testing data sets. For ANN3-1 model, the optimum number of HN is determined to be 13, and it is calibrated after 1100 iterations. The statistical results show that the ANN3-1 model is very accurate in predicting the MPC's physical and mechanical properties. For ANN3-1 model, R^2ts, R^2tr, and R^2val are calculated to be 0.96, 0.99, and 0.95 respectively. Moreover, the model yields an average square error (ASE) of 0.0017, 0.00066, and 0.0018 for testing, training, and validation respectively. All the statistical measurements of ANN3-1 model are summarized in table 24.

Table 24. Statistical measurements for ANN3-1 model.

Model	ANN Structure	MARE tr	MARE ts/val	R^2 tr	R^2 ts/val	ASE tr	ASE ts/val	ASE Com.
Training-testing	5-13-3 With 1100 iterations	6.40	9.96	0.99	0.96	0.00066	0.0017	0.0023
Training-validation		6.40	8.10	0.99	0.95	0.00066	0.0018	0.0025
Training all		7.99	NA	0.97	NA	0.00103	NA	NA

Figure 57 shows a comparison between the actual and the predicted data sets of ANN3-1 model for flow, initial setting time, and compressive strength respectively. It can be seen that a good agreement between the actual and the predicted values are achieved for all the outputs; while the low scatter of the data points around the equality line can demonstrate the high accuracy of the ANN3-1 model in predicting the desired outputs. Furthermore, using all the data sets to train the model leads to more accurate results. The ANN for training all process yields an $ASE_{(trall)}$ of 0.0013, $R^2_{(trall)}$ of 0.97, and $MARE_{(trall)}$ of 7.99. Figure 58 shows the graphical comparisons of the predicted data sets for the training all network.

.

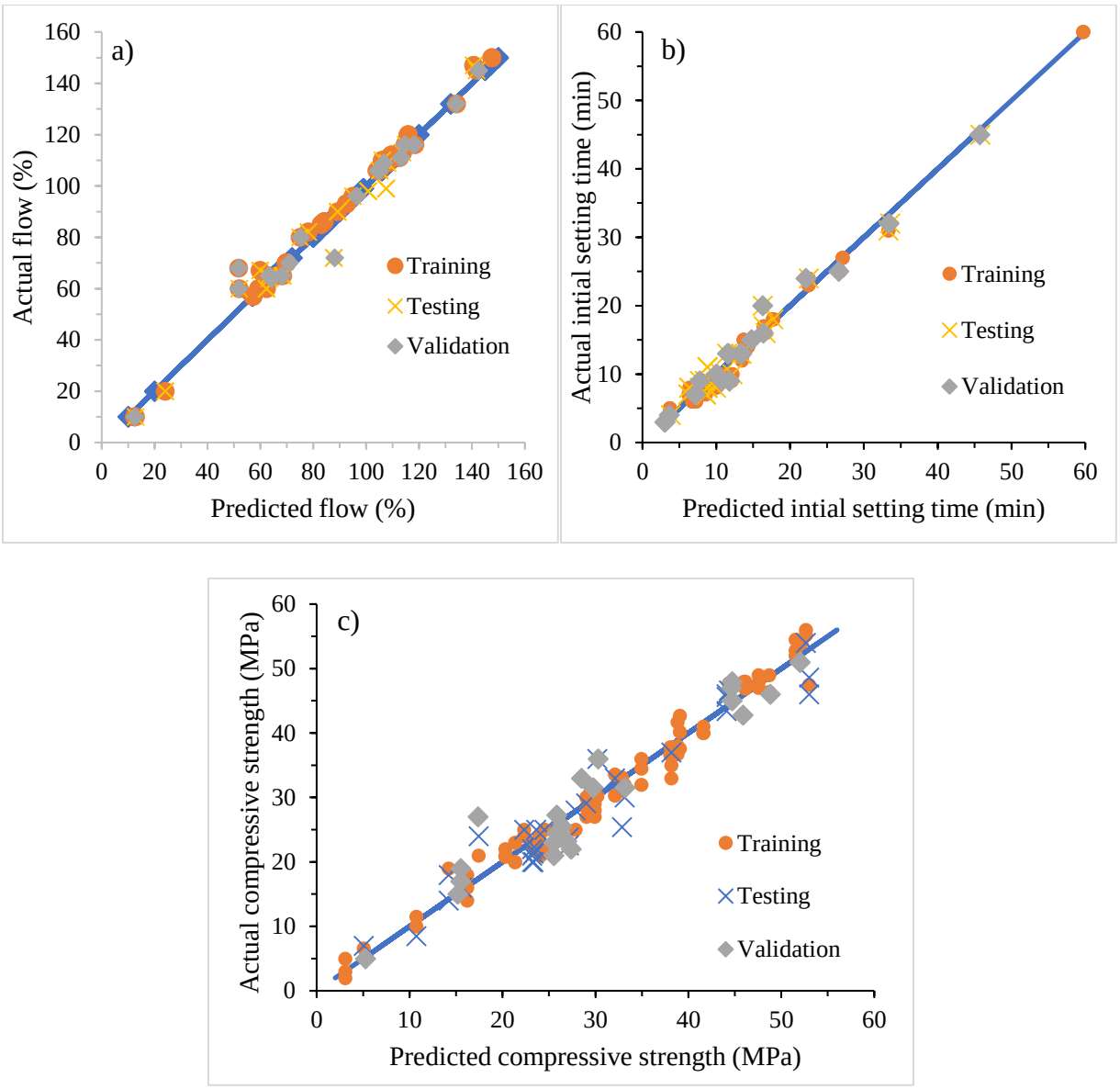

Figure 57. ANN3-1($_{tr\text{-}ts\text{-}val}$) model predictions accuracy for a) flow (%), b) initial setting time (min), and c) compressive strength (MPa).

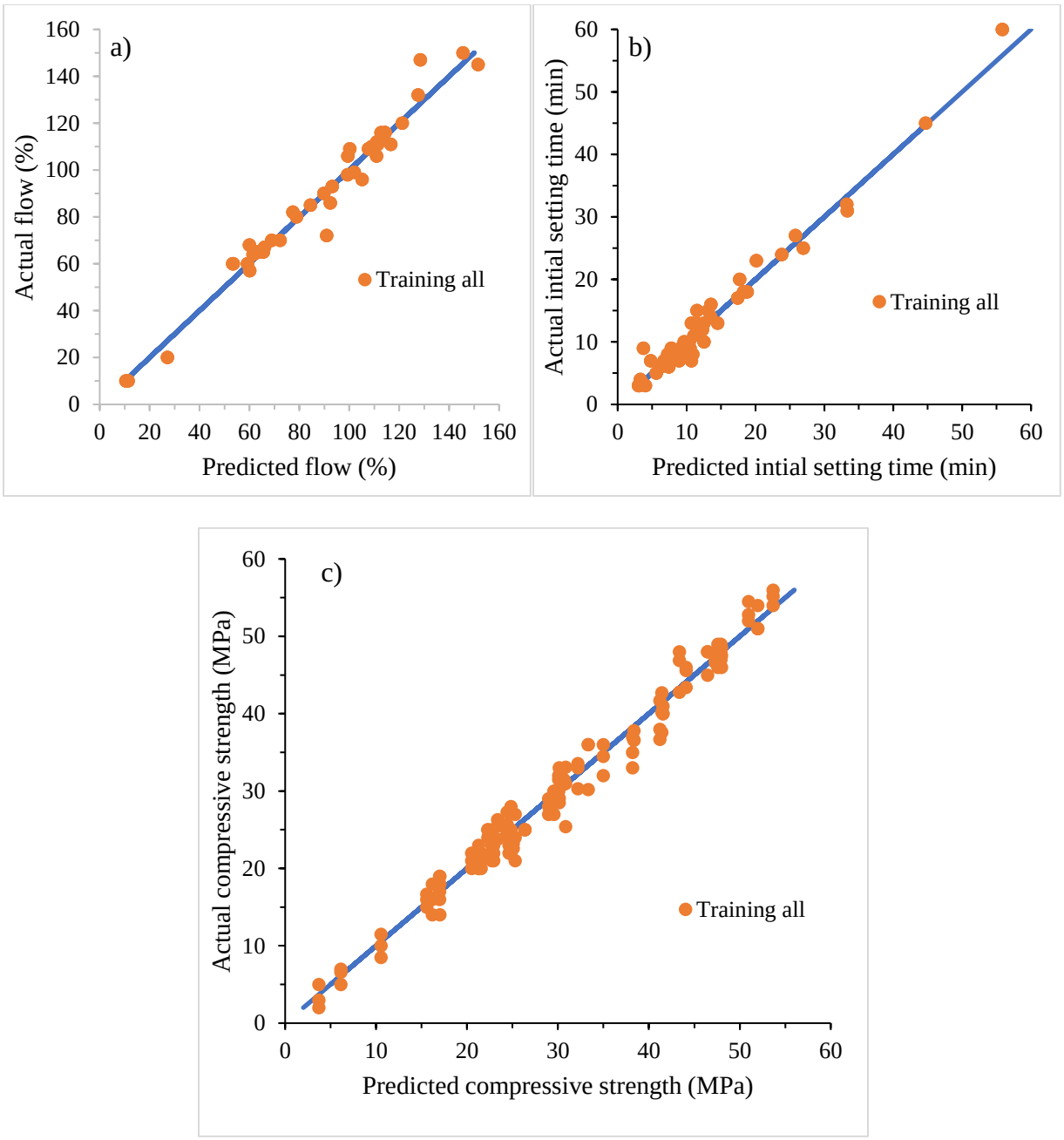

Figure 58. ANN3-1($_{\text{training all}}$) model predictions accuracy for a) flow (%), b) initial setting time (min), and c) compressive strength (MPa).

6.7.2 ANN3-2 MODEL

As previously noted, ANN3-2 model is developed to predict the mix proportions between different MPC paste components/additives, while the MPC properties are used as inputs. Table 16 summarizes all inputs and outputs of the ANN3-2 model. The optimum number of HN is found to be 13, and it is calibrated after 3000 iterations. The model has a final structure of 3 input nodes in the input layer, 13 nodes in the hidden layer, and 3 output nodes in the output layer.

ANN3-2 model shows a better performance than the ANN1-2 model but worse performance than the ANN2-2 model. The ANN3-2 model has an ASEts of 0.011, R^2ts of 0.72, and MAREts of 311.66 for testing data sets, and ASEtr of 0.0032 R^2tr of 0.94, and MAREtr of 326.33 for training data sets. Furthermore, the statistical measurements of the validation data sets are not as required. For the validation data sets, the corresponding statistical measurements are ASEval of 0.0099, R^2val of 0.64, and MAREval of 356.06. All the statistical measurements of the ANN3-2 model are shown in table 25.

Figure 59 shows a comparison between the actual and the predicted data sets of ANN3-2 model for M/P ratio, W/P ratio, B/M ratio, AAC, and GNP/S ratio respectively. As seen in the figures, the model is not much accurate in predicting the mix proportions of the MPC paste. The model is not able to predict the M/P ratio correctly. Besides, the model has a major problem in predicting the B/M ratio. As previously mentioned, the reason behind the bad predictions is attributed to the possibility of getting the same property value by using multiple mix proportions. However, the overall performance of the model is acceptable as experimental results predicter and inverse problem solver. On the other hand, the accuracy of this model can be significantly improved by using the training all technique. The statistical measurements of the training all model

are yielding ASE(trall) of 0.0036, R^2(trall) of 0.94 and MARE(trall) of 326.28. Figure 61 shows a comparison between the actual and the predicted parameters for ANN3-2$_{(\text{training all})}$

Table 25. Statistical measurements of the ANN3-2 model.

Model	ANN Structure	MARE tr	MARE ts/val	R^2 tr	R^2 ts/val	ASE tr	ASE ts/val	ASE Com.
Training-testing	3-13-5 With 3000 iterations	326.66	311.66	0.94	0.72	0.0032	0.011	0.014
Training-validation		326.66	356.06	0.94	0.64	0.0032	0.0099	0.013
Training all		326.28	NA	0.92	NA	0.0036	NA	NA

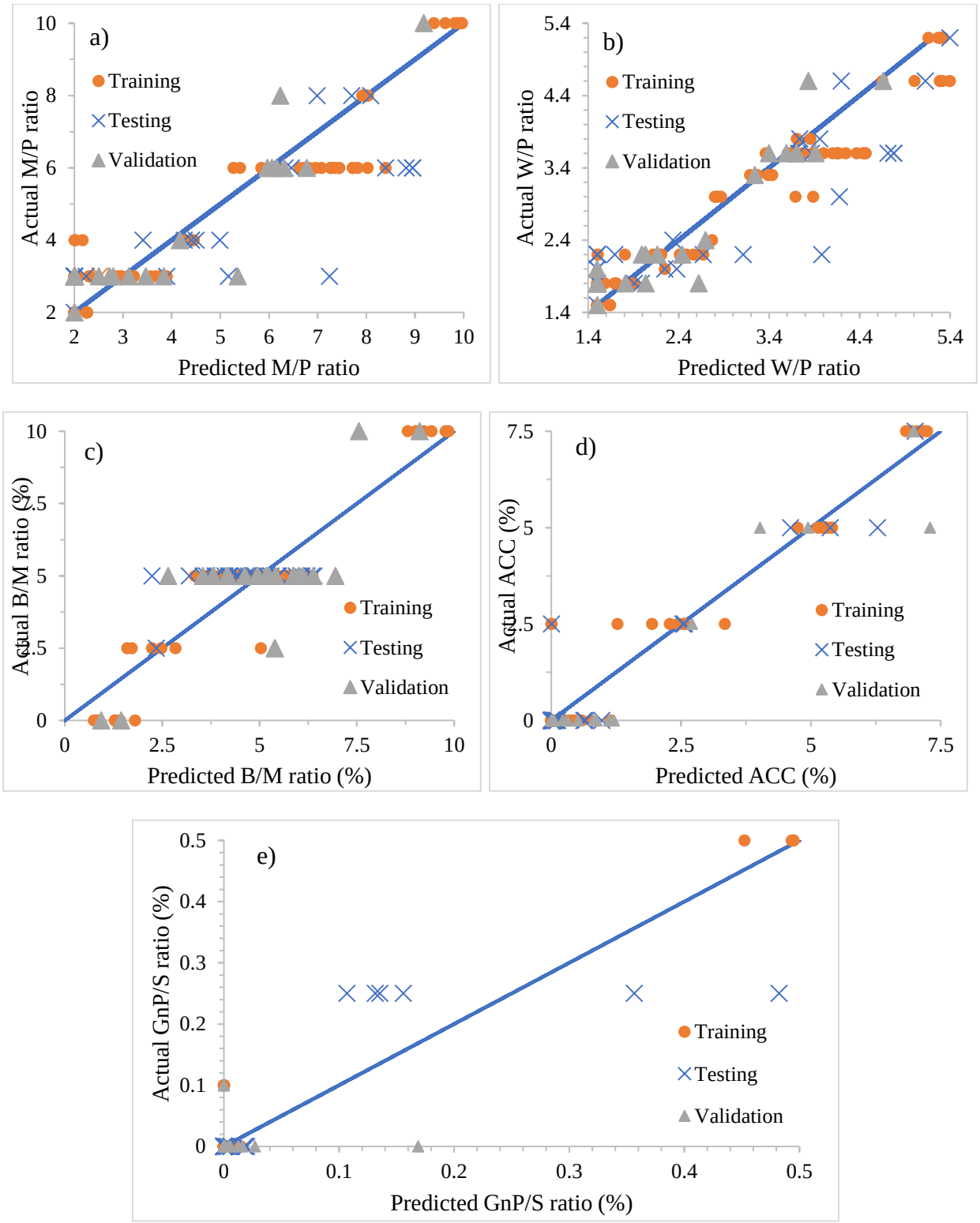

Figure 59. ANN3-2($_{tr\text{-}ts\text{-}val}$) model predictions accuracy for a) M/P ratio, b) W/P ratio, and c) B/M ratio, d) AAC ratio, and e) GnP/S ratio.

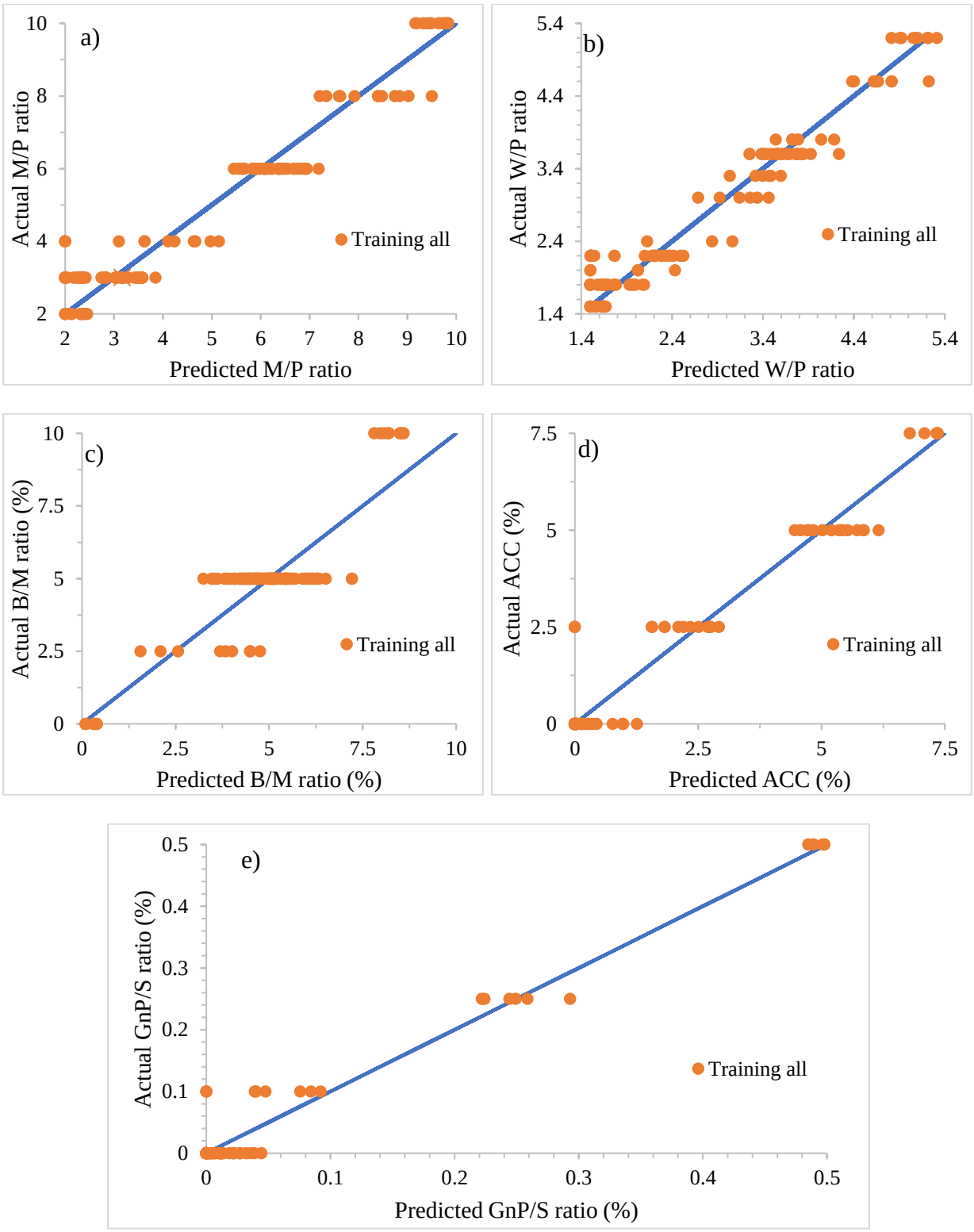

Figure 60. ANN3-2($_{\text{training all}}$) model predictions accuracy for a) M/P ratio, b) W/P ratio, and c) B/M ratio, d) AAC ratio, and e) GnP/S ratio.

6.8 MODELS COMPARISON

As previously showed, a total of twelve different ANN models have been developed in order to represent the available data. Six ANN models are performed to predict the physical and mechanical properties of the MPC paste including (1) ANN1-1$_{(tr\text{-}ts\text{-}val)}$, (2) ANN1-1 $_{(training\ all)}$, (3) ANN2-1$_{(tr\text{-}ts\text{-}val)}$, (4) ANN2-1 $_{(training\ all)}$ (5) ANN3-1$_{(tr\text{-}ts\text{-}val)}$, and (6) ANN3-1 $_{(training\ all)}$. The other six models are optimized to predict the mix proportions of the MPC paste by using the physical and mechanical properties as input variables. These models are: (1) ANN1-2$_{(tr\text{-}ts\text{-}val)}$, (2) ANN1-2 $_{(training\ all)}$, (3) ANN2-2$_{(tr\text{-}ts\text{-}val)}$, (4) ANN2-2 $_{(training\ all)}$ (5) ANN3-2$_{(tr\text{-}ts\text{-}val)}$, and (6) ANN3-2 $_{(training\ all)}$. Since the performance of the training all models are better for all cases, two ANN training all models have been selected to represent the data. The first model is selected to predict the MPC physical and mechanical properties while the other is selected to predict the MPC mix proportions.

Based on the statistical measurements and the graphical accuracy figures, ANN2-1 $_{(training\ all)}$ model has been selected to predict the physical and the mechanical properties of the MPC pastes. The model has the lowest measured error including ASE and MARE in addition to the highest R^2. Table 26 shows the statistical measurements for all the ANN training all models that used to predict different MPC properties.

Table 26. Statistical measurements of ANN1-1(training all), ANN2-1(training all), and ANN3-1(training all) models.

Model	ANN Structure	MARE	R^2	ASE
ANN1-1$_{(training\ all)}$	5-5-3	17.28	0.89	0.0042
ANN2-1$_{(training\ all)}$	5-11-3	6.735	0.98	0.0007
ANN3-1$_{(training\ all)}$	5-13-3	7.99	0.97	0.00103

On the other hand, ANN2-2$_{(\text{training all})}$ model has been selected in order to predict the mix proportions of the MPC pastes. The model has been selected due to its low ASE and MARE measurements in addition to its high R^2. Table 27 summarizes the statistical measurements for all the ANN training all models that used to predict the mix proportions of MPC pastes.

Table 27. Statistical measurements of ANN1-2(training all), ANN2-2(training all), and ANN3-2(training all) models.

Model	ANN Structure	MARE	R^2	ASE
ANN1-2$_{(\text{training all})}$	3-2-5	336.46	0.28	0.043
ANN2-2$_{(\text{training all})}$	3-11-5	303.4	0.92	0.0035
ANN3-2$_{(\text{training all})}$	3-13-5	326.28	0.92	0.0036

After selecting the best ANN models to represent the experimental data sets, the models are used for sensitivity analysis and data simulations.

6.9 SENSITIVITY ANALYSIS AND DATA SIMULATION

Many previous studies have proved that the physical and chemical properties of MPC paste could be influenced by several factors include magnesia to phosphate molar ratio (M/P), water to the sold ratio (W/S), boric acid to magnesia ratio (B/M), and the physical and chemical characteristics of the used additives. In this research, a new expression is used to describe the amount of the used water. The water content is calculated based on phosphate to water molar ratio (W/P). This expression can provide more reliable information about the impact of the water

content. Moreover, two different additives are used in this research to enhance the performance of the MPC paste. The first additive is selected to be the acetic acid, this additive is used to enhance the initial setting time of the MPC paste. The content of the acetic acid is calculated based on its concentrations in the aqueous solvent (AAC). Since the MPC system is very sensitive to the water content, adding or dropping a small amount of water can make a big difference in term of fluidity. Therefore, the graphene nanoplatelets (GnP) is selected to control the fluidity of the system in case of using high water content. The amount of this additive is calculated based on the graphene nanoplatelets to the total solid ratio (GnP/S).

In this section, ANN2-1 model has been used for sensitivity analysis and data simulations. These processes involve changing the value of one input while keeping all other input parameters constant. These processes are applied to the three desired MPC output properties including flow, initial setting time, and compressive strength.

Sensitivity analysis is performed by changing one variable and keeping all the other variables constant. Figure 61 shows the flow prediction of the MPC paste based on a) B/M ratio, b) W/P molar ratio, c) AAC, and d) GnP/S ratio. At first, B/M ratio is changed from 0 to 10% while all the other variables are kept constant (figure 61.a). In figure 61.b, W/P ratio is changed from 3 to 4.6 while the other parameters are kept constant. Then, AAC is changed from 2.5 to 7.5% and all the others variable are kept constant (figure 61.c). Finally, in figure 61.d, the flow prediction is conducted based on changing the GnP/S from 0.1 to 0.5 % and keeping the other variable constant. For all cases, it can be seen that the ANN2-1 model is capable to predict the flow of the MPC efficiently. Furthermore, the model did not generate any strange or negative output.

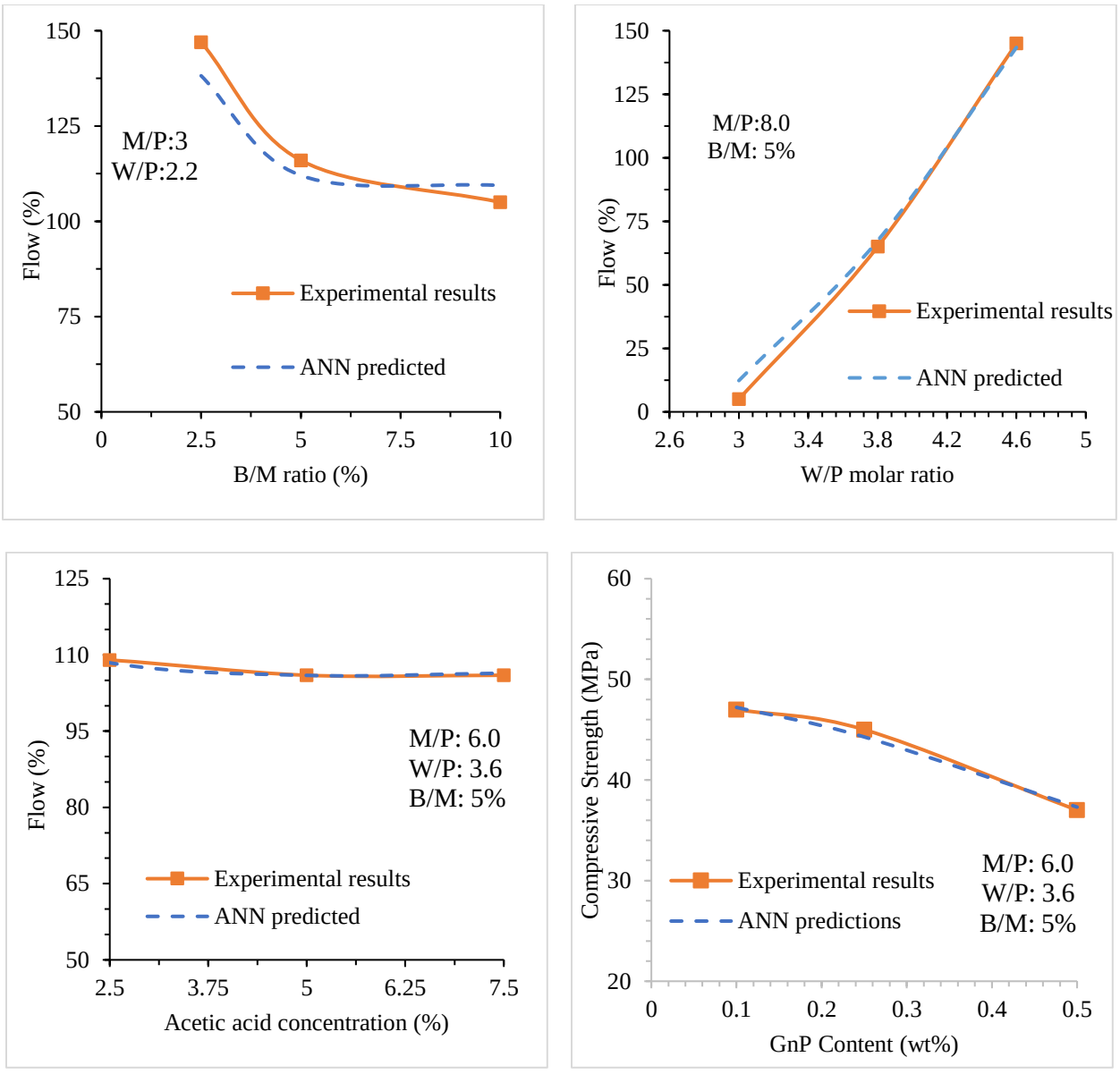

Figure 61. ANN2-1 model prediction of flow based on a) B/M ratio, b) W/P molar ratio, c) AAC, and d) GnP/S ratio.

In the same manner, the ANN2-1 model is used to predict the initial setting time of the MPC by changing the proportions between the MPC paste components. Figure 62 shows the prediction of initial setting time based on a) B/M ratio, b) W/P molar ratio, c) AAC, and d) GnP/S ratio. The sensitivity analysis indicates that the ANN2-1 model is very consistent in predicting the

initial setting time. For example, the model confirms that the optimum B/M ratio for the initial setting time is around 5% which is the same finding of the experimental results. Moreover, the model can predict the initial setting time in the presence of acetic acid or graphene nanoplatelets efficiently. For example, the model can predict that increasing the ACC will enhance the initial setting time of the paste.

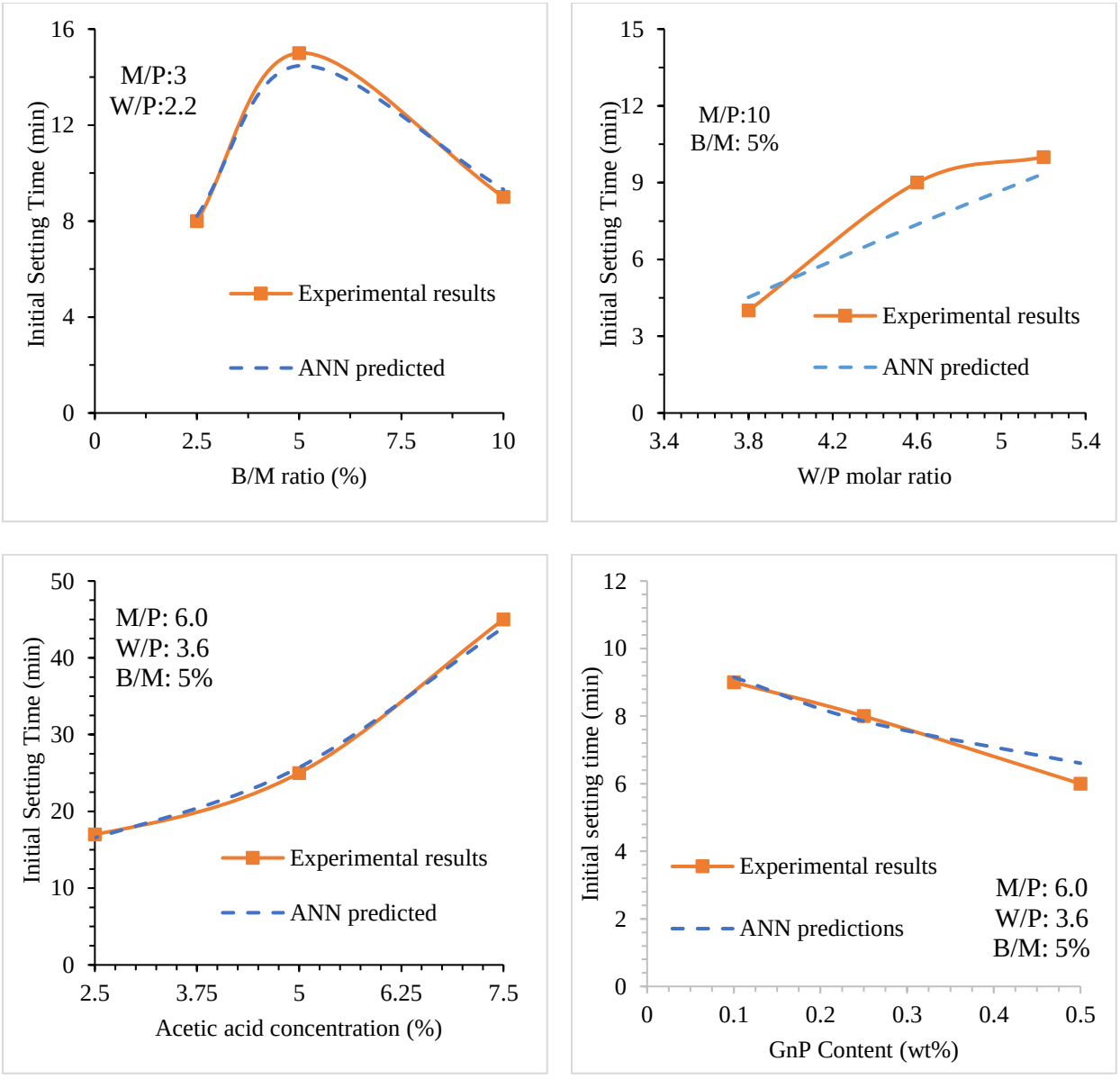

Figure 62. ANN2-1 model prediction of initial setting time based on a) B/M ratio, b) W/P molar ratio, c) AAC, and d) GnP/S ratio.

Finally, the ANN2-1 model is found to be very accurate in predicting the compressive strength. Figure 63 shows the prediction of compressive strength based on a) B/M ratio, b) W/P molar ratio, c) AAC, and d) GnP/S ratio. figure 64.a is performed by fixing all the MPC variables and changing only the B/M ratio. It can be seen that the model is able to predict that increasing the boric acid content can decrease the compressive strength. Furthermore, for M/P molar ratio of 10 and by using the ANN model, the optimum W/P molar ratio is found to be 4.6. it is worth to mention that the same results can be achieved from the experimental results. Also, the model shows an accurate prediction if the acetic acid or the graphene nanoplatelets is added to the mixture. For example, increasing the acetic acid concentrations in the MPC paste can reduce its compressive strength.

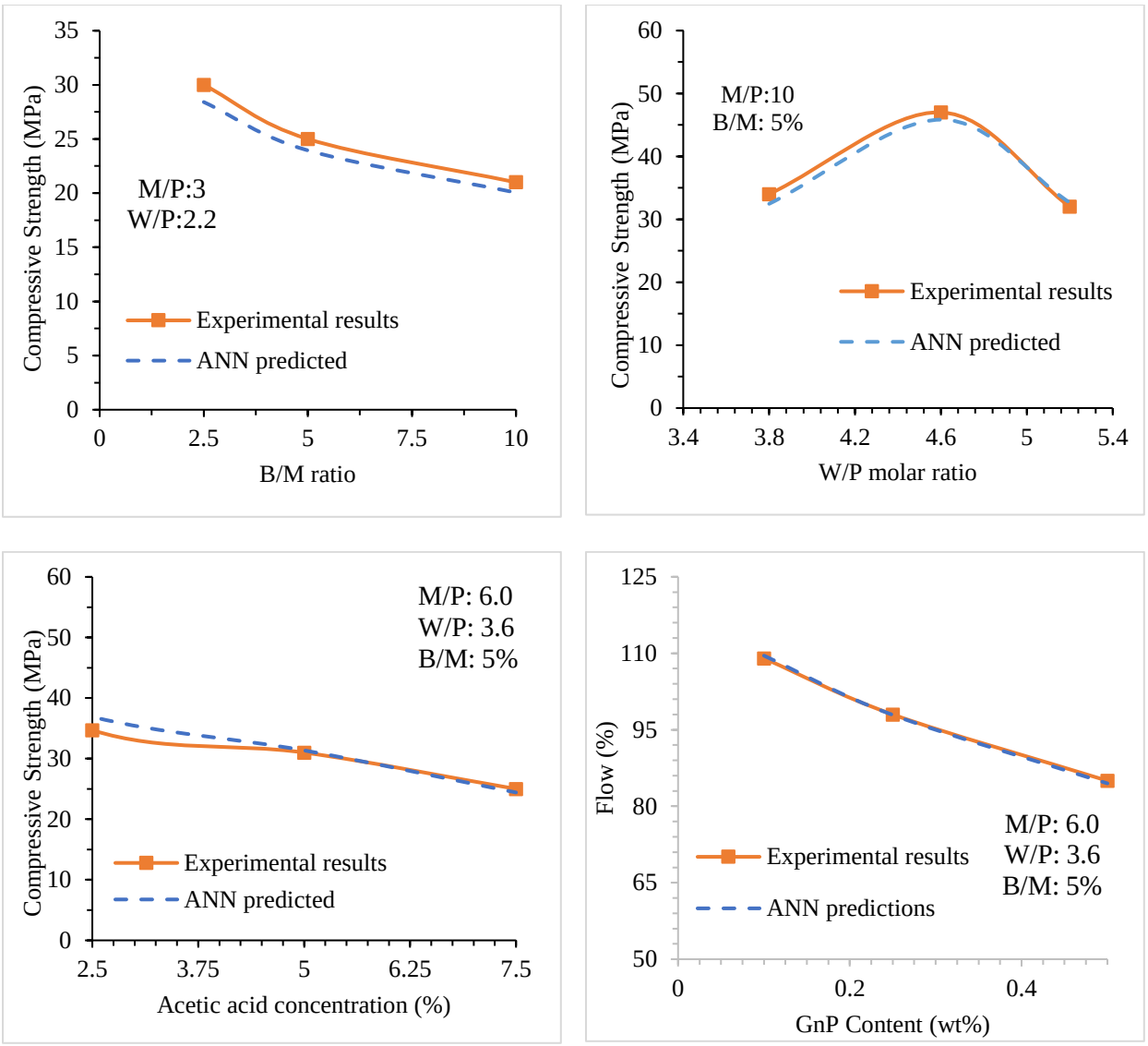

Figure 63. ANN2-1 model prediction of compressive strength based on a) B/M ratio, b) W/P molar ratio, c) AAC, and d) GnP/S ratio.

CHAPTER VII

CONCLUSIONS AND RECOMMENDATIONS

7.1 CONCLUSIONS

In the last few decades, magnesium phosphate cements (MPC) has received significant attention from researchers due to its superior properties such as the high early strength, rapid setting time, very good volume stability, fire-proof behavior, good resistance to abrasion, and excellent bonding to old concrete structures. Moreover, the MPC is considered as eco-friendly cement. Compared to OPC, MBCs production is considered to be low energy consumer and low carbon dioxide emitter.

This research aims to give more insight about the physical, mechanical, thermal, and chemical performance of the MPC paste mainly with the addition of the boric acid for retardation behavior. On the other hand, two different additives have been used to enhance the performance of the boric acid including (1) graphene nanoplatelets (GnP), and (2) acetic acid (AA). Then, the influence of each additive on the MPC paste has been studied and evaluated. Finally, the experimental results are collected and employed to develop an artificial neural network (ANN) model that can describe the behavior of the MPC paste under different conditions.

7.1.1 CONCLUSIONS BASED ON CHAPTER III (INFLUENCE OF BORIC ACID)

As previously mentioned, the behavior of the MPC paste specimens can be driven by three main factors including magnesia to phosphate molar ratio (M/P), water to solid mass ratio (W/S) and boric acid to magnesia mass ratio (B/M). In this chapter, the authors chose to represent the

MPC pastes ingredients in molar ratios rather than the mass ratios terminology to capture the impact of the different MPC mix proportions (M/P, W/P, and B/M ratios) on the acid-base reaction, in addition to the influence of these factors on physical, mechanical, and thermal properties of the MPC system with the addition of boric acid as a retarder. Based on the experimental results and observations of this chapter, the following conclusions can be made:

1. The behavior of the MPC paste can be greatly influenced by several factors including M/P ratio, W/P ratio, and B/M ratio. Using the molar ratio between water and monopotassium phosphate compound (W/P) to calculate the amount of the used water can provide better understanding of the MPC behavior under different conditions.
2. The presence of the boric acid greatly influences the physical behavior of the MPC paste. The boric acid can significantly decrease the workability of the system and increase the fluidity loss with time. On the other hand, using B/M ratio of 5% can undoubtedly improve the initial setting time of the MPC paste, while adding more than 5% can reduce the initial setting time due to increase the fluidity loss of the MPC paste.
3. The MPC system is found to be very susceptible to water content. Adding or dropping a small amount of water can make a big difference in term of fluidity. For M/P ratio of 3, changing W/P ratio from 1.8 to 2.2 can increase the fluidity by more than 70%.
4. The presence of boric acid changes the mechanical behavior of the MPC system. The compressive strength can be significantly reduced when the boric acid is added to an MPC paste with low M/P ratio. On the other side, the reduction of the compressive becomes marginal if the boric acid is added to an MPC paste with high M/P molar ratio.
5. The optimal M/P molar ratio can be affected by the amount of the used W/P, while the optimal W/P molar ratio can be affected by the amount of the used M/P ratio. The

experimental results improve that for each W/P molar ratio there is an optimal M/P molar ratio and for each M/P molar ratio there is an optimal W/P molar ratio.

6. The boric acid can change the impact of the water content on the mechanical behavior of the MPC paste. For M/P ratio of 3, the reduction in the compressive strength due to increasing the W/P molar ratio from 1.8 to 2.2 is 19%. Adding 5% of boric acid to the same mixtures can reduce the compressive strength by only 4%.
7. The XRD analysis demonstrates that the only magnesium phosphate crystal that exists in the final products of the MPC system is the well-known K-struvite, where no other magnesium phosphate crystalline phases are found including Cattiite ($H_{44}Mg_3O30P_2$) and Newberyite (H_7MgO_7P). On the other side, no boron-containing crystalline phases are appeared in the final products of the system including Luneburgite $B_2H_{18}Mg_3O_{20}P_2$ and Szaibelyite $BHMgO_3$. These crystalline phases could be formed during the hydration processes and dissolved again during the hydration process.
8. The microstructure of the MPC paste is greatly influenced by adding the boric acid. The boric acid can prevent the reaction between the MgO and the KDP and reduce the amount of the K-struvite in the final product. Moreover, the presence of the boric acid with the MPC system leads to a considerable reduction in the crystallinity degree of K-struvite.
9. The FTIR analysis demonstrate that no new crystalline product has been achieved when the boric acid is added to the MPC system. However, adding the boric acid is reducing the intensity of the observed vibration bands.
10. The SEM images demonstrate that the microstructure of the K-struvite can be in several forms including prism-like microstructure, needle-like microstructure, and plate-like

microstructure. Furthermore, adding the boric acid to the MPC paste can change its morphology and reduce the crystallinity of the K-struvite.

11. The boric acid has the ability to reduce the thermal conductivity of the MPC paste due to the reduction in the dry density. Moreover, this reduction becomes more obvious when the M/P ratio is becoming high.

7.1.2 CONCLUSIONS BASED ON CHAPTER IV (INFLUENCE OF GNP)

In chapter IV, the GNP modified MPC specimens are prepared by using two different techniques: (1) the GNP is added to the mixture directly by using the sonication process, and (2) the GnP is added with using the polyethyleneimine (PLE) as a surfactant to improve the dispersion of the GnP. The behavior of the GnP modified MPC specimens is studied to investigate the influence of the GnP on the physical, chemical, mechanical, thermal, and microstructure properties of the MPC paste. The following conclusions can be drawn:

1. The presence of the GnP can significantly affect the physical and the mechanical properties of the MPC. The GnP can significantly reduce the initial setting time, the fluidity and the compressive strength. For example, adding 0.5 wt% of GnP can reduce the initial setting time, the fluidity, and the compressive strength by 67%, 19%, and 40% respectively. These reductions are due to the ability of GnP to absorb Mg^{+2} ions and reduce the amount of the final products.
2. Using the PLE to enhance the dispersion of the graphene can reduce the effect of the GnP on the fresh and hardened properties of the MPC paste. The presence of the PLE alone has an adverse effect on the compressive strength. However, using the PLE with the GnP is better than using the GnP alone. This observation can be attributed to the role of the

surfactant inside the aqueous solvent. The PLE can cover the GnP particles leading to reduce its ability to absorb the Mg^{+2} particles.

3. Both the GnP and the surfactant can change the phase compositions of the MPC paste. Although the XRD results demonstrated that there is no any chemical reaction between the graphene and the main ingredients of the MPC paste (MgO, KDP, and B), but the presence of the GnP reduced the amount of the reacted particles and reduced the amount of the crystalline k-struvite in the system. This reduction in the k-struvite is due to the tendency of the dissolved particles (Mg^{+2} and $PO4^{-3}$) to stick with the graphene surface during the hydration process.
4. The FTIR analysis demonstrated that no new crystalline product could be achieved when the GnP is added. However, adding the GnP can reduce the intensity of the observed vibration bands.
5. The GnP has the ability to improve the thermal conductivity of the MPC paste due to its high surface area. The addition of 0.1 wt%, 0.25wt%, and 0.5 wt% of the GNP improves the thermal conductivity of the paste by 3%, 12%, and 16% respectively.

7.1.3 CONCLUSIONS BASED ON CHAPTER V (INFLUENCE OF AA)

In chapter V, the acetic and the boric acids are used to improve the initial setting time of the MPC system. At first, the acetic acid is added alone to investigate its influence on the MPC paste behavior. Then, a hybrid system of both acids is added to different MPC mixtures to enhance the setting behavior of the MPC. Based on the finding of this research, the following conclusions can be made:

1. Using the acetic acid alone can increase the volumetric expansion/cracks of the MPC specimens during the curing process. Adding 7.5% of acetic acid can destroy the MPC paste sample during the reaction process due to the volumetric expansion.
2. Adding the acetic acid to the MPC mixtures can enhance the initial setting time of the paste by preventing the reaction between MgO and KDP particles. For example, using an acetic acid concentration of 5% can increase the initial setting time of the paste from 3 minutes to 12 minutes.
3. Using the boric acid with the acetic acid can prevent the volumetric expansion cracks. Moreover, using a hybrid system of both acids is found to be more efficient regarding the initial setting time.
4. The acetic acid has the ability to decrease the compressive strength of the MPC paste.
5. Using the acetic acid can change the phase compositions of the MPC paste. Based on the XRD analysis, it can be seen that the MPC specimen with no acetic acid exhibit stronger k-struvite characteristic peaks. This observation concludes that the existence of the acetic acid leads to poor crystal growth and maybe less amount of the k-struvite phase. On the other side, the MPC specimen that has high AAC exhibits stronger KDP characteristic peak which indicates that the presence of the acetic acid increases the amount of unreacted KDP.
6. The experimental results indicate that the thermal conductivity of the MPC paste decreases when the AAC increases. For example, adding 2.5% and 7.5 % of AAC can decrease the thermal conductivity from 1.31 to 1.29 and from 1.31 to 0.96 W/mk respectively. One possible reason of this reduction is the high volumetric expansion of

the acetic acid-containing specimens which can provide more voids in the paste and decrease its density and its thermal conductivity.

7.1.4 CONCLUSIONS BASED ON CHAPTER VI (ANN)

The work in chapter VI aims to predict the behavior of the MPC paste by using the mix proportions of its main ingredients in addition to two different additives including acetic acid (AA) and graphene nanoplatelets (GnP). The relation between the MPC properties and its mix proportions is highly non-liner. Therefore, performing a mathematical model to predict the MPC behavior is very difficult. The statistical measurements and the graphical accuracy plots demonstrate that the ANN approach is capable of predicting the MPC physical and mechanical properties by using its mix proportions. Moreover, The ANN approach is able to predict the behavior of the MPC paste by using different additives/retarders.

By developing several ANN models to predict the MPC behavior, the result shows that using of the training-all technique can improve the accuracy of the ANN model when the number of the available data sets is not enough to train the network.

On the other hand, the ANN results demonstrate that the manipulation of the available data sets can improve the accuracy of the ANN models. After replicating the AA and the GnP data sets for three times, the R^2 of the ANN1-1 and ANN2-1 models is increased from 0.89 to 0.98 respectively.

Furthermore, the statistical measurements approve that the ANN technique can predict the MPC mix proportions by using its physical and mechanical properties as input variables. For example, the ASE, MARE, and R^2 of the ANN2-2($_{\text{training-all}}$) model are found to be 0.0035, 303.4, and 0.92 respectively. The problem of such inverse data sets is the discontinuity and the non-

uniqueness. Therefore, modeling of such data sets is not possible in many cases especially when the data sets are collected from experimental measurements.

The proposed models can significantly provide a great insight about the MPC behavior under different conditions. At first, the ANN2-2 model can be used to provide initial guesses of the MPC mix proportions by using the desired material properties. Then, these proportions can be used as input variables of the ANN1-2 model to check the given mix proportions. Besides, the proposed ANN models can be used for several real-life applications such as MPC paste casting and 3D-printing application.

7.2 RECOMMENDATIONS

Based on the finding of this research, the following recommendations and future works are needed to provide more understanding of some related aspects of the MPC behavior:

1- The boric acid retardation mechanism of the MPC paste can be deeply understood by conducting the XRD test during the reaction processes of the MPC system. This can provide more information about the phase forming and the real impact of the boric acid during the acid-base reaction.

2- A rheological study of the MPC paste under different conditions is highly recommended to understand the impact of the boric and the acetic acids on the fluidity loss of the MPC material. Conducting such studies may solve the fluidity loss problem of the MPC and provide more information to use this material for the 3DP techniques.

3- Studying the change in the phase compositions of the MPC paste with time is highly recommended to understand the impact of each additive on the mechanical behavior of the MPC system.

4- Studying the effect of acetic acid on the volume expansion of MPC paste is recommended to understand the real impact of this additive on the MPC behavior.

5- Studying the mechanical and chemical behavior of the acetic acid modified MPC paste after 28 days is recommended to provide full understanding of the MPC behavior when this additive is used.

BIBLIOGRAPHY

1. Yap, Y. L., Y. M. Lai, H. F. Zhou, and W. Y. Yeong Yeong. "Compressive strength of thin-walled cellular core by inkjet-based additive manufacturing." Proceedings of the 1st International Conference on Progress in Additive Manufacturing. Singapore: NTU Additive Manufacturing Centre, School of Mechanical and Aerospace Engineering, Nanyang Technological Universit. 333-338.
2. Ngo, Tuan D., Alireza Kashani, Gabriele Imbalzano, Kate TQ Nguyen, and David Hui. "Additive manufacturing (3D printing): A review of materials, methods, applications and challenges." Composites Part B: Engineering (2018).
3. Jean-Claude, Andre. "Disdpositif pour realiser un modele de piece industrielle" (http://bases-brevets.inpi.fr/fr/do cument/FR2567668/publications.html). National De La Propriete Industrielle.
4. Hull, Charles W. "Apparatus for production of three-dimensional objects by stereolithography." U.S. Patent 4,575,330 issued March 11, 1986.
5. Freedman, David H. "Layer by layer." Technology Review 115, no. 1 (2012): 50-53.
6. Crump, S. Scott. "Apparatus and method for creating three-dimensional objects." U.S. Patent 5,121,329 issued June 9, 1992.
7. Yampolskiy, Mark, Wayne E. King, Jacob Gatlina, Sofia Belikovetskyc, Adam Browna, Anthony Skjellumd, and Yuval Elovicic. 2018. "Security of additive manufacturing: Attack taxonomy and survey." Additive Manufacturing (Elsevier) 431-457.

8. Vu, Ivan Q., Lindsey B Bass, Christopher B. Williams, and David A. Dillard. 2018. "Characterizing the effect of print orientation on interface integrity of multi-material jetting additive manufacturing." Additive Manufacturing 447-461.
9. Bass, Lindsey, Nicholas Alexander Meisel, and Christopher B. Williams. "Exploring variability of orientation and aging effects in material properties of multi-material jetting parts." *Rapid Prototyping Journal* 22, no. 5 (2016): 826-834.
10. He, Yinfeng, Ricky D. Wildman, Chris J. Tuck, Steven DR Christie, and Steven Edmondson. "An investigation of the behavior of solvent based polycaprolactone ink for material jetting." *Scientific reports* 6 (2016): 20852.
11. Additive Manufacturing Research Group (AMRG), Loughborough University. 2018. *About Additive Manufacturing.* http://www.lboro.ac.uk/research/amrg/about/.
12. Vlasea, Mihaela L., B. Lane, F. Lopez, Sergey Mekhontsev, and A. Donmez. "Development of powder bed fusion additive manufacturing test bed for enhanced real-time process control." In *Proceedings of the International Solid Freeform Fabrication Symposium*, pp. 527-539. 2015.
13. Gao, Wei, Yunbo Zhang, Devarajan Ramanujan, Karthik Ramani, Yong Chen, Christopher B. Williams, Charlie CL Wang, Yung C. Shin, Song Zhang, and Pablo D. Zavattieri. "The status, challenges, and future of additive manufacturing in engineering." *Computer-Aided Design* 69 (2015): 65-89.
14. 3D Print. 2017. *Comparison of Metal 3D Printing — Part Two: Directed Energy Deposition.* Jul. https://3dprint.com/182367/directed-energy-deposition/.

15. Lee, Hyub, Chin Huat Joel Lim, Mun Ji Low, Nicholas Tham, Vadakke Matham Murukeshan, and Young-Jin Kim. "Lasers in additive manufacturing: a review." *International Journal of Precision Engineering and Manufacturing-Green Technology*4, no. 3 (2017): 307-322.
16. Lim, Sungwoo, Richard A. Buswell, Thanh T. Le, Simon A. Austin, Alistair GF Gibb, and Tony Thorpe. "Developments in construction-scale additive manufacturing processes." *Automation in construction* 21 (2012): 262-268.
17. De Schutter, Geert, Karel Lesage, Viktor Mechtcherine, Venkatesh Naidu Nerella, Guillaume Habert, and Isolda Agusti-Juan. "Vision of 3D printing with concrete—Technical, economic and environmental potentials." *Cement and Concrete Research* (2018).
18. Bos, Freek, Rob Wolfs, Zeeshan Ahmed, and Theo Salet. "Additive manufacturing of concrete in construction: potentials and challenges of 3D concrete printing." *Virtual and Physical Prototyping* 11, no. 3 (2016): 209-225.
19. Panda, Biranchi, and Ming Jen Tan. "Experimental study on mix proportion and fresh properties of fly ash based geopolymer for 3D concrete printing." *Ceramics International*44, no. 9 (2018): 10258-10265.
20. Lim, Sungwoo, Richard A. Buswell, Thanh T. Le, Simon A. Austin, Alistair GF Gibb, and Tony Thorpe. "Developments in construction-scale additive manufacturing processes." *Automation in construction* 21 (2012): 262-268.

21. Labonnote, Nathalie, Anders Rønnquist, Bendik Manum, and Petra Rüther. "Additive construction: State-of-the-art, challenges and opportunities." *Automation in Construction* 72 (2016): 347-366.
22. Le, Thanh T., Simon A. Austin, Sungwoo Lim, Richard A. Buswell, Alistair GF Gibb, and Tony Thorpe. "Mix design and fresh properties for high-performance printing concrete." *Materials and structures* 45, no. 8 (2012): 1221-1232.
23. Anastasiou, Athanasios, Charalambos Tsirmpas, Alexandros Rompas, Kostas Giokas, and Dimitris Koutsouris. "3D printing: Basic concepts mathematics and technologies." In *Bioinformatics and Bioengineering (BIBE), 2013 IEEE 13th International Conference on*, pp. 1-4. IEEE, 2013.
24. ASTM. "Standard test methods for time of setting of hydraulic cement by Vicat needle." *C191-08* (2008).
25. Cullen, P. J., B. K. Tiwari, and V. Valdramidis. "Novel Thermal and Non-Thermal Technologies for Fluid Foods. 2012."
26. Liew, K. M., A. O. Sojobi, and L. W. Zhang. "Green concrete: Prospects and challenges." *Construction and Building Materials* 156 (2017): 1063-1095.
27. ASTM C181-11, Standard Test Method for Workability Index of Fireclay and High-Alumina Refractory Plastics, ASTM International, West Conshohocken, PA, 2011.
28. Jianchao, Zhu, Tao Zhang, Mansour Faried, and Chen Wengang. "3D printing cement-based ink, and it's application within the construction industry." In *MATEC Web of Conferences,*vol. 120, p. 02003. EDP Sciences, 2017.

29. Paul SC, Tay YWD, Panda B, Tan MJ. Fresh and hardened properties of 3D printable cementitious materials for building and construction. Arch Civil Mech Eng2018;18(1):311–9.
30. Zhang, Yu, Yunsheng Zhang, Guojian Liu, Yonggan Yang, Meng Wu, and Bo Pang. "Fresh properties of a novel 3D printing concrete ink." Construction and Building Materials 174 (2018): 263-271.
31. Soltan, Daniel G., and Victor C. Li. "A self-reinforced cementitious composite for building-scale 3D printing." Cement and Concrete Composites 90 (2018): 1-13.
32. Asprone, Domenico, Ferdinando Auricchio, Costantino Menna, and Valentina Mercuri. "3D printing of reinforced concrete elements: Technology and design approach." Construction and Building Materials 165 (2018): 218-231.
33. Kazemian, Ali, Xiao Yuan, Evan Cochran, and Behrokh Khoshnevis. "Cementitious materials for construction-scale 3D printing: Laboratory testing of fresh printing mixture." Construction and Building Materials 145 (2017): 639-647.
34. Perrot, A., D. Rangeard, and E. Courteille. "3D printing of earth-based materials: Processing aspects." Construction and Building Materials 172 (2018): 670-676.
35. Ketel, Sabrina, Gabriel Falzone, Bu Wang, Newell Washburn, and Gaurav Sant. "A printability index for linking slurry rheology to the geometrical attributes of 3D-printed components." Cement and Concrete Composites (2018).

36. Achillas, Ch, D. Aidonis, E. Iakovou, M. Thymianidis, and D. Tzetzis. "A methodological framework for the inclusion of modern additive manufacturing into the production portfolio of a focused factory." Journal of Manufacturing Systems 37 (2015): 328-339.
37. Li Yue, Sun Jia, Chen Bing, Experimental study of magnesia and M/P ratio influencing properties of magnesium phosphate cement, Construction and Building Materials 65 (2014) 177–183.
38. Yang, Nan, Caijun Shi, Jianming Yang, and Yuan Chang. "Research progresses in magnesium phosphate cement–based materials." Journal of Materials in Civil Engineering 26, no. 10 (2013): 04014071.
39. U. Klammert, E. Vorndran, T. Reuther, F.A. Müller, K. Zorn, U. Gbureck, Low temperature fabrication of magnesium phosphate cement scaffolds by 3D powder printing, J. Mater. Sci. – Mater. Med. 21 (11) (2010) 2947–2953.
40. J.A. Inzana, D. Olvera, S.M. Fuller, J.P. Kelly, O.A. Graeve, E.M. Schwarz, et al., 3D printing of composite calcium phosphate and collagen scaffolds for bone regeneration, Biomaterials 35 (13) (2014) 4026–4034.
41. EcoSmart Concrete. Accessed October 24, 2018. http://ecosmartconcrete.com/?page_id=208.
42. Li, Zongjin. Advanced concrete technology. John Wiley & Sons, 2011.
43. C.K. Chau, Fei Qiao, Zongjin Li, Microstructure of magnesium potassium phosphate cement, Construction and Building Materials 25 (2011) 2911–2917.

44. Formosa, J., J. M. Chimenos, A. M. Lacasta, and M. Niubó. "Interaction between low-grade magnesium oxide and boric acid in chemically bonded phosphate ceramics formulation." Ceramics International 38, no. 3 (2012): 2483-2493.
45. SORRE, CHARLES A., and Charles R. Armstrong. "Reactions and Equi ibria in Magnesium Oxych oride Cements." Journal of the American Ceramic Society 59, no. 1-2 (1976): 51-54.
46. Hwang, Byung Wook, Jeong Hwan Lim, Ho Jin Chae, Ho-Jung Ryu, Doyeon Lee, Joong Beom Lee, Hana Kim, Soo Chool Lee, and Jae Chang Kim. "CO2 capture and regeneration properties of MgO-based sorbents promoted with alkali metal nitrates at high pressure for the sorption enhanced water gas shift process." Process Safety and Environmental Protection 116 (2018): 219-227.
47. Hongyan Ma, Biwan Xu, Jun Liu, Huafu Pei, Zongjin Li, Effects of water content, magnesia-to-phosphate molar ratio and age on pore structure, strength and permeability of magnesium potassium phosphate cement paste, Materials and Design 64 (2014) 497–502.
48. Walling, Sam A., and John L. Provis. "Magnesia-based cements: a journey of 150 years, and cements for the future?." Chemical reviews 116, no. 7 (2016): 4170-4204.
49. Chuanlin Hu, Biwan Xu, Hongyan Ma, Binmeng Chen, Zongjin Li, Micromechanical investigation of magnesium oxychloride cement paste, Construction and Building Materials 105 (2016) 496–502.
50. Demediuk, Thaisa, W. F. Cole, and H. V. Hueber. "Studies on magnesium and calcium oxychlorides." Australian Journal of Chemistry 8, no. 2 (1955): 215-233.

51. Dehua, Deng, and Zhang Chuanmei. "The formation mechanism of the hydrate phases in magnesium oxychloride cement1." *Cement and concrete research* 29, no. 9 (1999): 1365-1371.
52. Li, Zongjin, and C. K. Chau. "Influence of molar ratios on properties of magnesium oxychloride cement." *Cement and Concrete Research* 37, no. 6 (2007): 866-870.
53. Beaudoin, James Joseph, and Vangipuram Seshachar Ramachandran. "Strength development in magnesium oxychloride and other cements." *Cement and Concrete Research* 5, no. 6 (1975): 617-630.
54. S. Sorel, Sur un Nouveau cement magnesium, Comp. Rend. 65 (1867) 102–104.
55. Qin, Ling, Xiaojian Gao, Wengui Li, and Huan Ye. "Modification of magnesium oxysulfate cement by incorporating weak acids." *Journal of Materials in Civil Engineering* 30, no. 9 (2018): 04018209.
56. Wu, Chengyou, Hongfa Yu, Huifang Zhang, Jinmei Dong, Jing Wen, and Yongshan Tan. "Effects of phosphoric acid and phosphates on magnesium oxysulfate cement." *Materials and structures* 48, no. 4 (2015): 907-917.
57. Chengyou Wu, Wenhai Chen, Huifang Zhang, Hongfa Yu, Wuyu Zhang, Ningshan Jiang, Lianxin Liu, The hydration mechanism and performance of Modified magnesium oxysulfate cement by tartaric acid, Construction and Building Materials 144 (2017) 516–524
58. Demediuk, Thaisa, W. F. Cole, and H. V. Hueber. "Studies on magnesium and calcium oxychlorides." *Australian Journal of Chemistry* 8, no. 2 (1955): 215-233.

59. Tao Guo, Hefang Wang, Hongjian Yang, Xiaosen Cai, Qiu Ma, Shaoming Yang, The mechanical properties of magnesium oxysulfate cement enhanced with 517 phase magnesium oxysulfate whiskers, Construction and Building Materials 150 (2017) 844–850.
60. Biwan Xu, Hongyan Ma, Zongjin Li, Influence of magnesia-to-phosphate molar ratio on microstructures, mechanical properties and thermal conductivity of magnesium potassium phosphate cement paste with large water-to-solid ratio, Cement and Concrete Research 68 (2015) 1–9.
61. Li Yue, Sun Jia, Chen Bing, Experimental study of magnesia and M/P ratio influencing properties of magnesium phosphate cement, Construction and Building Materials 65 (2014) 177–183.
62. Qiao, Fei, C. K. Chau, and Zongjin Li. "Property evaluation of magnesium phosphate cement mortar as patch repair material." Construction and Building Materials 24, no. 5 (2010): 695-700.
63. Masuda T, Ogino I, Mukai SR. Optimizing the dimensions of magnesium ammonium phosphate to maximize its ammonia uptake ability. Adv Powder Technol 2013; 24:520–4.
64. Soudée, E., and J. Péra. "Mechanism of setting reaction in magnesia-phosphate cements." Cement and Concrete Research 30, no. 2 (2000): 315-321.
65. Li Yue, Shi Tongfei, Chen Bing, Li Yaqiang, Performance of magnesium phosphate cement at elevated temperatures, Construction and Building Materials 91 (2015) 126–132.

66. Mathew M, Schroeder LW. Crystal structure of a struvite analogue, MgKPO4_6H2O. Acta Crystallogr 1979;B35(1):11–3.
67. Mathieu Le Rouzic, Thierry Chaussadent, Gérard Platret, Lavinia Stefan, Mechanisms of k-struvite formation in magnesium phosphate cements, Cement and Concrete Research 91 (2017) 117–122.
68. Zhu Ding, Biqin Dong, Feng Xing, Ningxu Han, Zongjin Li, Cementing mechanism of potassium phosphate based magnesium phosphate cement, Ceramics International 38 (2012) 6281–6288.
69. Fei Qiao, C. K. Chau, Zongjin Li, Calorimetric study of magnesium potassium phosphate cement, Materials and Structures (2012) 45:447–456.
70. Li Yue a, Chen Bing, Factors that affect the properties of magnesium phosphate cement, Construction and Building Materials 47 (2013) 977–983.
71. Quanbing Yang, Xueli Wu, Factors influencing properties of phosphate cement-based binder for rapid repair of concrete, Cement and Concrete Research 29 (1999) 389–396.
72. Quanbing Yan, Beirong Zhu, Shuqing Zhang, Xueli Wu, Properties and applications of magnesia-phosphate cement mortar for rapid repair of concrete, Cement and Concrete Research 30 (2000) 1807-1813.
73. Xiaojie Fu, Zhenyu Lai, Xinchun Lai, Zhongyuan Lu, Shuzhen Lv, Preparation and characteristics of magnesium phosphate cement based porous materials, Construction and Building Materials 127 (2016) 712–723.

74. D.A. Hall, R. Stevens, B. El-Jazairi, The effect of retarders on the microstructure and mechanical properties of Magnesia-phosphate cement mortar, Cement and Concrete Research 31 (2001) 455-465.
75. J. Formosa, J.M. Chimenos, A.M. Lacasta, M. Niubo, Interaction between low-grade magnesium oxide and boric acid in chemically bonded phosphate ceramics formulation, Ceramics International 38 (2012) 2483–2493.
76. Lahalle, Hugo, Céline Cau Dit Coumes, Adel Mesbah, David Lambertin, Céline Cannes, Sylvie Delpech, and Sandrine Gauffinet. "Investigation of magnesium phosphate cement hydration in diluted suspension and its retardation by boric acid." Cement and Concrete Research 87 (2016): 77-86.
77. Tan, Hongbo, Xun Zhang, Yulin Guo, Baoguo Ma, Shouwei Jian, Xingyang He, Zhenzhen Zhi, and Xiaohai Liu. "Improvement in fluidity loss of magnesia phosphate cement by incorporating polycarboxylate superplasticizer." Construction and Building Materials 165 (2018): 887-897.
78. Li, Jiusu, Wenbo Zhang, and Yong Cao. "Laboratory evaluation of magnesium phosphate cement paste and mortar for rapid repair of cement concrete pavement." Construction and Building Materials 58 (2014): 122-128.
79. YANG Jianming, QIAN Chunxiang, Effect of Borax on Hydration and Hardening Properties of Magnesium and Pottassium Phosphate Cement Pastes, Journal of Wuhan University of Technology-Mater. Sci. Ed. Aug.2010.

80. Li, Yue, Yaqiang Li, Tongfei Shi, and Jiaqi Li. "Experimental study on mechanical properties and fracture toughness of magnesium phosphate cement." Construction and Building Materials 96 (2015): 346-352.
81. Zheng, Deng-Deng, Tao Ji, Can-Qiang Wang, Chun-Jing Sun, Xu-Jian Lin, and Khandaker Muhammed Anwar Hossain. "Effect of the combination of fly ash and silica fume on water resistance of Magnesium–Potassium Phosphate Cement." Construction and Building Materials 106 (2016): 415-421.
82. Xu, Biwan, Hongyan Ma, Hongyu Shao, Zongjin Li, and Barbara Lothenbach. "Influence of fly ash on compressive strength and micro-characteristics of magnesium potassium phosphate cement mortars." Cement and Concrete Research99 (2017): 86-94.
83. Li, Jun, Yong-sheng Ji, Guo-dong Huang, Zhan-zhan Xu, and Gui-hong Yan. "Properties and reaction mechanisms of magnesium phosphate cement mixed with acetic acid." KSCE Journal of Civil Engineering 22, no. 1 (2018): 231-235.
84. Lu, Zeyu, Dongshuai Hou, Hongyan Ma, Tianyuan Fan, and Zongjin Li. "Effects of graphene oxide on the properties and microstructures of the magnesium potassium phosphate cement paste." Construction and Building Materials 119 (2016): 107-112.
85. Onal, Okan, and Ali Ugur Ozturk. "Artificial neural network application on microstructure–compressive strength relationship of cement mortar." Advances in Engineering Software 41, no. 2 (2010): 165-169.

86. Arslan, M. Hakan. "Predicting of torsional strength of RC beams by using different artificial neural network algorithms and building codes." *Advances in Engineering Software* 41, no. 7-8 (2010): 946-955.
87. Zadeh, E. Eftekhari, S. A. H. Feghhi, G. H. Roshani, and A. Rezaei. "Application of artificial neural network in precise prediction of cement elements percentages based on the neutron activation analysis." *The European Physical Journal Plus* 131, no. 5 (2016): 167.
88. Nazari, Ali, Hadi Hajiallahyari, Ali Rahimi, Hamid Khanmohammadi, and Mohammad Amini. "Prediction compressive strength of Portland cement-based geopolymers by artificial neural networks." *Neural Computing and Applications* (2012): 1-9.
89. Lee, Seung-Chang. "Prediction of concrete strength using artificial neural networks." Engineering Structures 25, no. 7 (2003): 849-857.
90. Mohamed, Ashraf Ragab, Adel El Kordy, and Mona Elsalamawy. "Prediction of SEM–X-ray images' data of cement-based materials using artificial neural network algorithm." *Alexandria Engineering Journal* 53, no. 3 (2014): 607-613.
91. Dias, W. P. S., and S. P. Pooliyadda. "Neural networks for predicting properties of concretes with admixtures." *Construction and Building Materials* 15, no. 7 (2001): 371-379.
92. Hanle, L. J., Jayaraman K. R., and Smith J. S. (2004). CO2 emissions profile of the U.S. cement industry. U.S. Environmental Protection Agency, Washington, D.C.
93. Ellis M. Gartner, Donald E. Macphee, A physico-chemical basis for novel cementitious binders, Cement and Concrete Research 41 (2011) 736–749.

94. Environment Agency (EA), Waste Protocol Project, A technical report on the manufacture of products from pulverised fuel ash and furnace bottom ash (online). Available from: <www.wrap.org.uk>, 2006 (accessed 04.02.10).

95. M. Mavroulidou, T. Morrison, C. Unsworth, M.J. Gunn, Properties of concrete made of multicomponent mixes of low-energydemanding binders, Construction and Building Materials 101 (2015) 1122–1141.

96. M. C. G. Juenger, F. Winnefeld, J. L. Provis and J. H. Ideker, Advances in alternative cementitious binders, Cement and Concrete Research (in press).

97. Walling, Sam A., and John L. Provis. "Magnesia-based cements: a journey of 150 years, and cements for the future?." *Chemical reviews* 116, no. 7 (2016): 4170-4204.

98. Itani, O., & Najjar, Y. (2000). Three-dimensional modeling of spatial soil properties via Artificial Neural Networks. Transportation Research Record: Journal of the Transportation Research Board, (1709), 50-59.

99. Yasarer, H., & Najjar, Y. M. (2013). Characterizing the Permeability of Kansas Concrete Mixes Used in PCC Pavements. International Journal of Geomechanics, 14(4), 04014017.

100. Najjar, Y. M., & Huang, C. (2007). Simulating the stress–strain behavior of Georgia kaolin via recurrent neuronet approach. Computers and Geotechnics, 34(5), 346-361.

101. "Magnesium Compounds for Heat Emission Fillers." Research and Development Magnesium Compounds for Heat Emission Fillers- [Konoshima Chemical Co.,Ltd.]. Accessed April 07, 2019. http://www.konoshima.co.jp/eng/resdev/resdev04.html.

102. Ropp, Richard C. Encyclopedia of the alkaline earth compounds. Newnes, 2012.

103. "Dead Burned Magnesium Oxide." Martin Marietta Magnesia Specialties, LLC. Accessed April 07, 2019. https://magnesiaspecialties.com/dead-burned-magnesium-oxide/.

104. American Elements. "Potassium Dihydrogen Phosphate." American Elements. June 13, 2017. Accessed April 07, 2019. https://www.americanelements.com/potassium-dihydrogen-phosphate-7778-77-0#section-synonyms.

105. "Potassium Dihydrogen Phosphate." National Center for Biotechnology Information. PubChem Compound Database. Accessed April 07, 2019. https://pubchem.ncbi.nlm.nih.gov/compound/Potassium_dihydrogen_phosphate.

106. "Premier Magnesia, LLC." Premier Magnesia, LLC. Accessed April 07, 2019. https://www.premiermagnesia.com/.

107. "Granular Boric Acid, 8 Oz." Granular Boric Acid, 8 Oz [boric08oz] | DudaDiesel Biodiesel Supplies. Accessed April 07, 2019. https://www.dudadiesel.com/choose_item.php?id=boric08oz.

108. "Acetic Acid Formula." Math. Accessed April 07, 2019. http://www.softschools.com/formulas/chemistry/acetic_acid/328/.

109. Garg, Pulkit, Pallav Gupta, Devendra Kumar, and Om Parkash. "Structural and mechanical properties of graphene reinforced aluminum matrix composites." J. Mater. Environ. Sci 7, no. 5 (2016): 1461-1473.

110. Cheap Tubes Inc. "Understanding Graphene Nanoplatelets." AZoNano.com. July 05, 2018. Accessed April 08, 2019. https://www.azonano.com/article.aspx?ArticleID=4846.

111. "Graphene Nano-Platelets." World-Leading Graphene Company - XG Sciences. Accessed April 08, 2019. https://xgsciences.com/materials/graphene-nano-platelets/.

112. "Polyethylenimine." Wikipedia. February 10, 2019. Accessed April 07, 2019. https://en.wikipedia.org/wiki/Polyethylenimine.

113. Hall, David A., Ronald Stevens, and Bayhass El Jazairi. "Effect of water content on the structure and mechanical properties of magnesia-phosphate cement mortar." Journal of the American Ceramic Society 81, no. 6 (1998): 1550-1556.

114. Stefov, V., B. Šoptrajanov, F. Spirovski, I. Kuzmanovski, H. D. Lutz, and B. Engelen. "Infrared and Raman spectra of magnesium ammonium phosphate hexahydrate (struvite) and its isomorphous analogues. I. Spectra of protiated and partially deuterated magnesium potassium phosphate hexahydrate." Journal of Molecular Structure 689, no. 1-2 (2004): 1-10.

115. Liao, Wenyu, Hongyan Ma, Hongfang Sun, Yan Huang, and Yaocheng Wang. "Potential large-volume beneficial use of low-grade fly ash in magnesia-phosphate cement based materials." Fuel 209 (2017): 490-497.

116. Qiu, Xinhong, Keiko Sasaki, Kwadwo Osseo-Asare, Tsuyoshi Hirajima, Keiko Ideta, and Jin Miyawaki. "Sorption of H3BO3/B (OH) 4− on calcined LDHs including different divalent metals." Journal of colloid and interface science 445 (2015): 183-194.

117. Sasaki, Keiko, Xinhong Qiu, Yukiho Hosomomi, Sayo Moriyama, and Tsuyoshi Hirajima. "Effect of natural dolomite calcination temperature on sorption of borate onto calcined products." Microporous and Mesoporous Materials 171 (2013): 1-8.

118. Sasaki, Keiko, Xinhong Qiu, Sayo Moriyama, Chiharu Tokoro, Keiko Ideta, and Jin Miyawaki. "Characteristic sorption of H3BO3/B (OH) 4− on magnesium oxide." Materials transactions 54, no. 9 (2013): 1809-1817.

119. Wang, Baomin, Ruishuang Jiang, and Zhenlin Wu. "Investigation of the mechanical properties and microstructure of graphene nanoplatelet-cement composite." Nanomaterials6, no. 11 (2016): 200.

120. Du, Hongjian, and Sze Dai Pang. "Dispersion and stability of graphene nanoplatelet in water and its influence on cement composites." Construction and Building Materials 167 (2018): 403-413.

121. Tong, Teng, Zhou Fan, Qiong Liu, Sen Wang, Susheng Tan, and Qiang Yu. "Investigation of the effects of graphene and graphene oxide nanoplatelets on the micro- and macro-properties of cementitious materials." Construction and Building Materials 106 (2016): 102-114.

122. Sedaghat, Ahmadreza, Manoj K. Ram, A. Zayed, Rajeev Kamal, and Natallia Shanahan. "Investigation of physical properties of graphene-cement composite for structural applications." Open journal of composite materials 4, no. 01 (2014): 12.

123. Cui, Xia, Shengwei Sun, Baoguo Han, Xun Yu, Jian Ouyang, Shuzhu Zeng, and Jinping Ou. "Mechanical, thermal and electromagnetic properties of nanographite platelets

modified cementitious composites." Composites Part A: Applied Science and Manufacturing 93 (2017): 49-58.

124. Li, Yue, and Hui Lin. "Experimental study on the effect of different dispersed degrees carbon nanotubes on the modification of magnesium phosphate cement." Construction and Building Materials 200 (2019): 240-247.

125. Li, Xiangyu, Yan Ming Liu, Wen Gui Li, Chen Yang Li, Jay G. Sanjayan, Wen Hui Duan, and Zongjin Li. "Effects of graphene oxide agglomerates on workability, hydration, microstructure and compressive strength of cement paste." Construction and Building Materials 145 (2017): 402-410

126. C.P. Lazar, F. Karlický, P. Jurečka, M. Kocman, E. Otyepková, K. Šafářová, and M. Otyepka, “Adsorption of Small Organic Molecules on Graphene,” J. Am. Chem. Soc., vol. 135, no. 16, pp. 6372–6377, Apr. 2013

127. Pan, Zhu, Li He, Ling Qiu, Asghar Habibnejad Korayem, Gang Li, Jun Wu Zhu, Frank Collins, Dan Li, Wen Hui Duan, and Ming Chien Wang. "Mechanical properties and microstructure of a graphene oxide–cement composite." Cement and Concrete Composites 58 (2015): 140-147.

128. Ramakrishnan, Sayanthan, Xiaoming Wang, and Jay Sanjayan. "Thermal enhancement of paraffin/hydrophobic expanded perlite granular phase change composite using graphene nanoplatelets." Energy and Buildings 169 (2018): 206-215.

129. Di Crescenzo, Antonello, Pietro Di Profio, Gabriella Siani, Romina Zappacosta, and Antonella Fontana. "Optimizing the interactions of surfactants with graphitic surfaces and clathrate hydrates." Langmuir 32, no. 26 (2016): 6559-6570.

130. Tachikawa, Hiroto, Tetsuji Iyama, and Hiroshi Kawabata. "MD simulation of the interaction of magnesium with graphene." Thin Solid Films 518, no. 2 (2009): 877-879.

131. Yu, Yan-Zi, Jian-Gang Guo, and Yi-Lan Kang. "An analytical model for adsorption and diffusion of atoms/ions on graphene surface." Journal of Nanomaterials 16, no. 1 (2015): 321.

132. Alilou, Vahid K., and Mohammad Teshnehlab. "Prediction of 28-day compressive strength of concrete on the third day using artificial neural networks." International journal of Engineering 3, no. 6 (2010): 565-576.

133. Chopra, Palika, Rajendra Kumar Sharma, and Maneek Kumar. "Artificial neural networks for the prediction of compressive strength of concrete." International Journal of Applied Sciences & Engineering 13, no. 3 (2015): 187-204.

134. Alshihri, Marai M., Ahmed M. Azmy, and Mousa S. El-Bisy. "Neural networks for predicting compressive strength of structural light weight concrete." Construction and Building Materials 23, no. 6 (2009): 2214-2219.

HASHEM ALMASHAQBEH

EDUCATION

University of Mississippi - Oxford, MS, United States
Ph.D. in Engineering Science- Civil Engineering **2019**
Dissertation: "Decoding and Optimizing Magnesium Phosphate Cement for Additive Construction Applications"
Jordan University of Science and Technology
Master of Engineering Science – Civil/ Structural Engineering **2014**
Thesis: "Strengthening of Reinforced Concrete Beams Using Nano-composites reinforce with Carbon Fiber Sheet"
Jordan University of Science and Technology
Bachelor's in Civil Engineering **2012**

ACADEMIC EXPERIENCE

University of Mississippi - Oxford, MS, United States
Teaching Assistant – to Professor Hunain Alkhateb "Material Science' **2019**
Collaborated in teaching, and class preparation.

University of Mississippi - Oxford, MS, United States
Teaching Assistant **2015-2019**
Collaborated in preparing and teaching some classes, HomeWorks and final exam grading.

University of Mississippi - Oxford, MS, United States
Research Assistant – to Professor Hunain Alkhateb **2015-2019**

PUBLICATIONS AND PAPERS

Irshidat, Mohammad R., Mohammed H. Al-Saleh, and Hashem Almashagbeh. "Effect of carbon nanotubes on strengthening of RC beams retrofitted with carbon fiber/epoxy composites." Materials & Design 89 (2016): 225-234.